4258

A Theoretical Study of the Variations of NO_x in the Upper Atmosphere

Yutaka Kondo

Geophysical Institute

University of Tokyo

CONTENTS

ABSTRACT

The behavior of minor constituents in the upper atmosphere at mid-latitudes and high latitudes is studied by using one-dimensional photochemical-diffusive model.

The diurnal variation of odd nitrogen in the mid-latitudes atmosphere is investigated first. Introducing the $N(^2D)$ quenching by O with k_q = 0.6-1.0x10^{-12} cm^{3}s^{-1} around 100 km, the quantum yield of $N(^2D)$ production in the reactions energetically capable of producing $N(^2D)$ such as $NO^+ + e \rightarrow N + O$, $N_2^+ + O \rightarrow NO^+ + N$, and the dissociation of N_2 by photoabsorption of solar EUV and photoelectron impact, is determined to be about 0.9 by comparing the calculated and measured daytime NO profiles below 110 km. Above 140 km $k_q \simeq 1.0 \times 10^{-12}$ cm^{3}s^{-1} is recommended to be consistent with NI(5200 Å) dayglow measurements.

NO density goes through large diurnal variation above 100 km caused by the diurnal variation of the thermospheric temperature: the daytime density of 10^7 cm^{-3} decreasing to $\leq 10^6$ cm^{-3} at night around 110 km if the thermopause temperature T_∞ is $\leq$ 900 K after sunset. Highly temperature dependent reaction $N(^4S) + O_2 \rightarrow NO + O$, which contributes to the production of NO and loss of $N(^4S)$, is the key reaction which controls the nighttime NO concentration. Small concentration of NO measured in the early morning by rockets can be attributed to the lowered temperature during night.

Nighttime $N(^4S)$ profile is also very sensitive to the thermospheric temperature change. Midnight N density at 120 km could vary by more than two orders of magnitude with the change of T_∞ by about 200 K. Daytime N density does not depend so greatly on T_∞ and the noon value has its maximum of 2-5 x 10^7 cm^{-3} at about 130 km. The measurement of N density by Feldman and Takacs(1974) is in agreement with our calculated profile which

assumed T_∞ appropriate for the time of the observation and k_q of 4-5 x 10^{-12} $cm^3 s^{-1}$ above 130 km based on the laboratory experiment.

Secondly height distribution of minor constituents in the mesosphere and lower thermosphere in the polar region is simulated assuming the auroral precipitation to induce a temporal variation of the source terms for minor species. The dissociation of molecular nitrogen by impacts of precipitating electrons, together with the production of neutral odd nitrogen through ionic reactions caused by auroral ionizations, plays an essential role in determining the distribution of neutral odd nitrogen (N and NO) densities. Temporal variations of the N and NO densities during the auroral perturbations are quite different with different values of the quantum yield η of $N(^2D)$ in the dissociation of N_2. Enhancement of the NO density to a value more than a factor 10 larger than the normal value is possible above the height of 100 km in an IBC III aurora, as far as $\eta \gtrsim 0.5$. The atomic nitrogen density grows rapidly during the precipitation, and decreases through the reaction with NO as soon as the perturbation ends. Alternatively if $\eta \lesssim 0.1$, the N density would increase to be comparable with that of NO, resulting in lower NO density. A large value of η ($\gtrsim 0.5$) is in favor of the recent observations of NO which revealed the larger density of NO in the polar thermosphere than in the low and middle latitude. The prolonged enhancement of NO density may influence the electron density and the ionic composition in the ionospheric E region, during a pause of the auroral precipitation. The more abundant NO^+ density than the O_2^+ density would be maintained throughout the day even under the condition of intermittent precipitations of auroral electrons.

CHAPTER I. GENERAL INTRODUCTION

Odd nitrogen chemistry

There are various kinds of minor chemical compounds, which are produced from chemically stable species such as N_2, O_2, H_2, and H_2O in the upper atmosphere. Nitrogen, hydrogen, oxygen, and their ionic compounds constitute such minor species. They are known to play important roles in the upper atmosphere in spite of their small relative abundances. For example, radiation from OH is an interesting subject in the fields of airglow, O_3 is important as a heat source in the stratosphere and mesosphere, and NO is crucial to the ion chemistry in the ionospheric D and E regions. Of these minor constituents we are mainly concerned with the aeronomy of odd nitrogen here.

Nitric oxide was first considered as an important constituent in the upper atmosphere by Nicolet(1945). He pointed out the important role played by this molecule through photoionization in the D-region. This was confirmed by Watanabe, Marmo, and Inn(1953) by the measurement of the absorption coefficients of NO, O_2, and other molecules. They concluded that the formation of the D-region by NO as indicated by Nicolet(1945) can be a satisfactory explanation, since Ly-α, which photoionizes NO molecules, lies in an atmospheric window. Bates(1952) was the first to discuss the photochemistry of nitrogen. N_2 dissociation by photoabsorption in the bands of the Lyman-Birge-Hopfield(L-B-H) system and electron impact, and dissociative recombination of N_2^+ were already considered as a source of atomic nitrogen in his study

The effect of dynamic processes such as diffusion and mixing(today we call these as molecular and eddy diffusion) on nitrogen species was pointed out by Nicolet(1955). He concluded that departure from static chemical equilibrium has to be considered in the computation of the relative population of nitrogen oxides.

The concentration of nitric oxide was first estimated quantitatively by measuring the resonance fluorescence of the NO gamma bands in the lower thermosphere by means of scanning ultraviolet spectrometer flown on a rocket(Barth, 1964). The value indicated by this experiment was considerably larger than that predicted by Nicolet(1960) and Barth(1961), and some unknown sources of NO had to be considered.

Nicolet(1965a) reviewed the photochemistry of nitric oxide in detail. It was concluded that the hydrogen compounds do not play an important role in the chemistry of odd nitrogen and all their reactions with NO and NO_2 can be neglected in the mesosphere. But chemical reactions, which contribute to the production of NO, considered to be important by that time were three body reaction $N + O + M \rightarrow NO + M$ and the reaction $N + O_2 \rightarrow NO + O$. Since these reactions are slow below 100 km, the estimation of NO density including only these NO sources leads to small NO concentration.

Nicolet(1965b) proposed the reaction $N_2 + O_2^+ \rightarrow NO^+ + NO$ as a source of NO to explain the observation by Barth(1964). However, the rate coefficient of the reaction has been found to be less than 10^{-15} $cm^3 sec^{-1}$ at several hundred degrees in the laboratory(Ferguson,1967;Ferguson et al., 1968). Although Barth(1966a) suggested that this reaction may be fast enough if N_2 is vibrationally excited, excess vibrational energy in N_2 is rapidly transferred to CO_2, which radiates it in the 4.3μ band system. In this way this reaction failed to explain the observed NO density.

Instead, Hunten and McElroy(1968) suggested the reaction of $O_2(^1\Delta_g)$ with N as the most important source of NO. They speculated that the electronic excitation of $O_2(^1\Delta_g)$ might reduce the activation energy of the reaction making the reaction rapid enough to explain the NO density observed. But this couldn't be accepted as an important source since it was not supported by experimental data in the laboratory(Clark and Wayne,1969;

Findlay et al.,1969) which showed the rate coefficient of this reaction to be of the order of 2×10^{-15} cm^3sec^{-1} at 200 K.

Norton and Barth(1970) and Nicolet(1970) pointed out the importance of the production of NO by the reaction $N(^2D) + O_2 \rightarrow NO + O$. This was favored by the laboratory experiments of Black et al.(1969) and Lin and Kaufman(1971), and the reported value for the rate coefficient for the removal of $N(^2D)$ by O_2 were 7×10^{-12} and 5×10^{-12} cm^3sec^{-1} respectively. By this reaction observations of NO densities by Barth(1964,1966b) and Pearce(1969) were fundamentally explained by considering the dissociative recombination of NO^+ and N_2^+ and the reaction of N_2^+ with O as sources of $N(^2D)$ (Norton and Barth,1970;Nicolet,1970).

Calculation of the concentrations of NO and N incorporating molecular and eddy diffusion was first carried out by Strobel et al.(1970). They solved continuity equation for odd nitrogen following the steady state treatment of the combined chemistry of O and O_2 by Colegrove et al.(1965,1966). In this calculation N_2 dissociation by photoelectron impact was introduced as a new source of atomic nitrogen and metastable $N(^2D)$ was included to obtain large NO densities in the mesosphere in agreement with the measurement by Barth(1966b). Strobel(1971a) calculated the diurnal variation of NO and N by solving the time dependent continuity equation. This detailed theoretical model with measured values of solar flux, absorption cross section and chemical rate coefficients for input data, succeeded to be in accord with the new rocket measurement of NO density by Meira(1971).

The predissociation of NO was introduced by Bates(1952) as a dissociation process of NO. Bates(1954) and Nicolet(1965a) deduced a photodissociation coefficient of NO $J_{NO}=10^{-7}sec^{-1}$ at zero optical depth and Nicolet(1970) obtained $J_{NO}=5\times10^{-6}sec^{-1}$ considering $\delta(1,0)$ band of the system $C^2\Pi-X^2\Pi$ of NO as the principal band leading to a direct predissociation

process. Strobel et al.(1970) deduced $J_{NO}=4x10^{-6}$ sec^{-1} for the γ bands (v'>3) and the β bands (v'>6). Strobel(1971b) introduced all δ and ε bands in his detailed model and obtained a large $J_{NO}>10^{-5}$ sec^{-1} which results in a large NO dissociation rate throughout the mesosphere. The photodissociation coefficient of NO in the mesosphere is difficult to calculate accurately since the atmospheric attenuation depends on the absorption by the Shumann-Runge bands of O_2. Such a calculation was made by Cieslik and Nicolet(1973) by using detailed cross sections values of molecular oxygen determined by Ackerman et al.(1970). They concluded that major contribution to the dissociation of NO in the mesosphere and stratosphere is the predissociation of the δ(1,0) and δ(0,0) bands and obtained photodissociation coefficient for δ(0,0) and δ(1,0) bands which are $6.9x10^{-6}sec^{-1}$ and $7.2x10^{-6}$ sec^{-1} respectively at zero optical depth.

More comprehensive calculations including some new reactions of odd nitrogen were carried out by Oran et al.(1975) and Ogawa and Shimazaki (1975). Photodecomposition of N_2 by solar EUV radiation between 800-1000 Å was newly added in their calculations based on the laboratory experiments of Hudson and Carter(1969) and Cook et al.(1973). Photodissociation in the Lyman-Birge-Hopfield(L-B-H) bands with v'>6, which contributes to a small part of the production of the ground state $N(^4S)$ has already been taken into account by Bates(1952,1954), Nicolet(1965a,1970), and Strobel(1971b). Important reactions which can produce metastable $N(^2D)$ are the dissociation of N_2 by photoelectron impact and photoabsorption of solar EUV, dissociative recombination of NO^+ and N_2^+ with electron, and the reaction of N_2^+ with O. Quantum yield of $N(^2D)$ production in these reactions energetically capable of producing $N(^2D)$ was found to be greater than 0.5 by comparing the calculated NO profiles with those measured by Meira(1971), Tisone(1973), and Tohmatsu and Iwagami(1975).

$N(^2D)$ thus produced was considered to react with O_2 to form NO and the quenching reaction of $N(^2D)$ by O or electron was neglected or considered to be small. However, Rusch et al.(1975) obtained the value of the quenching rate coefficient of $N(^2D)$ by O from the simultaneous measurement of the NI(5200 Å) dayglow, neutral, and ion densities, and photoelectron fluxes by a satellite. The value found was $1.4\text{-}6.3\times10^{-13}$ cm^3sec^{-1}. Torr et al. (1976) deduced $1.5\text{-}2.5\times10^{-12}$ cm^3sec^{-1} for the reaction from the NI(5200 Å) nightglow profile measurement. Davenport et al.(1976) has measured the rate coefficient in the laboratory and obtained a value 1.8×10^{-12} cm^3sec^{-1} at 315 K increasing with temperature. With these large values of the rate coefficient the quenching reaction cannot be neglected in the calculation of odd nitrigen densities in the thermosphere where the quenching competes with the reaction of $N(^2D)$ with O_2. If $N(^2D)$ produced is quenched to $N(^4S)$, it leads to the loss of NO by the reaction $N + NO \rightarrow N_2 + O$ instead of producing NO.

Recently NO concentration, which is considerably smaller above its peak than that obtained in the midday, in the early morning has been obtained by Tohmatsu and Iwagami(1976) up to 140 km. In addition, a reevaluation of the fluorescence coefficient for the $\gamma(1,0)$ band of NO has revealed that it must be increased by a factor 2(C.A.Barth, private communication,1975). Consequently it has become necessary to reduce NO concentrations measured by Meira(1971), Tisone(1973), and Tohmatsu and Iwagami(1975) by a factor 2.

N density in the thermosphere has been estimated by Feldman and Takacs (1974) and Gerard(1975) from the NO δ-band twilight observations by a rocket and a satellite, respectively, and it also can be estimated from the NO γ and δ bands emission rate at night observed on a ballon(Cohen-Sabban and Vuillemin,1973), as these band emissions of NO nightglow are excited by the

chemiluminescent reaction of N with O.

Considering these new circumstances, it seems necessary to revise the previous model including the $N(^2D)$ quenching reaction to explain consistently the observational results of NO and N in the thermosphere.

Role of NO in the ionospheric E and D region

Nicolet and Swider(1963) recognized that a conversion process for $O_2^+ \rightarrow NO^+$ was required in the E-region and suggested processes like $O_2^+ + N_2 \rightarrow NO^+ + NO$ and $O_2^+ + N \rightarrow NO^+ + O$. However, the former reaction is known to be too slow from laboratory experiments as noted earlier and the latter is not effective in the E-region owing to the small concentration of N(Strobel,1971;Oran et al.,1975;Ogawa and Shimazaki,1975). It is now known that there is sufficient NO in the E-region to explain the conversion $O_2^+ \rightarrow NO^+$ by the reaction $O_2^+ + NO \rightarrow NO^+ + O_2$ (Keneshea et al.,1970;Swider, 1972).

In the daytime N_2^+ is a major initially-formed ion in the E-region and its conversion to NO^+ or O_2^+ is dependent upon the O/O_2 ratio. On the contrary at night the effect of NO is more straightforward. The ionization of the mid-latitude night-time E-region below about 100 km is a result of photoionization of NO by scattered H Ly-α(Ogawa and Tohmatsu,1966; Keneshea et al.,1970;Strobel,1972;Strobel et al.1974). In addition, the major ion observed at night is not O_2^+ but NO^+ in spite of the fact that above 100 km ionization at night is mainly due to the photoionization of O_2 by H Ly-β. This is because with the lower electron concentration by night as compared to day, the process $O_2^+ + NO \rightarrow NO^+ + O_2$ becomes the major loss process as compared to $O_2^+ + e \rightarrow 2O$.

Nicolet and Aikin(1960) suggested that under normal conditions ionization of about 85 km is produced by the photoionization of NO by Ly-α in the daytime. If NO density by Barth(1966b) and Meira(1971), which is about 3 orders of magnitude larger than that used by them, is adopted, photoionization of NO becomes the dominant source of ionization in the entire D-region both in the daytime and at night(Bourdeau et al.,1966; Thomas,1971). NO^+ ion is also important to the chemical reactions in the D-region. It has been suggested that NO^+ thus produced may represent the precursor ion of the water cluster production chain as well as O_2^+ ion:reaction chain starting with NO^+ may be important in the production of positive water-cluster ions(Hunt,1971;Sechrist,1972). In this way accurate knowledge of NO concentration is essential to discuss the behavior of the ionospheric E and D region.

The aeronomy of minor constituents in the polar atmosphere

There are still scarce observational results and theoretical study concerning the minor constituents in the atmosphere at high latitudes compared to those at mid-latitudes(observational results of high latitude atmosphere are reviewed by Swider(1977)). The behavior of these species is expected to go through large changes compared to those at mid-latitudes caused by

(1) precipitation of electrons and protons associated with various disturbances in the polar atmosphere,

(2) difference in photodissociation and photoionization rates due to the different insolation,

(3) latitudinal variation of the thermal structure,

and

(4) configuration of meridional transport.

Item (1), (2), and (3) would be easily included in the one-dimensional model which was originally developed to study the atmosphere at mid-latitudes. Item (4) is not important to the discussion of the temporal behavior of constituents with chemical time constants shorter than a day such as odd nitrogen, but is expected to influence the concentration of species with time constants longer than a day such as O and H in the thermosphere. Quantitative estimate of the effect of horizontal transport awaits the development of the two-dimensional model.

Among these effects (1) has attracted most attension because of its optical feature. The calculation of ionization and excitation rates of various atoms and molecules has been the first step of the study of the aurora. There have been a lot of attempts to investigate quantitatively the processes of interaction of precipitating electrons with the earth's upper atmosphere. (Tohmatsu and Nagata,1960;Takayanagi and Yonezawa,1961;Rees,1963;Rees,1964; Maeda,1965;Kamiyama,1966;Kamiyama,1967;Rees,1969;Judge,1972;Banks et al.,1974).

Calculated auroral intensities from various excited states were compared with observed ones on the ground or by rockets and calculated spectra of electron fluxes at various altitudes were compared with those measured.

Walker and Rees(1968) calculated the electron density in aurorae assuming chemical equilibrium on steady state condition.

Time dependent behavior of minor neutral constituents during and after the precipitation of auroral electrons were first studied by Maeda and Aikin(1968) and Maeda(1968). They discussed the variation of O, O_3, and OH taking into account the related photochemical reactions, but assumed values for electron fluxes are too large to assess adequately the realistic effects of auroral perturbations.

Jones and Rees(1973) calculated the ion, $N(^4S)$, and $N(^2D)$ densities after turning on a primary flux of bombarding electrons by solving a time dependent continuity equation incorporating ionic and neutral chemical reactions and diffusion to represent the characteristic aeronomic feature of aurorae. But they didn't include the variation of NO density and their model does not give the initial background profiles of the species cocerned in a self-consistent manner. Characteristic buildup time for ions are concluded to be of the order of 1 sec to 1 minute and for N its longer.

Ion compositions in aurorae have been measured by Swider and Narcisi (1970), Donahue et al.(1970), and Narcisi et al.(1974) by positive ion mass spectrometers flown on rockets. All these observations showed large NO^+/O_2^+ ratio suggesting increases of NO in aurorae. Swider and Narcisi (1974) deduced NO concentration from their observed ion concentration in an aurora. NO density was more than order of magnitude larger than those observed at mid-latitudes.

More direct measurement of NO density using mass spectrometer was carried out by Zipf et al.(1970), but their derived value at 120 km is 3.5×10^{11} cm^{-3} which seems too large.

More comprehensive and reliable observations of NO was made by Rusch et al.(1975). NO $\gamma(1,0)$ band emission measured by a satellite at high latitudes showed that NO concentrations are highly variable in both time and space, the average values being 3-4 times higher at high latitudes than at mid-latitudes. They speculate that increase of NO density is caused by the efficient $N(^2D)$ production by auroral processes.

As there is no satisfactory quantitative study concerning the behavior of odd nitrogen in aurorae including the chemistry of odd nitrogen and ions, it seems worth estimating the effect of the perturbations based on a one-dimensional photochemical-diffusive model.

CHAPTER II. A Temperature Dependent Model of the Thermospheric Distribution of Odd Nitrogen

1. Introduction

The behavior of odd nitrogen, especially its diurnal variation in the thermosphere has been discussed by Strobel (1971), Oran et al.(1975), and Ogawa and Shimazaki(1975) by taking into account the photochemical reactions related to odd nitrogen, including ionic reactions, and its vertical diffusion. By comparing calculated NO profiles with those deduced from NO γ(1,0) airglow measurements below 110 km, they concluded that quantum yield of $N(^2D)$ is ≥ 0.5 in the dissociative recombination of NO^+ and the dissociation of N_2 by photoabsorption between 800 and 1000 Å and by photoelectron impact which are the major sources of $N(^2D)$.

$N(^2D)$ produced has been considered to react with O_2 to form NO and the quenching rate coefficient of $N(^2D)$ by O has been estimated to be small or neglected in their calculations. However, Rusch et al.(1975) deduced the value of the quenching coefficient to be $\leq 6.0 \times 10^{-13}$ cm^3s^{-1} from the observed emission rates of NI(5200 Å) dayglow and the physical quantities above 140 km which are necessary to determine the coefficient. Torr et al. (1976) have obtained $1.5\text{-}2.5\times10^{-12}$ cm^3s^{-1} for the reaction from the NI(5200 Å) nightglow profile measurement. Davenport et al.(1976) has measured this rate coefficient in the laboratory and obtained a value of 1.8×10^{-12} cm^3s^{-1} at 315 K increasing with temperature. Although these values differ one another, the quenching reaction cannot be neglected in modeling the odd nitrogen distribution, as it is expected to be more important than the reaction of $N(^2D)$ with O_2 above 140 km.

Recently NO concentration in the early morning, which is considerably smaller than that in the midday, has been measured by Tohmatsu and Iwagami (1976). In addition, it has become necessary to reduce NO concentration already published by Meira(1971), Tisone(1973), and Tohmatsu and Iwagami (1975) due to the correction of the fluorescence coefficient for the NO

$\gamma(1,0)$ band (Barth, C.A., private communication, 1975). N density in the thermosphere has been derived by Feldman and Takacs(1974) and Gerard(1975) by the NO δ band twilightglow observations. These new observations necessitates us to revise the previous model calculation.

In this paper, we try to calculate the diurnal vatiation of odd nitrogen incorporating the quenching reaction of $N(^2D)$ by O, in order to interpret the measurements of odd nitrogen synthetically.

2. Numerical model

Minor constituents involved in the present calculation are $N(^2D)$, $N(^4S)$, NO, N_2^+, O_2^+, NO^+, O^+, N^+, and electron. Photochemical reactions and their rate coefficients incorporated in this study are listed in Tables II. 1, 2, and 3. Vertical eddy and molecular diffusion for neutral species, and ambipolar diffusion for ions and electron, are taken into account. For $[N_2]$, $[O_2]$, and [O], results by Ogawa and Shimazaki(1975) are utilized between 70 and 120 km, and above 120 km they are calculated assuming diffusive equilibrium. ([ ] represents the number density of the assigned particle.)

Lower boundary is chosen to be 70 km where the density of NO which has the chemical time constant of order of 1 day, is kept constant. $N(^2D)$, $N(^4S)$ and ionic species with much shorter time constants than that of NO, are calculated neglecting the dynamical term at the lower boundary. The effect of the lower boundary condition on [NO] is considered to become unimportant above 80 km(by more than 1 scale height apart from the lower boundary). Molecular diffusion flux is set to be 0 at the upper boundary which is chosen to be 200 or 400 km.

Temperature profile is given as Ogawa and Shimazaki(1975): below 110 km it's based on U.S. Standard Atmosphere and is extended above 110 km

by the relation

$$T = T_\infty - (T_\infty - T_{110}) \exp (-0.02(Z-110)) \qquad (II.1)$$

where height Z is given in kilometers, T_{110} is the temperature at 110 km, and T_∞ is the thermopause temperature.

Height and time steps in the numerical integration, which is carried out for 45°N latitude at the equinox, are 1 km and 180 sec respectively.

3. Photochemistry of odd nitrogen in the thermosphere

Before discussing the results of the diurnal variation of odd nitrogen in detail, we will summarize how each density is determined by the photochemical reactions based on the calculated chemical rates.

Fig. II.1 is a reaction scheme representing the chemical budget of odd nitrogen above 90 km.

Production rates of $N(^2D)$ by the reactions J2, J3, J7, R8, RI1, RI10, RI12, and RI14, which are energetically capable of producing $N(^2D)$, are depicted in Fig. II.2a. N_2 dissociation rate by photoelectron impact is approximated to be $0.18Q_e$ $cm^{-3}s^{-1}$, where Q_e is the total photoelectron production rate. This approximation is thought to be valid within a factor two below 200 km where R8 becomes important. Above 120 km, ionic reactions RI1 and RI14 are the major sources of $N(^2D)$, R8 and RI12 becoming also important with altitude, and below this height J2 and J3 are important. Here we have assumed the quantum yield η for $N(^2D)$ in the reactions mentioned above to be 0.9. The validity of this value is discussed in detail later.

The production rates of $N(^4S)$ are shown in Fig. II.2b. The most important source of $N(^4S)$ above 110 km is the quenching reaction R3 which is also ~~being~~ the major sink of $N(^2D)$ above 140 km. Below 110 km, JI1 and the other branching to yield $N(^4S)$ in the reactions J2, J3, J7, R8, RI1, RI10, RI12, and RI14 mostly contribute to the production of $N(^4S)$.

In Figs. II.2c and II.2d are shown the production and loss rates of NO. R1 is the most important source of NO above 120 km, while R4 dominates below this altitude. Dominance of R1 at higher altitude is due to the increased rate coefficient for R1 owing to the temperature increase as well as large [N] caused by the significant production of $N(^4S)$ through R3. NO is mainly lost to form N_2 through the association reaction with N. RI9 and J4 are important as a sink of NO below 110 km. R1 and R2, which are the important source and loss of NO above 120 km respectively, constitute the sink of $N(^4S)$. $N(^2D)$ is mostly converted to NO through R4 below 120 km, whereas above this altitude it is quenched to $N(^4S)$ by the reaction with O(R3).

Also the production rates of NO^+ are shown in Fig. 2e. NO^+ comes from N_2^+ above 110 km and also from O^+ above 170 km. O_2^+ is an important source of NO^+ below 110 km together with N_2^+.

In the daytime the rates of the production (P) and loss (L) for each constituent are of the order of 10^3 $cm^{-3}s^{-1}$ being by about a factor 10 greater than the divergence term due to the eddy and molecular diffusion. At night Q and L decrease to about 10^2 $cm^{-3}s^{-1}$ whereas the dynamical term remains the same order of magnitude. It may be concluded that the concentration of odd nitrogen is determined mainly by the photochemical reactions above 90 km in the daytime, whereas the dynamical process has an important effect on the behavior of odd nitrogen during the night.

4. Quantum yield of $N(^2D)$

Although Oran et al.(1975), Ogawa and Shimazaki(1975) and Rusch et al.(1975) have treated the quantum yield of $N(^2D)$ in the reactions RI1, RI4, J2, J3, and R8 separately, only the total $N(^2D)$ production rate is an important physical quantity as a source of NO when calculated and

observed NO profiles are compared around 100 km, as these reaction rates are in the same order of magnitude there. So we have calculated the diurnal variation of [NO] assuming the same quantum yield η for each reaction. Noon profiles for various values of η are shown in Fig. II.3 together with [NO] by Meira(1971) and Tohmatsu and Iwagami(1975) deduced from NO $\gamma(1,0)$ airglow observations. Here it must be noted that the observed values have been reduced a factor 2.07 from their original ones considering the revision of the fluorescence coefficient for the NO $\gamma(1,0)$ band. Although these measurments differ in latitude, season, local time, and solar activity, they coincide well with each other below 110 km. By comparing the calculated and measured profiles around 100 km it can be concluded that η must be much larger than 0.5. Hereafter η is taken to be 0.9 as an optimum value.

5. Effect of the quenching of $N(^2D)$ by O

The rate coefficient for R3 used in our present calculation is $k_3 = 8.5 \times 10^{-12} \exp(-500/T)$ cm^3s^{-1} which is based on the laboratory experiment by Davenport et al.(1976). k_3 reaches 5×10^{-12} cm^3s^{-1} for T = 1000 K which commonly occurs in the thermosphere. However, Rusch et al.(1975) and Torr et al.(1976) have obtained $k_3 = 1.4 - 6.3 \times 10^{-13}$ cm^3s^{-1} and $1.5 - 2.5 \times 10^{-12}$ cm^3s^{-1}, respectively from the observed NI(5200 Å) airglow intensities.

Calculated $N(^2D)$ profile at noon is compared with the observation by Rusch et al.(1975) in Fig. II.4 (labeled as case A). [NO] and $[N(^4S)]$ are also shown in the same figure. As is expected from the disagreement of the laboratory value with those obtained by the airglow analysis, the calculated $[N(^2D)]$ is about 5 times smaller than the observed. This discrepancy of $[N(^2D)]$ becomes larger by more than 1.5 times for the 5200 Å intensities observed by Wallace and McElroy(1966). If the coefficient is chosen to be 1.0×10^{-12} cm^3s^{-1} at all altitudes (case B), $[N(^2D)]$ becomes 3-4 times larger and nearly equal to the observed as seen from

Fig. II.4.

The variation of the daytime [NO] and [N(^{4}S)] due to the difference of k_3 between the cases A and B is most prominent around 120 km as seen from Fig.II.4. Above 140 km the difference of [NO] between the two cases is small. This is because the increase of [N(^{2}D)] does not directly lead to the increase of [NO] owing to the dominating production of NO through R1. Below 120 km k_3 differs little each other between the cases A and B, and at the same time, the reaction R3 is no more important owing to the decrease of $[O]/[O_2]$. This leads to the small variance of [NO] between the two cases again at the lower altitude.

In summary it may be said that k_3 of about 1×10^{-12} $cm^3 s^{-1}$ is preferable above 140 km so as to accord with the observations of NI(5200 Å) dayglow. On the other hand, [N(^{4}S)] and [NO] in the daytime do not depend seriously on the choice of the k_3 value except around 120 km. It has been around 100 km that we have determined the quantum yield η by comparing the calculated and measured daytime NO profiles. At this height the variance of [NO] due to the different k_3 is negligibly small. Consequently, the conclusion that η must be close to unity need not be changed by the different choice of k_3.

6. Effect of the temperature variation

So far the thermopause temperature T_∞ in (II.1) has been kept 1050 K through the diurnal cycle. The temperature change is expected to influence greatly the concentration of odd nitrogen owing to the large temperature dependence of the rate coefficient for R1. Now we try to investigate the effect of the diurnal variation of the thermospheric temperature on the behavior of odd nitrogen.

The diurnal variation of the thermopause temperature is given

according to Jacchia(1971): T_∞ is the highest at 14 h LT(T_{max}) and the lowest at 04 h LT, the difference between the maximum and minimum temperature being 150-200 K.

NO profiles at 12 h and 0 h LT for T_{max} = 900, 1000, and 1100 K are presented in Fig.II.5.The corresponding diurnal minimum temperatures are 750, 830, and 910 K at 04 h LT, respectively. NO profiles at 07 h LT for the case A and B are shown in FigII.6. In this figure [NO] for T_{max} = 800 K (case B) is also dipicted. The major change of [NO] brought about by introducing the diurnal temperature variation occurs when $T_{max} \lesssim$ 1000 K; i.e. [NO] continues to decrease after sunset and remain reduced until post-sunrise. Nighttime NO density is very sensitive to the thermospheric temperature: Around 110 km it becomes smaller by about an order of magnitude with decreasing T_{max} by 100 K from 1000 K. It is also sensitive to the rate coefficient for R3 as seen from FigII.6. The difference of the profiles in FigII6 between the cases A and B is nearly equivalent to that caused by the difference of T_{max} by about 100 K in the case A. It should be emphasized that when $T_{max} \lesssim$ 900 K the nighttime dip of [NO] appears regardless of the rate coefficient.

The vertical profiles of [N(^{4}S)] at noon and midnight for the case A are represented in Fig.II.7.Midnight [N] becomes much larger with decresing thermopause temperature in contrast to [NO]. This can be explained as follows: The smaller rate of conversion from N to NO through R1 for lower temperature results in a decrease of the production of NO and the loss of N. The increased [N] augments the loss of NO through R2, whereas the decreased [NO] sets off the loss of N. Thus the variation will be accelarated.

The results from rocket observations of NO at sunrise(SZA = 90°) by Tisone(1973) and at 07 h LT(SZA = 82°) by Tohmatsu and Iwagami(1976) are compared with the theoretical profiles at 07 h LT in FigII.6. As theoretical

NO concentrations for the local times of two observations differ little in the altitude region concerned, the profile for 07 h LT can be representative. As seen from Fig.II6 the two observed profiles in the morning are smaller than the daytime profiles by Meira(1971) above 90 km. The present calculation also shows that [NO] from sunset to post-sunrise is considerably smaller than the daytime value. Again, the observed profiles in the morning coincide well with the theoretical curve for T_{max} = 1000 K (case A) or T_{max} = 900 K (case B). Considering the solar activity, which controls the thermospheric tmeperature, at the time of the observation of Tohmatsu and Iwagami(1976), the profile for T_{max} = 900 K (case B) seems preferable. [NO] at typical local times calculated assuming T_{max} = 1000 K for the case A are shown in Fig.II8 together with those measured. Correspondence of the observations to the calculated profiles is as follows: Meira(1971)-12 h, Tohmatsu and Iwagami(1975)-18 h, Tisone(1973) and Tohmatsu and Iwagami (1976)-06 h, Rusch et al.(1976)- 12h or 18h LT. It may be said that NO profiles calculated from 90 to 200 km, which show a large diurnal change, are consistent with those measured at various local times.

[N] has been estimated by Feldman and Takacs(1974) to be 1.9×10^7 cm^{-3} at 140 km on the basis of the twilight chemiluminescent emission of NO δ bands above 140 km. Gerard(1975) has also deduced [N] reaching its maximum about 9×10^7 cm^{-3} at 180 km by a satellite observation. The solar zenith angle and the thermopause temperature at the time of two observations were about 110° and 800 K respectively. T_∞ becomes about 800 K at about this time when T_{max} = 900 K in this model. Our model for the case A and 20 h LT(SZA=110°) predicts [N] = 4×10^7, 2×10^7, and 7×10^6 at 120, 140, and 180 km, respectively, and is in quantitative agreement with the result by Feldman and Takacs. However, [N] by Gerard is more than order of magnitude larger than the calculated value at 180 km, and is in contradic-

tion to both our present calculation and the observation of Feldman and Takacs.

7. Concluding remarks

Daytime [NO] and [N] above 160 km and below 110 km do not depend seriously on the choice of the rate coefficient for the $N(^2D)$ quenching by O. This enables us to determine the quantum yield of $N(^2D)$ η in the reactions RI1, RI4, J2, J3, R8, and RI2, by comparing the calculated and measured daytime NO profiles below 110 km. Optimum value of η is evaluated to be about 0.9. On the contrary $[N(^2D)]$ above 140 km is very sensitive to the rate coefficient for R3. It differs especially above 120 km between those deduced from the laboratory experiment and the NI(5200 Å) airglow observations. Further accurate measurement of $N(^2D)$ vertical profile would be of importance in order to confirm the rate coefficient value.

Lower temperature at night than in the daytime decreases [NO] greatly during the night. Absolute values of the nighttime [NO] and [N] are highly dependent on the nighttime temperature which can vary corresponding to the solar and geomagnetic activities and with season. This is due to the large temperature dependence of the rate coefficient for R1.

The calculated $[N(^4S)]$ agrees well with the observation by Feldman and Takacs(1974) which infers as much [N] as 2×10^7 cm^{-3} at 140 km. The satellite observation by Gerard(1975) contradicts both the calculation and the Feldman and Takacs observation. An improved measurement would be necessary to discuss [N] in detail.

CHAPTER III. Odd Nitrogen in the Lower Thermosphere under Auroral Perturbations

1. INTRODUCTION

A model of the diurnal variation for various minor constituents in the mesosphere and thermosphere has been constructed by taking the vertical eddy and molecular diffusion as well as photochemical reactions into considerations (e.g., Shimazaki and Laird, 1970; Thomas and Bowman, 1972; Hunt, 1973; Isaksen, 1973). This model predicts minor constituents with short (less than one day) chemical time constant such as O_3, $O_2(^1\Delta_g)$, NO, and OH in agreement with direct and indirect observations, although a two-dimensional model including the horizontal transport is necessary in order to give a better agreement for the atomic oxygen and hydrogen in the thermosphere.

The one-dimensional model which was developed originally for the mid-latitude atmosphere may be applicable to the polar atmosphere as far as we adequately consider the conditions specific to the polar region. Differences between the polar and mid-latitude atmospheres are caused mainly by

(1) precipitation of electrons and protons associated with various disturbances in the polar atmosphere,

(2) difference in photodissociation and photoionization rates due to the different insolation,

(3) latitudianl variation of the thermal structure,

and

(4) configuration of meridional transport.

The item (1) is of essential importance in the polar atmosphere. Modeling of the atmospheric composition under the influence of auroral precipitations is the principal purpose of this study. The items (2) and (3) are easily incorporated. The item (4) is neglected in this study, because this study concerns mainly the temporal behavior of the odd nitrogen.

Since tbe chemical time constant of odd nitrogen species is generally in the order of or less than 1 day in the thermosphere, the distribution of odd nitrogen density is determined mainly by the local production and loss, and partly by the vertical diffusion:the horizontal transport could not directly affect the distribution of odd nitrogen species. It must be noted, however, that the densities of O and H in the polar thermosphere are greatly affected by the transport from the mid-latitude thermosphere, because of longer chemical time constant.

Recent observations of ion composition suggest the substantial enhancement of odd nitrogen species in the auroral thermosphere (Danahue et al., 1970; Swider and Narcisi, 1970; Narcisi et al., 1974). This enhancement could be ascribed to the increased ionization caused by precipitating particles, together with the collisional dissociation of N_2 by the precipitating particles. To model these situation in the thermosphere, it is necessary to treat the odd nitrogen and ionic species simultaneously, because these species are closely coupled with one another through the chemical reactions (Ogawa and Shimazaki, 1975). In this study, we will try to simulate the temporal variation of the various atmospheric constituents under the influence of various types of the electron influx, with special attention to the responce of N, NO and electron densities and the ion composition to the auroral perturbation.

2. UNDISTURBED ATMOSPHERE

First of all, diurnal variations for various minor constituents in the polar mesosphere and thermosphere under aurorally quiet conditions must be calculated in order to assess the background on which the perturbation incorporates. The calculation was excecuted by the use of one-dimensional photochemical-diffusive model essentially identical with that of Ogawa and

Shimazaki (1975). The temperature distribution was chosen so as to represent the 70° latitude in equinoxes: the US Standard Atmosphere for 60°N was used below 90 km, and the Jacchia model (1971) for the exospheric temperature of 1000°K above 90 km. Upper and lower boundaries were set at the heights of 150 and 40 km, respectively. The diurnal variation was traced with time integration for 5 days starting from the steady state solution at a solar zenith angle of 80°. The 5 days integration resulted in a good diurnal reproducibility for species other than H and O. The number densities of O, O_3, $O_2(^1\Delta_g)$, and NO above 70 km calculated at 70° latitude are about a factor 2 less than those at 45° lati tude, as expected from the difference in the solar zenith angle. On the other hand, N shows little latitudinal variation. This may be explained as follows: The principal source and sink of N above 70 km are the photo-dissociation of NO and the reaction with NO, respectively. Equating the rates of these processes, the number density of N is found to be determined only by the photodissociation coefficient and the rate coefficient for the reaction of N with NO. Since the former coefficient varies little with solar zenith angle and the latter is constant with respect to latitude, the number density of N is almost invariant with respect to latitude.

3. IONIZATION AND DISSOCIATION BY AURORAL ELECTRONS

The perturbation in the polar atmosphere is caused mainly by the precipitating electrons associated with auroras. Evaluating the ionization and dissociation rates due to precipitating electrons in the next step of this study. First of all well will describe the method of calculation for these rates in the following three subsections.

3.1 Calculation of the primary electron flux

Energy loss rate of an electron with the energy E per unit length through collisions with atmospheric molecules is represented as

$$-\frac{dE}{ds} = \sum_j \sum_i (\Delta E)_{j,i}\, \sigma_{j,i}(E)\, n_j(z) = \sum_j S_j(E)\, \chi_j(z)\, n(z), \qquad (\text{III}.1)$$

where $\sigma_{j,i}(E)$, and $(\Delta E)_{j,i}$ are the cross section and the energy lost by the i-th collision with the j-th gas, respectively, and the product of these two is called the stopping cross section; $S_j(E)$ is total electron stopping cross section of the j-th gas. $n_j(z)$ is the number density of the j-th gas at the height z; $n(z) = \sum_j n_j(z)$, and $\chi_j(z) = n_j(z)/n(z)$. When the energy of electrons which is in the range $(\varepsilon, \varepsilon + \delta\varepsilon)$ at the top of the atmosphere reduces to the energy in the range $(E, E + \delta E)$ at the height z,

$$\int_{E+\delta E}^{\varepsilon+\delta\varepsilon} \frac{dE}{\sum_j S_j(E)\, \chi_j(z)} = \int_E^{\varepsilon} \frac{dE}{\sum_j S_j(E)\, \chi_j(z)}, \qquad (\text{III}.2)$$

or

$$\frac{\delta E}{\sum_j S_j(E)\, \chi_j(z)} = \frac{\delta\varepsilon}{\sum_j S_j(\varepsilon)\, \chi_j(\infty)}. \qquad (\text{III}.3)$$

Conservation law for the electron flux yields the relation between the incident flux $F(\infty,\varepsilon)$ and the flux at the height z, $F(z,E)$, i.e..

$$F(\infty, \varepsilon)\, \delta\varepsilon = F(z, E)\, \delta E. \qquad (\text{III}.4)$$

From (III.3) and (III.4), we have

$$F(z,E) = F(\infty,\varepsilon)\frac{\delta\varepsilon}{\delta E} = F(\infty,\varepsilon)\frac{\sum_j S_j(\varepsilon)\chi_j(\infty)}{\sum_j S_j(E)\chi_j(z)} \quad . \qquad (\text{III}.5)$$

E and ε are not independent of each other, but the following relation must hold:

$$E(z) = \varepsilon - \sum_j \int_z^\infty S_j(E(z'))\eta_j(z')dz' \sec\alpha \operatorname{cosec}\omega , \qquad (\text{III}.6)$$

where α and ω denote the pitch angle of electrons and the geomagnetic inclination, respectively.

The electron flux at the height z will be calculated numerically as follows. The energy space is divided into n intervals (ε_1, ε_2, ····, ε_n) for the incident energy, and (e_1, e_2, ····, e_n) for the energy at the height z. Correspondence of the energy e_i with the energy ε_i is determined from (III.6) and the flux $F(z,e_i)$ at the energy e_i from (III.5). Since the flux $F(z,e_i)$ is expressed at a different energy from ε_i, $F(z,e_i)$ is converted to $F(z,\varepsilon_i)$ by a linear interpolation. Calculation of the primary flux has been made for the energy above 10 eV, because primary electron fluxes below 10 eV are not responsible for ionizing collisions, and are generally much less than secondary electron fluxes.

The pitch angle of an electron varies through collisions with atmospheric gases. A complete treatment of this process is beyond the scope of this study; an approximation is made by introducing an average pitch angle. Stolarski (1972), and Cicerone et al.(1973) have found that an average pith angle of about 60° leads to a good appoximation for the ionospheric photoelectrons. We assume $\sec\alpha \cdot \operatorname{cosec}\omega = \langle\sec\alpha\rangle \cdot \sec 10°$ = 2.033 for the geomagnetic inclination of 80°.

The processes of excitation, dissociation and ionization of atoms

and molecules considered in this study are given in TableIII.1. For the convenience of numerical calculation we use the analytical representation for cross sections similar to the method of Green and Stolarski (1973). The energy distribution of secondary electrons ejected at ionizing collisions is another important quantity, because the secondary electrons carry kinetic energy. Banks et al. (1974) developed the following expression for the partial cross section based on the experiments by Opal et al. (1971):

$$\sigma_{j,ion}(E,E') = \frac{2}{\pi \tilde{E}_j} \cdot \frac{\sigma_{j,ion}(E)}{1+(E'/\tilde{E}_j)^2} , \qquad (\text{III}.7)$$

where $\sigma_{j,ion}(E)$ is the total ionization cross section, $\tilde{E}_j$ is a constant which depends on the species of atmospheric gases, and E and E' are energies of incident and secondary electrons, respectively.

The energy loss factor $(\Delta E)_{j,i}$ for ionizing collisions is evaluated by assuming (III.7)to be representative of various ionization processes of the j-th molecule. Denoting the average excitation energy of an ion by $E_{x,j}$, the ionization potential by I_j, and the average energy of secondary electrons by $\overline{E'}_j$, the average energy loss per ionizing collision with the j-th molecule is written as

$$\overline{(\Delta E)}_j = I_j + E_{x,j} + \overline{E'}_j , \qquad (\text{III}.8)$$

where the average energy of a secondary electron is given by

$$\overline{E'}_j = \frac{\int_0^{E'_{max}} E' \sigma_{j,ion}(E,E')\,dE'}{\int_0^{E'_{max}} \sigma_{j,ion}(E,E')\,dE'} \qquad (\text{III}.9)$$

with

$$E'_{max} = \frac{1}{2}(E - I_j - E_{x,j}) .$$

$\bar{E}'_j$ calculated by (III.9) is represented in Fig.III.1. The average energy of secondary electrons is found to be 10 - 100 eV in the case of the incident electrons with energies between 100 eV and 10 keV, and it differs little for N_2, O_2, and O.

Cross sections for all processes incorporated in this work are depicted in Figs.III.2a, III.2b, and III.2c. The total stopping cross sections calculated by the use of these cross sections are also shown in Fig.III.3.

3.2 Calculation of secondary and total electron fluxes

If the total electron flux at the height $z + \Delta z$, $F_t(z + \Delta z, E)$ is known, the production rate of secondary electrons at the height $z + \Delta z$ can be calculated with the aid of the relation

$$q(z+\Delta z, E) = \sum_j n_j(z+\Delta z) \int F_t(z+\Delta z, E') \sigma_{j,ion}(E', E) dE'. \qquad (III.10)$$

Then the secondary electron flux at the height $z + \Delta z$ is evaluated as

$$F_2(z+\Delta z, E) = \frac{\int_E^\infty q(z+\Delta z, E') dE'}{\sum_j S_j(E) n_j(z)} \qquad (III.11)$$

Calculation of the secondary electron flux at the height z can be made quite similarly to the case of the primary flux. As an example, the primary and total electron fluxes calculated at various heights for the incident flux $F(\infty,E) = 1\times10^6 \exp(-E/5)$ electrons$\cdot cm^{-2} sec^{-1} eV^{-1} str^{-1}$ at 300 km (E in keV) are presented in Fig.III.4.

3.3 Dissociation and ionization by photoelectrons produced by the Bremsstrahlung X-ray

Since incident electrons with the energy of about 5 keV, which are responsible for exciting the auroral emissions, cannot penetrate to the heights below 100 km, the effect of direct impact ionizations by the precipitating electrons can be neglected at the heights below 90 km in case of usual auroral events. Alternatively the impact ionization of the photoelectrons produced by the Bremsstrahlung X-ray emitted from incident electrons may become important at these heights.

In the energy range concerned in this study the emission cross section of the Bremsstrahlung X-ray is given by the equation obtained by the same approximation as the Bethe-Heitler formula (Gluckstern and Hull, 1953);

$$
\begin{aligned}
d\sigma_x(E_0,k,\theta) = & \\
& \frac{Z^2}{8\pi}\cdot\frac{r_0^2}{137}\cdot\frac{dk}{k}\cdot\frac{P}{P_0}\left\{\frac{8\sin^2\theta_0(2E_0^2+1)}{P_0^2\Delta_0^4}-\frac{2(5E_0^2+2EE_0+3)}{P_0^2\Delta_0^2}-\frac{2(P_0^2-k^2)}{Q^2\Delta_0^2}\right. \\
& +\frac{4E}{P_0^2\Delta_0}+\frac{L}{P_0P}\left[\frac{4E_0\sin^2\theta_0(3k-P_0^2E)}{P_0^2\Delta_0^4}+\frac{4E_0^2(E_0^2+E^2)}{P_0^2\Delta_0^2}\right. \\
& \left.\left.+\frac{2-2(7E_0^2-3EE_0+E^2)}{P_0^2\Delta_0^2}+\frac{2k(E_0^2+EE_0-1)}{P_0^2\Delta_0}\right]-\frac{4\Pi}{P\Delta_0}\right. \\
& \left.+\frac{\Pi'}{PQ}\left[\frac{4}{\Delta_0^2}-\frac{6k}{\Delta_0}-\frac{2k(P_0^2-k^2)}{Q^2\Delta_0}\right]\right\}, \qquad \text{(III.12)}
\end{aligned}
$$

with

$$
\begin{aligned}
L &= \ln\left[\frac{EE_0-1+PP_0}{EE_0-1-PP_0}\right], \\
\Delta_0 &= E_0-P_0\cos\theta_0, \\
Q^2 &= P_0^2+k^2-2P_0k\cos\theta_0, \\
\Pi &= \ln\left[\frac{E+P}{E-P}\right], \quad \text{and} \quad \Pi' = \ln\left[\frac{Q+P}{Q-P}\right].
\end{aligned}
$$

where the notations are as follows:

$\underset{\sim}{P}_o$, $\underset{\sim}{P}$ = initial and final momentum of the electron in a collision, in $m_o c$ units,

E_o, E = initial and final total energy of the electron in a collision, in $m_o c^2$ units,

k, $\underset{\sim}{k}$ = energy and momentum of the emitted photon, in $m_o c^2$ and $m_o c$ units,

θ_o, θ = direction angles of $\underset{\sim}{P}_o$, and $\underset{\sim}{P}$ measured from the direction of $\underset{\sim}{k}$,

Z = atomic number of the target atom, and

$r_o = e^2/m_o c^2 = 2.818 \times 10^{-13}$ cm.

It is found from (III.12) that the X-ray is emitted dominantly in the forward with respect to the direction of electron motion. Since the moving direction of electrons in the atmosphere has a certain angular distribution, we must sum up the emission rates of the X-ray from electrons moving in various directions. Denoting the moving direction of an electron by (ζ,ϕ) and the emitting direction of the X-ray by (ξ,ϕ_0), the emission rate of the X-ray from the electron flux $f(E,\zeta,\phi)$ is represented as

$$I(E,k,\theta)=\int_0^{\pi}\int_0^{2\pi}\frac{d\sigma_x(E,k,\theta)}{dk}f(E,\zeta,\phi)\sin\zeta\,d\zeta\,d\phi\,, \qquad (III.13)$$

where

$$\cos\theta = \cos\xi\cos\zeta + \sin\xi\sin\zeta\cos(\phi-\phi_0).$$

For the electron flux isotropic over the downward hemisphere, i.e.

$$f(E,\zeta,\phi)=\begin{cases} f\,, & \text{for } \pi/2\geq\zeta\geq 0 \text{ and } 2\pi\geq\phi\geq 0, \\ 0\,, & \text{for } \zeta\geq\pi/2 \text{ and } 2\pi\geq\phi\geq 0. \end{cases} \qquad (III.14)$$

$I(E,k,\theta)$ normalized by the value at $\theta = 0°$ are calculated for various sets of E and k values. As shown in Fig.III.5, anisortopy of the emission

rate becomes more remarkable as E and k increase. However, this anisortopy is not so large for the energy between several keV and several 10 keV. For higher energies (E $\geq$ 100keV) where the anisotropy becomes apparent, the direct impact ionization dominates over the photoelectron impact ionization produced by the Bremsstrahlung X-ray above the heights of 50 to 60 km. As a result we can safely assume an isotropic emission rate of the X-ray.

Integrating (III.12) with respect to angle, the emission cross section per photon energy is obtained (Heitler, 1949) as

$$\sigma_{j,X}(E,h\nu) = \frac{8}{3}\gamma_0 \frac{m_0c^2}{E} \ln\left\{\frac{E^{1/2}+(E-h\nu)^{1/2}}{h\nu}\right\}\frac{1}{h\nu}, \qquad (\text{III}.15)$$

where

$$\gamma_0 = \frac{Z^2 r_0^2}{137} = 5.795 \times 10^{-28} Z^2 \quad cm^2,$$

E is the electron energy, and the photon energy k has been replaced by $h\nu$. The X-ray emission rate per unit photon energy (in $cm^{-3}sec^{-1}h\nu^{-1}$) caused by the omnidirectional electron flux F(z,E) is

$$I(z,h\nu) = \sum_j n_j(z) \int_{1keV}^{\infty} \sigma_{j,X}(E,h\nu)\, F(z,E)\, dE. \qquad (\text{III}.16)$$

As far as the height range below 100 km is concerned, we can neglect the X-ray with energies smaller than 1 keV, and correspondingly the electrons with energies smaller than 1 keV. Downward and Upward fluxes of the X-ray at the height z are given by the following equations (Kamiyama, 1966):

$$J_D(z,h\nu) = \frac{1}{2}\int_z^{\infty} I(z',h\nu)\, E_1(t)\, dz', \qquad (\text{III}.17)$$

and

$$J_U(z,h\nu) = \frac{1}{2}\int_0^{z} I(z',h\nu)\, E_1(t)\, dz', \qquad (\text{III}.18)$$

where t is the optical thickness between the heights z and z' defined by

$$t = \sum_j \sigma_{j,abs}(h\nu) \left| \int_z^{z'} n_j(z'')\, dz'' \right|, \qquad (\text{III}.19)$$

and

$$E_1(t) = \int_1^{\infty} \frac{e^{-tx}}{x}\, dx, \qquad (\text{III}.20)$$

where $\sigma_{j,abs}(h\nu)$ is the absorption cross section of the j-th atmospheric gas for the X-ray with the energy $h\nu$ (Veigele, 1973). The production rate of photoelectrons with the energy E is then given by

$$q_x(z,E) = \sum_j \sigma_{j,ion}(h\nu)\, n_j(z) \left\{ J_D(z,h\nu) + J_U(z,h\nu) \right\}, \qquad (\text{III}.21)$$

where $\sigma_{j,ion}(h\nu)$ is the photoionization cross section for the X-ray with the energy $h\nu$. The photoelectron energy E has been calculated as $E = h\nu - I_j^n$, where I_j^n is ionization potential for ejection of an inner shell electron.

Photoelectron fluxes caused by the Bremsstrahlung X-ray for the incident electron flux $F(\infty, E) = 1\times10^6 \exp(-E/5)$ electrons$\cdot$cm^{-2}sec^{-1}eV^{-1}str^{-1} are shown in Fig. III.6.

3.4 Ionization and dissociation rates by auroral electrons and X-ray

The ionization and dissociation rates are then calculated from electron fluxes thus calculated considering the direct collisional ionization, and the photoionization by Bremsstrahlung X-ray which becomes important below 80 km.

Four spectral distributions of incident electron fluxes are adopted in the calculation:

$$\text{Case A,} \quad F(\infty, E) = 1 \times 10^{6} \exp(-E/5),$$

$$\text{Case B,} \quad F(\infty, E) = 1 \times 10^{5} \exp(-E/5),$$

$$\text{Case C,} \quad F(\infty, E) = 1 \times 10^{3} \exp(-E/40),$$

and

$$\text{Case D,} \quad F(\infty, E) = 1 \times 10^{2} \exp(-E/40),$$

where the electron energy E is expressed in kilo-electronvolts, and the flux in $cm^{-2}sec^{-1}eV^{-1}str^{-1}$. Cases A and B are representative of the electron flux in the auroras of IBC Classes III and II, respectively, and Cases C and D of events with a harder electron spectrum (Frank and Ackerson, 1971; Hones et al., 1971).

Examples of calculated ionization and dissociation rates for the incident fluxes of Cases A and C are depicted in Figs.III.7a and b. The main peak of the production rate of ionization or dissociation occurs at the height of 100 km for Cases A and B, and at 85 km for Cases C and D. It is a natural consequence of the large dissociation cross section for electron impact on N_2 that the production rate of N exceeds the other production rates. Difference of the scale height between the production rates of $O(^1D)$ and other species above the peak height is due to the difference in the scale heights of target molecules; i.e., $O(^1D)$ is produced

mainly by the electron impact on O, while the others by the impact on N_2 and O_2.

It is interesting to compare the magnitudes of production rates for O, N, and electron by the auroral precipitation with those by the solar EUV radiation. The production rates of $O(^3P)$ and $O(^1D)$ in Case A are in comparable order of magnitude with those by the solar photodissociation of O_2 at the height around 110 km, whereas the production rate of N and the total ionization rate are larger by 3 and 2 orders of magnitude, respectively, than those in the sunlit condition.

4.RESULTS AND DISCUSSION

4.1 Odd oxygen

Atomic oxygen is produced by the electron impact dissociation of O_2 in the auroral thermosphere:

$$O_2 + e \rightarrow O + O + e, \text{ and } O + O^+ + 2e.$$

Production of atomic oxygen occurs mainly above 90 km for the precipitating electrons with the energy spectrum of characteristic energy of about 5 keV. As described in the previous section, the electron flux of Case A, corresponding to an IBC III aurora, results in the peak production rate of $\sim 10^5$ $cm^{-3}sec^{-1}$, which is of the same order of magnitude as the daytime production rate due to the O_2 photodissociation. Since the density of atomic oxygen is $\sim 10^{11}$ cm^{-3} at the heights of 90 - 100 km, the growth time for the perturbation by an IBC III aurora is $\sim 10^6$ sec. Consequently, the atomic oxygen density would hardly follow such a short-term variation of its production rate as is caused in each auroral break-up. Again, ozone does not change as far as atomic oxygen is unchanged, because ozone is nearly in

chemical equilibrium with atomic oxygen.

Precipitating electrons with energy above 100 keV give a different effect on the atmosphere. It can produce substantial amount of atomic oxygen below 80 km where the atomic oxygen density is very low at night. The effect of the electron precipitation on O and O_3 densities will be apparent below 80 km at night. However, it must be mentioned that such a large incident flux at around 100 keV as adopted by Maeda and Aikin (1968) has hardly been observed.

Investigating the effect of long-term continual electron precipitations on the thermospheric composition is beyond the scope of this study. It must be noted, however, that this long-term influence coupled with the horizontal transport would be important in simulating the atomic oxygen distribution in the polar thermosphere.

4.2 Odd nitrogen

The major production processes of atomic nitrogen in the undisturbed thermosphere are (1) photodissociation of N_2, (2) dissociation of N_2 by photoelectron impact, (3) dissociative recombination of NO^+ with electron, (4) ion-neutral reaction of N_2^+ with O, and (5) photodissociation of NO (see, e.g., Strobel, 1971; Ogawa and Shimazaki, 1975). In the auroral atmosphere, (6) the dissociation of N_2 by precipitating electrons

$$N_2 + e \rightarrow N + N + e, \quad \text{and} \quad N + N^+ + 2e$$

will be an essential source of odd nitrogen, whose cross sections have been measured by Winters (1966) and Rapp and Englander-Golden (1965). As seen in Fig.III.7a, the electron flux of Case A leads to the dissociation rate of N_2 to be in the order of magnitude of 10^6 $cm^{-3}sec^{-1}$ at the peak height, 3

orders of magnitude greater than that in the normal daytime thermosphere. Dissociative recombination of NO^+, whose rate will be increased by the auroral ionization, may also contribute to the production of N, in addition to the electron impact dissociation of N_2. As a matter of fact, the production rate of N due to this reaction is found to be 10 to 20 % of the total production rate.

The atomic nitrogen produced in the above reactions except the process (5) may be in the electronically excited state ^2D as well as in the ground state ^4S. Although a large part of $N(^2D)$ may be deexcited to the ground state in the heights above $\sim$ 150 km (Rusch et al., 1975), it will be converted into NO through the reaction with O_2 in the lower thermosphere (Norton and Barth, 1970). On the other hand, $N(^4S)$ removes NO into N_2 through the combination reaction. Consequently, the efficiency of the $N(^2D)$ production is an important parameter determining the relative population of N and NO in the odd nitrogen system. Comparison of observed $N(^2D)$ and NO profiles with model calculations has led to the quantum yield of $N(^2D)$ in the processes (1) through (4) of 0.5 - 1.0 (Ogawa and Shimazaki, 1975; Oran et al., 1975; Rusch et al., 1975).

Although the process (6) is likely to produce $N(^2D)$ with a quantum yield as large as the processes (1) through (4), the quantum yield of $N(^2D)$ is not determined with a sufficient accuracy. Therefore, we are obliged to allow variability of this value in our present calculation. As an example to show the sensitivity of odd nitrogen density with respect to the $N(^2D)$ quantum yield, [N] and [NO] profiles ([ ] denotes the number density of the assigned particle) after 30 minutes electron precipitation for the flux Case A are depicted in Fig. III.8, where [N] and [NO] have been calculated for three typical values of the $N(^2D)$ quantum yield η for the process (6). Variations of [N] and [NO] are remarkable for the change of η between 0.1 and

1. In case of $\eta \lesssim 0.1$, [N] increases to a value exceeding 1×10^9 cm^{-3} at the peak height, whereas [NO] remains around the quiet level in the lower thermosphere. On the other hand, in case of $\eta \gtrsim 0.5$, [NO] increases more than one order of magnitude larger than that in the lower thermosphere under quiet conditions. In this case, [N] also increases to a value equal or larger than that could be found in the quiet daylight hours.

Variations of [N] and [NO] during the auroral perturbation depends on height and the $N(^2D)$ quantum yield. In Figs. III.9a and b are shown typical diurnal variations of [N] and [NO] calculated for some chosen values of η, where the electron precipitation of the flux Case A occurs in the time interval 0000-0030 LT. At 80 km where the production of $N(^2D)$ or $N(^4S)$ is not significant, the auroral perturbation can modify only the nocturnal decay of [N], and hardly affect [NO]. On the other hand, above $\sim$ 100 km, rapid changes of [N] and [NO] occur during the auroral perturbation. The effect of perturbation on [N] and [NO] differs greatly with the values of η. For $\eta \gtrsim 0.5$, [NO] remains almost constant after the rapid increase caused by the auroral perturbation, while [N] enhanced in the auroral perturbation decreases rapidly after the end of the perturbation. For $\eta \lesssim 0.1$, [NO] decreases and [N] increases rapidly during the perturbation, and both remain almost invariant after the end of the perturbation, in spite of the sunlit condition. This contrasting response of [N] and [NO] variations caused by the change of η can be attributed to that the main loss of both N and NO at night is their mutual combination into N_2. The removal of either N or NO ceases when the other is completely removed. As a result, [N] decreases and [NO] remains invariant in case of larger [NO] than [N]. On the contrary, once [N] would exceed [NO], [N] could remain unchanged and [NO] decreased. Since the time constant for the chemical removal of odd nitrogen is much longer than that for the

dynamical transport in the lower thermosphere, the enhancement of either N or NO will continue until the vertical and horizontal transports modify it.

Precipitating electrons of an energy spectrum with a characteristic energy of 40 keV can affect [N] and [NO] mainly in the heights between 70 and 100 km. In Figs. III.10a and b are compared the auroral effect on [N] and [NO] at 70 and 80 km for the flux Cases A and C, together with those under non-auroral conditions. In Case C the precipitation affects both [N] and [NO] below $\sim$ 90 km much more significantly than Case A, while Case A does above $\sim$ 100 km. The auroral perturbation on [N] is rather temporal in Case C, although some after-effects through the next daylight hours are found in the heights of 70 - 80 km. These after-effects are caused by the enhanced photodissociation of NO into N due to the increased [NO]. Again, the faster nocturnal decay of [N] at 80 km after the cessation of the electron precipitation for Case C than that for Case A is due to the large enhancement of [NO]. Variation of [NO] below $\sim$ 70 km after the auroral enhancement are different from that above $\sim$ 80 km. The nocturnal decay of [NO] becomes remarkable below $\sim$ 70 km; this is due to the reaction with O_3 which converts NO into NO_2. With the start of sunshine, NO_2 is rapidly changed into NO through the photodissociation, and [NO] increases.

Fig. III.11 compares the height distributions of [NO] at 0030 LT(i.e., after the 30 minutes electron precipitation) for various spectra of the electron influx. Cases A and B are representative of the usual auroral event with a characteristic energy of 5 keV, while Cases C and D of 40 keV. The difference of the height range where the electron precipitation can affect [NO] substantially is apparent with respect to different spectral characteristics of the electron influx; Cases A and B affect [NO] above $\sim$ 80 km, and Cases C and D in the heights 70 - 100 km.

4.3 Electron and ions

Electron and ion densities will be modified in the auroral ionosphere by two different causes: One is due to impact ionization of N_2, O and O_2, and the other is caused by the increase of odd nitrogen density in the auroral mesosphere and thermosphere. Variations of electron and ion densities by the former cause are of temporal nature and lasts only during the precipitation, since the chemical time constant for growth and removal of ionic species are in the order of magnitude of 10 sec (Jones and Rees, 1973). On the other hand, the latter will make a long-lasting effect after the cessation of the auroral precipitation, since the increased odd nitrogen density at the auroral precipitation remains stable after the auroral event.

Diurnal variations of electron and ion densities allowing auroral disturbances have been calculated simultaneously by solving the coupled continuity equations for neutral and ionic species as done in the paper by Ogawa and Shimazaki (1975). Chemical reactions incorporated in the present study are essentially the same as those in their paper, but some revisions of the rate coefficients have been made according to recent measurements by Burt (1972), Payzant et al. (1973), McFarland et al. (1974a, b), Lindinger et al. (1974), Heimerl and Vanderhoff (1974), Johnsen et al. (1975) and Moseley et al. (1975).

One of the physical quantities that show drastic changes following the auroral disturbance may be the ratio of $[NO^+]$ to $[O_2^+]$. Jones and Rees (1973) calculated the effect of auroral precipitation on ionic composition, but their calculation did not include the variation of odd nitrogen. Fig.III.12 represents the $[NO^+]/[O_2^+]$ ratio of 10 - 100 in the nighttime E region of the ionosphere decreasing to a value less than unity within a few minutes after

the beginning of the precipitation. This decrease is ascribed to the rapid increase of O_2^+ due to the addition of O_2 ionization by electron impact. The ratio then increases with increasing conversion rate of O_2^+ into NO^+ through the reaction with the increasing NO. There begins a sudden increase of the ratio at the cessation of the precipitation, when the O_2^+ production by electron impact ionization turns off. The $[NO^+]/[O_2^+]$ ratio in the E region after the auroral precipitation can increase to a value $\sim$ 100 times larger than that before the precipitation, as a consequence of the accumulation of NO during the 30 minutes electron precipitation of the flux Case A.

As seen in Fig. III.12, $[O_2^+]$ in the E region is in comparable magnitude with $[NO^+]$ during the auroral event, and the $[NO^+]/[O_2^+]$ ratio does not exceed 10 even for the 30 minutes duration of an IBC III aurora. Several observations of ion composition in the auroral ionosphere (Donahue et al., 1970; Swider and Narcisi, 1970, 1974; Narcisi et al., 1974) have revealed that in spite of large production rate of O_2^+, the $[NO^+]/[O_2^+]$ ratio in the E region amounts $\sim$10 in auroral conditions. This observational fact may suggest that [NO] must be in some increased level before the auroral event. Intermittent auroral precipitations would keep a persistently larger [NO] than in the middle and low latitudes.

Fig. III.13 represents the ionic composition after 30 minutes electron precipitation of the flux Case A. $[NO^+]$ and $[O_2^+]$ are dependent on the quantum yield of $N(^2D)$ in the electron impact dissociation of N_2, although other species are independent of this. The conversion of O_2^+ into NO^+ occurs mainly through the reaction $O_2^+ + NO \rightarrow NO^+ + O_2$ for the case of η = 0.9 ([NO] >> [N]), whereas it occurs mainly through the reaction $O_2^+ + N$ $NO^+ + O$ for the case of η = 0.1 ([NO] << [N]). The rate coefficient for the reaction of O_2^+ with NO is about a factor 3 larger than that for the

reaction of O_2^+ with N (Golden et al., 1966; Lindinger et al., 1974). Consequently, the $[NO^+]/[O_2^+]$ ratio in the E region is by a factor 3 - 5 larger for $\eta = 0.9$ than for $\eta = 0.1$. This result may suggest that $\eta \gtrsim 0.5$ is preferable so as to meet the $[NO^+]/[O_2^+]$ ratio observed in the auroral ionosphere.

There are depicted in Figs. III.14a and III.14b diurnal variations of electron densities at 80 km and 100 km for 4 spectral cases of the auroral electron influx and for a non-auroral case. The rapid response of the electron density to the variation of auroral ionization rates is evident at the onset and end of the precipitation. It is also found in these figures that the electron density in the E region remains increased after the cessation of the precipitation. This is mainly because of an enhancement of [NO]. The increased [NO] leads to an enhancement of the NO photoionization rate by the geocoronal or solar EUV radiation, and eventually an enhancement of the total ion production rate. As is easily understood from the different height profiles of [NO] for spectrally different fluxes of precipitating electrons (see Fig. III.11), this after-effect in the electron density variation appears mainly above $\sim$ 90 km for the flux Cases A and B, and mainly below $\sim$ 90 km for the flux Cases C and D.

In order to see the after-effect in detail, ion compositions at 1200 LT for the cases of the electron precipitation at the previous midnight and of no auroral disturbance are compared in Fig. III.15. The auroral disturbance causes the enhancement of $[NO^+]$ and [e] in 80 - 120 km, whereas it causes a large decrease of $[O_2^+]$. These results may be natural consequences of the persistent enhancement of [NO] in the auroral-zone thermosphere, and would be demonstrated by a direct observation in the near future. It must be emphasized that the observation of ion compositions together with neutral odd nitrogen in the auroral zone under daylight conditions will provide interesting topics on auroral aeronomy.

4.4 Further comparison of the calculation with observations

There have been available data concerning the odd nitrogen in the polar thermosphere, suggesting the enhancement of the NO density under auroral perturbations. We will examine further the results of the present calculation in comparison with observations.

The latitudinal variation of the NO concentration can be evaluated from the γ-band airglow measured by Rusch and Barth(1975) and the result is shown in Fig.III.16 [NO] is 3-4 times larger at high geomagnetic latitude than at mid-latitude, varing rather sporadically in time and space. It can safely be said that the observed enhancement of [NO] is attributed to the augmented N_2 dissociation due to the auroral electron precipitation, as no additional source of odd nitrogen is expected in normal sunlit condition at high latitudes. However, the region of the high NO concentration is not confined to the auroral zone. This may suggest that the horizontal diffusion of NO must be included by a two dimentional model in order to simulate adequately the effect of the poleward and equaterward outflows of NO from the auroral zone.

The enhancement of [NO] during the auroral electron precipitation has been suggested by the measurements of ion composition in aurorae. Ions, which have chemical time constants of the order of 1 minute, can be considered to be highly in chemical euqilibrium in the auroral ionosphere, and $[NO^+]$ and $[O_2^+]$ are greatly affected by NO or N through the reaction $NO + O_2^+ \rightarrow NO^+ + O_2$. Swider and Narcisi(1974) derived [NO] from the measured ion concentration in an aurora by assuming chemical equilibrium of ions with NO and neglecting the effect of N. The result is reproduced in FigIII.17. [NO] shown in this figure is about an order of magnitude larger than that in the non-polar region. We can expect the [NO] of this amount in an aurora

somewhat larger than IBC II class from the present calculation. [NO] obtained in the IBC II aurora may well be explained considering the effect of the prolonged electron precipitation in auroral zone. On the other hand, $[NO^+]/[O_2^+]$ itself is expected to be a good index of [NO]. In Fig. III.18, $[NO^+]/[O_2^+]$ measured by Swider and Narcisi(1970), Donahue et al.(1970), and Narcisi et al.(1974) are compared with those calculated at 2 minutes and 30 minutes after the commencement of the electron bombardment. 30 minutes after the onset of the precipitation, the calculated [NO] is increased from 5×10^7 cm^{-3} to 10^9 cm^{-3} at 100-120 km. The calculated $[NO^+]/[O_2^+]$ for the enhanced [NO] is in fundamental agreement with the observed and are thus suggestive of the increase of [NO] in polar region.

5. CONCLUDING REMARKS

The major source of atomic oxygen during auroral precipitations is the dissociation of O_2 by electron impact. Although the dissociation rate of O_2 by the electron flux of an IBC III aurora above 90 km becomes comparable to the photodissociation rate of O_2 in the daytime, [O] would hardly follow temporal variations of the production rate because of the long growth time. An extremely large electron flux of high energy ($\sim$ 100 keV) only could make an apparent increase of [O] below 80 km.

On the other hand, [N] and [NO] can be greatly affected by auroral perturbations. The major sources of odd nitrogen in the auroral thermosphere are the dissociation of N_2 by electron impact, and the dissociative recombination of NO^+ whose rate is raised due to the auroral ionization. The production rate of odd nitrogen above 80 km in an IBC II aurora may exceed that in the usual sunlit thermosphere.

[N] and [NO] show different responses to an auroral perturbation according to different values of the quantum yield of $N(^2D)$ in the electron impact dissociation of N_2. In case of $\eta \gtrsim 0.5$, a large amount of NO is produced through the conversion reaction of $N(^2D)$ with O_2 into NO, and [NO] can easily raised to a value of a factor 10 larger than those in the normal daytime thermosphere. [N] during the auroral precipitation may also become temporally larger than that in the sunlit thermosphere, but decreases rapidly after the cessation of the precipitation through the reaction with the increased NO. On the contrary in case of $\eta \lesssim 0.1$, the production rate of NO from $N(^2D)$ is suppressed, and [N] can grow up to a constantly large value. In this case, the decay of NO occurs through the reaction with N. For the case of η between 0.1 and 0.5 it would be probable that both [N] and [NO] begin an apparent decrease after the auroral enhancement.

Recent observations by Rusch and Barth (1975) have revealed that [NO] in the polar thermosphere varies greatly with time and space, but that it hardly becomes less than those in the middle- and low-latitude thermosphere. This result may be suggestive of $\eta \gtrsim 0.5$.

A large value of η is also agreeable with ion compositions measured in the auroral ionosphere. Enhancement of [NO] in the auroral thermosphere may influence the electron density and ion composition in the E region in such a way that increases the photoionization rate of NO and the conversion rate of O_2^+ into NO^+. Since the time constant for removal of NO is in the order of a day, the enhancement of NO may hold until the next perturbation starts. The persistently increased [NO] will maintain the high $[NO^+]/[O_2^+]$ ratio in the polar ionosphere even though an appreciable amount of O_2^+ can be produced in the auroral precipitation or in the sunlit condition.

Acknowledgements

I wish to express my appreciation to Prof. T.Tohmatsu who has continuously advised and encouraged the author and to Dr. T. Ogawa who has inspired him through invaluable discussions in the course of this study. I also want to thank Profs. N. Fukushima, T. Oguti, T. Tamao, S. Kokubun, and T. Sato and Drs. E. Kaneda, T. Iijima, K. Suzuki, and K. Hayashi and Mr. N. Iwagami who encouraged the author by discussions with interest. Thanks are also to the other members of Geophysics Research Laboratory, Univ. of Tokyo. The calculation in this study has been carried out on the Hitac 8800-8700 computer at the computer center, Univ. of Tokyo.

References

Ackerman,M., F.Bianmé, G. Kockarts, Absorption cross sections of the Shuman-Runge bands of molecular oxygen, Planet. Space Sci., 18, 1639-1651,1970.

Banks,P.M., C.R. Chappell, and A.F. Nagy, A new model for the interaction of auroral electrons with the atmosphere: Spectral degradation, backscatter, optical emission, and ionization, J. Geophys. Res.,79, 1459-1470, 1974.

Barth, C.A., Nitrogen and oxygen atomic reactions in the Lower and Upper Atmosphere, 303, Interscience, New York, 1961.

Barth, C.A., Rocket measurement of nitric oxide dayglow, J. Geophys. Res., 69, 3301-3303, 1964.

Barth, C.A., Nitric oxide in the upper atmosphere, Ann. Geophys., 22, 198-207, 1966a.

Barth, C.A., Rocket measurement of nitric oxide in the upper atmosphere, Planet. Space Sci., 14, 623-630, 1966b.

Bates,D.R., Some reactions occurring in the earth's upper atmosphere., Ann. Geophys., 8, 194-204, 1952.

Bates,D.R., The physics of the upper atmosphere. Chapter 12 in The Earth as a Planet(Ed.G. Kuiper), PP.576-643. Univ. of Chicago Press., 1954.

Black,G., T.G. Slanger, G.A. St. John, and R.A. Young, Vaccuum-ultraviolet photolysis of N_2O, 4, Deactivation of $N(^2D)$, J. Chem. Phys., 51, 116-121, 1969.

Bourdeau,R.E., A.C. Aikin, and J.L. Donley, Lower ionosphere at solar minimum, J. Geophys. Res., 71, 727-740, 1966.

Cieslik,S., and M.Nicolet, The aeronomic dissociation of nitric oxide, Planet. Space Sci., 21, 925-938, 1973.

Clark, I.D., and R.P. Wayne, The reaction of $O_2(^1\Delta_g)$ with atomic nitrogen and with atomic oxygen, Chem. Phys. Lett., 3, 405-407, 1969.

Cohen-Sabban,J., and A.Vuillemin, Ultra-violet nightglow spectrum from 1900 Å to 3400 Å, Astrophys. Space. Sci., 24, 127-132, 1973.

Colegrove,F.D., W.B. Hanson, and F.S. Johnson, Eddy diffusion and oxygen transport in the lower thermosphere, J. Geophys. Res., 70, 4931-4941, 1965.

Colegrove,F.D., F.S. Johnson, and W.B. Hanson, Atmospheric composition in the lower thermosphere, J. Geophys. Res., 71, 2227-2236, 1966.

Cook, G.R., M. Ogawa and R.W. Carlson, Photodissociation continuums of N_2 and O_2, J. Geophys. Res., 78, 1663-1667, 1973.

Davenport, J.E., T.G. Slanger, and G. Black, The quenching of $N(^2D)$ by $O(^3P)$, J. Geophys. Res., 81, 12-16, 1976.

Donahue, T.M., E.C. Zipf,Jr., and T.D. Parkinson, Ion composition and ion chemistry in an aurora, Planet. Space Sci., 18, 171-186, 1970.

Feldman, P.D., and P.Z. Takacs, Nitric oxide gamma and delta band emission at twilight, Geophys. Res. Lett., 1, 169-171, 1974.

Ferguson, E.E., Ionospheric ion-molecule reaction rates, Rev. Geophys., 5, 305-327, 1967.

Ferguson, E.E., D.B. Dunkin, F.C. Fehsenfeld, and A.L. Schmeltekopf, Ion-molecule reaction rate constant measurements in the near thermal range, Bull. Amer. Phys. Soc., 13, 212, 1968.

Findlay, F.D., C.J. Fortin, and D.R. Snelling, Deactivation of $O_2(^1\Delta_g)$, Chem. Phys. Lett, 3, 204-206, 1969.

Gerard, J.-C., Satellite observations of the nitric oxide nightglow, Geophys. Res. Lett., 2, 179-182, 1975.

Hudson, R.D., and U.L. Carter, Atmospheric implications of predissociations in N_2, J. Geophys. Res., 74, 393-395, 1969.

Hunt, B.G., Cluster ions and nitric oxide in the D-region, 33, 929-942, 1971.

Hunter, D.M. and M.B. McElroy, Metastable $O_2(^1\Delta)$ as a major source of ions in the D region, J. Geophys. Res., 73, 2421-2428, 1968.

Jones, R.A. and M.H. Ress, Time dependent studies of the aurora-I. Ion density and composition, Planet. Space Sci., 21, 537-557, 1973.

Judge, R.J.R. Electron excitation and auroral emission parameters, Planet. Space Sci., 20, 2081-2092, 1972.

Kamiyama, H., Ionization and excitation by precipitating electrons., Rep. Ions. Space. Res. Japan, 20, 171-187, 1966.

Kamiyama, H., The electron density distribution in the lower ionosphere produced through impact ionization by precipitating electrons and through photoionization by the associated Bremsstrahlung X-ray, J. Geomag. Geoelectr., 19, 27-47, 1976.

Keneshea, T.J., R.S. Norcisi, and W. Swider, Diurnal model of the E region, J. Geophys. Res., 75, 845-854 1970.

Lin, C.L. and F. Kaufman, Reactions of metastable nitrogen atoms, J. Chem. Phys., 55, 3760-3770, 1971.

Maeda, K., Diffusion of low energy electrons in the atmosphere, J. Atmos. Terr. Phys., 27, 259-275, 1965.

Maeda, K, The auroral O_2-dissociation and the infrared OH-emission, Ann. Geophys., 173-184, 24, 1968.

Maeda, K. and A.C. Aikin, Variations of polar mesospheric oxygen and ozone during auroral events, Planet. Space Sci., 16, 371-384, 1968.

Meira, L.G., Jr., Rocket measurements of upper atmospheric nitric oxide and their consequences to the lower ionosphere, J. Geophys. Res., 76, 202-212, 1971.

Narcisi, R.S., C. Sherman, L.E. Wlodyka, and J.C. Ulwick, Ion composition in an IBC class II aurora 1, Measurements, J. Geophys. Res., 79, 2843-2847, 1974.

Nicolet, M., Contribution à l'étude de la structure de l'ionosphère, Inst. Roy. Météorol Belg. Mém., 19, 169, 1945.

Nicolet, M., Contribution à l'étude de la structure de l'ionosphère, Inst. Roy. Météorol Belg. Mém., 19, 169, 1945.

Nicolet, M., The aeronomic problem of nitrogen oxides, J. Atmos. Terr. Phys., 7, 152-169, 1955.

Nicolet, M., Aeronomic chemical reactions, in the Physics and Medicine of the Atmosphere and Space, edited by O.O. Benson, Jr., and H. Strughold, John Wiley and Sons, New York, 1960.

Nicolet, M., Nitrogen oxides in the chemosphere, J. Geophys. Res., 70, 679-689, 1965a.

Nicolet, M., Ionospheric processes and nitric oxide, J. Geophys. Res., 691-701, 1965b.

Nicolet, M., The origin of nitric oxide in the terrestrial atmosphere, Planet. Space Sci., 18, 1111-1118, 1970.

Nicolet, M., and A.C. Aikin, The formation of the D region of the ionosphere, 65, 1469-1483, 1960.

Nicolet, M., and W. Swider, Ionospheric conditions, Planet. Space Sci., 11, 1459-1482, 1963.

Norton, R.B. and C.A. Barth, Theory of nitric oxide in the earth's atmosphere, J. Geophys. Res., 75, 3903-3909, 1970.

Ogawa, T. and T. Shimazaki, Diurnal variations of odd nitrogen and ionic densities in the mesosphere and lower thermosphere: Simultaneous solution of photochemical-diffusive equations, J. Geophys. Res., 80, 3945-3960, 1975.

Ogawa, T., and T. Tohmatsu, Photoelectronic processes in the upper atmosphere, 2, The hydrogen and helium ultraviolet glow as an origin of the nighttime ionosphere, Rep. Ion. Space Res. Japan, 20, 395-417, 1966.

Oran, E.S., P.S. Julienne, and D.F. Strobel The aeronomy of odd nitrogen in the thermosphere, J. Geophys. Res., 80, 3068-3076, 1975.

Ress, M.H., Auroral ionization and excitation by incident energetic electrons, Planet. Space Sci., 11, 1209-1217, 1963.

Ress, M.H., Note on the penetration of energetic electrons into the earth's atmosphere, Planet. Space Sci., 12, 725-726, 1964.

Ress, M.H., Auroral electrons, Space Sci. Rev. 10, 413-441, 1969.

Rusch, D.W. and C.A. Barth, Satellite measurements of nitric oxide in the polar region, J. Geophys. Res., 80, 3719-3721, 1975.

Rusch, D.W., A.I. Stewart, P.B. Hays, and J.H. Hoffman, The NI(5200 A) dayglow, J. Geophys. Res., 80, 2300-2304, 1976.

Sechrist, C.F., Jr., Theoretical models of the D-region, J. Atmos. Terr. Phys., 34, 1565-1589, 1972.

Shahin, M.M., Use of corona discharges for the study of ion-molecule reactions, J. Chem. Phys., 47, 4392-4399, 1967.

Strobel, D.F., D.M. Hunten, and M.B. McElroy, Production and diffusion of nitric oxide, J. Geophys. Res., 75, 4307-4321, 1970.

Strobel. D.F., Diurnal variation of nitric oxide in the upper atmosphere, J. Geophys. Res., 76, 2441-2452, 1971a.

Strobel., D.F., Odd nitrogen in the mesosphere, J. Geophys. Res., 76, 8384-8393, 1971b.

Strobel, D.F., Nitric oxide in the D region, J. Geophys. Res., 77, 1337-1339, 1972.

Strobel, D.F., T.R. Young, R.R. Meier, T.P. Coffey and A.W. Ali, The nighttime Ionosphere: E region and lower F region, J. Geophys. Res., 79, 3171-3178, 1974.

Swider, W., E-region model parameters, J. Atmos. Terr. Phys., 34, 1615-1629, 1972.

Swider, W., Minor neutral mesospheric constituents at high latitudes, to be published in Space Research XVII, 1977.

Swider, W. and R.S. Narcisi, On the ionic constitution of class I auroras, Planet. Space Sci., 18, 379-385, 1970.

Swider, W. and R.S. Narcisi, Ion composition in an IBC class II aurora 2. Model, J. Geophys. Res., 79, 2849-2852, 1974.

Takayanagi, K. and T. Yonezawa, Collision processes in the auroral and ionization in the auroral zone, Rep. Ionos. Space Res. Japan, 15, 51-69, 1961.

Thomas,L., The lower ionosphere, J. Atmos. Terr. Phys., 33, 157-195, 1971.

Tisone, G.C., Measurement of NO densities during sunrise at Kauai, J. Geophys. Res., 78, 746-750, 1973.

Tohmatsu, T. and N. Iwagami, Measurement of nitric oxide distribution in the upper atmosphere, Space Research XV, 241-245, 1975.

Tohmatsu, T., and N. Iwagami, Measurement of nitric oxide abundance in equatorial upper atmosphere, submitted to J. Geomag. Geoelectr. 1976.

Tohmatsu, T. and T. Nagata, On earth storms VI. Energy and flux of corpuscular streams impinging the earth's atmosphere, Rep. Ions. Space Res. Japan, 14, 301-319, 1960.

Torr, M.R., R.G. Burnside, P.B. Hays, A.I. Stewart,D.G. Torr, and J.C.G. Walker, Metastable ^2D atomic nitrogen in the mid-latitude nocturnal ionosphere, J. Geophys. Res., 81, 531-537, 1976.

Walker, J.C.G. and M.H. Rees, Ionospheric electron densities and temperatures in aurora, Planet. Space Sci., 16, 459-475, 1968.

Watanabe, K., F. Marmo, and E.C.Y. Inn, Formation of the D layer, Phys. Rev., 90, 155-156, 1953.

Zipf, E.C., W.L. Borst, and T.M. Donahue, A mass spectrometer observation of NO in an auroral arc, J. Geophys. Res., 75, 6371-6376, 1970.

Table II.1 Photodissociation and Photo-Ionization Processes

No.	Reaction	Coefficient(sec^{-1})	References
J1	$N_2 + h\nu(1200\text{-}1250\mathring{A}) \rightarrow N + N$	1.50×10^{-11}	Ogawa and Shimazaki [1975]
J2	$N_2 + h\nu(800\text{-}1000\mathring{A}) \rightarrow N + N$	1.90×10^{-8}	
J3	$N_2 + h\nu(1\text{-}800\mathring{A}) \rightarrow N + N$	$= 0.1J_6$	
J4	$NO + h\nu(1750\text{-}1908\mathring{A}) \rightarrow N + O$	1.34×10^{-5}	
J5	$NO + h\nu(630\text{-}1325\mathring{A}) \rightarrow N + O$	3.92×10^{-7}	
J6	$N_2 + h\nu(1\text{-}800\mathring{A}) \rightarrow N_2^+ + e$	4.53×10^{-7}	
J7	$N_2 + h\nu(1\text{-}510\mathring{A}) \rightarrow N^+ + N + e$	$=0.02J_6$	
J8	$O + h\nu(1\text{-}911\mathring{A}) \rightarrow O^+ + e$	3.22×10^{-7}	
J9	$O_2 + h\nu(1\text{-}1027\mathring{A}) \rightarrow O_2^+ + e$	5.92×10^{-7}	
J10	$O_2 + h\nu(1\text{-}660\mathring{A}) \rightarrow O^+ + O + e$	$=0.15J_9$	
J11	$NO + h\nu(153\text{-}1340\mathring{A}) \rightarrow NO^+ + e$	1.38×10^{-6}	
J12	$N + h\nu(1\text{-}850\mathring{A}) \rightarrow N^+ + e$	2.15×10^{-7}	Henry[1968]

Table II.2 Neutral Reactions

No.	Reaction	Rate Coefficient	References
R1	$N + O_2 \rightarrow NO + O$	$1.1 \times 10^{-14} T \exp(-3150/T)$	Baulch et al.[1973]
R2	$N + NO \rightarrow N_2 + O$	2.7×10^{-11}	Baulch et al.[1973]
R3	$N(^2D) + O \rightarrow N + O$	$8.5 \times 10^{-12} \exp(-500/T)$ (see text)	Davenport et al.[1976]
R4	$N(^2D) + O_2 \rightarrow NO + O$	5.2×10^{-12}	Husain et al.[1974]
R5	$N(^2D) + N_2 \rightarrow N + N_2$	2.3×10^{-14}	Husain et al.[1972]
R6	$N(^2D) + NO \rightarrow N_2 + O$	6.1×10^{-11}	Husain et al.[1972]
R7	$N(^2D) + e \rightarrow N + e$	$1.0 \times 10^{-9} (T/300)^{1/2}$	Rusch et al.[1975]
R8	$N_2 + e \rightarrow N + N + e$		see text

Table II.3 Ionic Reactions

No.	Reaction	Rate Coefficient	References
RI1	$N_2^+ + O \rightarrow NO^+ + N$	$1.4 \times 10^{-10}(300/T)^{0.44}$	McFarland et al.[1974b]
RI2	$N_2^+ + O \rightarrow O^+ + N_2$	$1.0 \times 10^{-11}(300/T)^{0.23}$	McFarland et al.[1974b]
RI3	$N_2^+ + O_2 \rightarrow O_2^+ + N_2$	$5.0 \times 10^{-11}(300/T)^{0.8}$	McFarland et al.[1973]
RI3A	$N_2^+ + O_2 \rightarrow NO^+ + NO$	$\leq 3.0 \times 10^{-14}$	Warneck [1967]
RI4	$N_2^+ + NO \rightarrow NO^+ + N_2$	3.3×10^{-10}	Fehsenfeld et al.[1970]
RI5	$O^+ + N_2 \rightarrow NO^+ + N$	$1.2 \times 10^{-12}(300/T)$	McFarland et al.[1973]
RI6	$O^+ + O_2 \rightarrow O_2^+ + O$	$2.0 \times 10^{-11}(300/T)^{0.4}$	McFarland et al.[1973]
RI6A	$O^+ + NO \rightarrow NO^+ + O$	$\leq 8.0 \times 10^{-13}$	McFarland et al. [1974a]
RI7	$O_2^+ + N_2 \rightarrow NO^+ + NO$	$\leq 1.0 \times 10^{-15}$	Ferguson et al.[1965]
RI8	$O_2^+ + N \rightarrow NO^+ + O$	1.8×10^{-10}	Goldan et al.[1966]
RI9	$O_2^+ + NO \rightarrow NO^+ + O_2$	7.2×10^{-10}	Johnsen et al.[1970]
RI10	$N^+ + O_2 \rightarrow O_2^+ + N$	3.0×10^{-10}	Lindinger et al.[1974]
RI10A	$N^+ + O_2 \rightarrow NO^+ + O$	3.0×10^{-10}	Lindinger et al.[1974]
RI11	$O_2^+ + N(^2D) \rightarrow N^+ + O_2$	2.5×10^{-10}	Dalgarno [1970]
RI12	$N_2^+ + e \rightarrow N + N$	2.9×10^{-7}	Biondi [1969]
RI13	$O_2^+ + e \rightarrow O + O$	$2.3 \times 10^{-7}(300/T)$	Biondi [1969]
RI14	$NO^+ + e \rightarrow N + O$	$4.6 \times 10^{-7}(300/T)$	Biondi [1969]

Table III.1 Ionization and excitation processes

	State	Ionization potential (eV)	Source
N_2^+	$X^2\Sigma_g^+$	15.58	1, 2
	$A^2\Pi_u$	16.78	1, 2, 3
	$B^2\Sigma_u^+$	18.75	1, 2, 4, 5
	$D^2\Pi_g$	22.0	1, 2
	$C^2\Sigma_u^+$	23.6	1, 2
	total $N + N^+$	25.0	1, 2, 6
O_2^+	$X^2\Pi_g$	12.1	1, 2
	$a^4\Pi_u$	16.1	1, 2, 7, 8
	$A^2\Pi_u$	16.9	1, 2
	$b^4\Sigma_g^-$	18.2	1, 2
	unidentified state	23.0	1, 2
	$O + O^+(^4S)$	18.0	1, 2, 6
	$O + O^+(^2D)$	22.0	1, 2, 6
O^+	^4S	13.6	1, 2
	^2D	16.9	1, 2
	^2P	18.5	1, 2

Table (continued)

	State	Excitation energy (eV)	Source
N_2	$A^3\Sigma_u^+$	6.14	9
	$B^3\Pi_g$	7.30	10
	$C^3\Pi_u$	11.03	10
	$a^1\Pi_g$	8.55	11
	$b^1\Pi_u$	12.85	1
	$h^1\Sigma_u^+$	14.0	1
	Rydberg (total)	13.75	1
	Dissociation	13.0	12
	Vibration		13
O_2	$a^1\Delta_g$	0.98	14
	$b^1\Sigma_g^+$	1.64	14
	$A^2\Sigma_u^+$	4.5	1
	$B^3\Sigma_u^-$	8.4	1
	Unidentified state	9.9	1
	Rydberg (total)	13.5	1
O	^1D	1.96	15
	^1S	4.17	15
	^3S	9.53	16
	^5S	9.15	16
	total ($\Delta\ell=1, \Delta S=0$) state	14.2	1
	total ($\Delta s=1$) state	14.7	1
	total ($\Delta\ell=0$, $\Delta s=0$) state	13.5	1

References to table III.1

(1) Banks et al. (1974)

(2) Kieffer and Dunn (1966)

(3) Simpson and McConkey (1969)

(4) Borst and Zipf (1970)

(5) Srivastava and Mirza (1968)

(6) Rapp et al. (1965)

(7) McConkey and Woolsey (1969)

(8) Srivastava (1970)

(9) Borst (1972)

(10) Stanton and St. John (1969)

(11) Ajello (1970)

(12) Winters (1966)

(13) Schulz (1964)

(14) Trajmar et al. (1971)

(15) Henry et al. (1969)

(16) Stone and Zipf (1974)

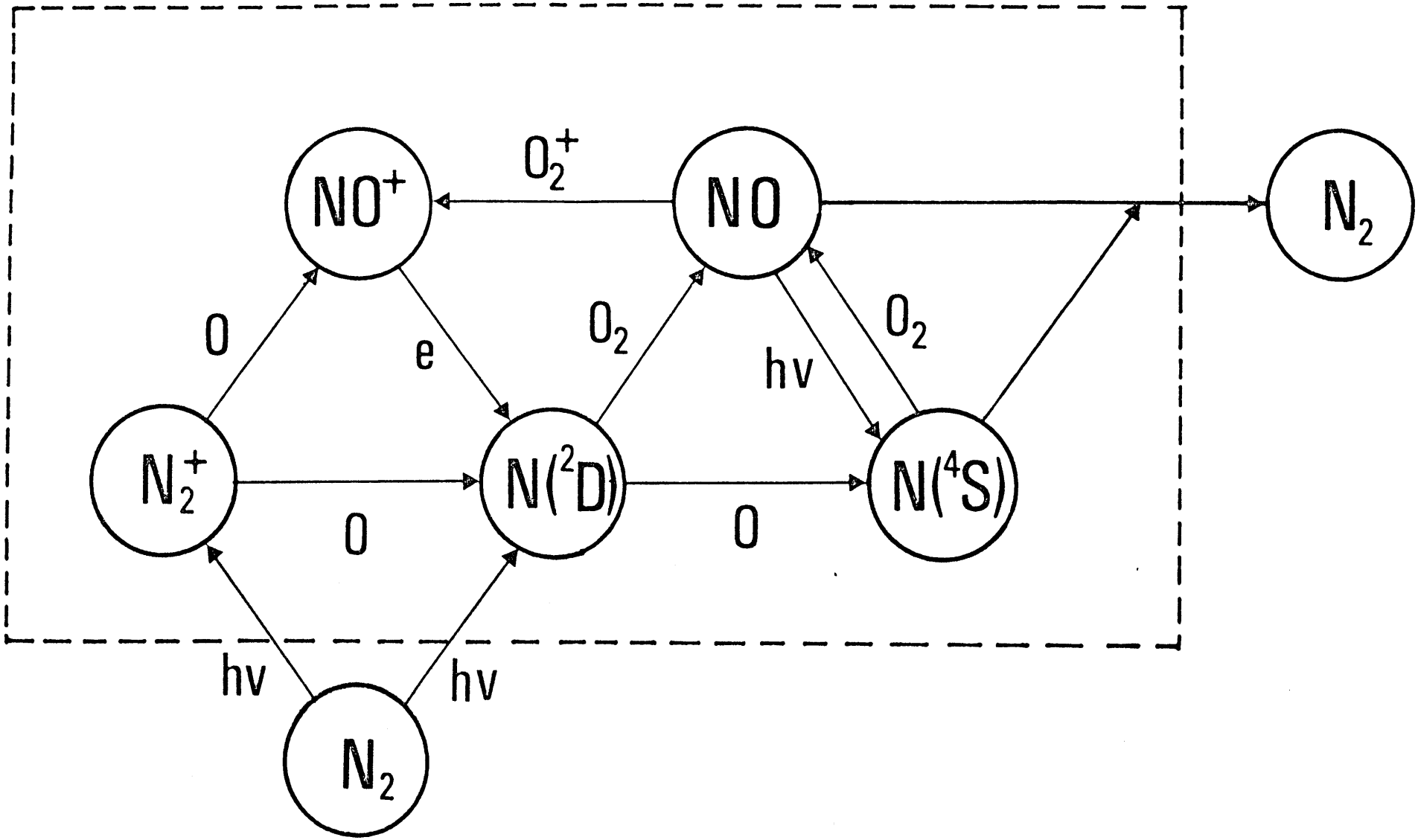

Fig. II.1 Simplified scheme of important chemical reactions above 90 km.

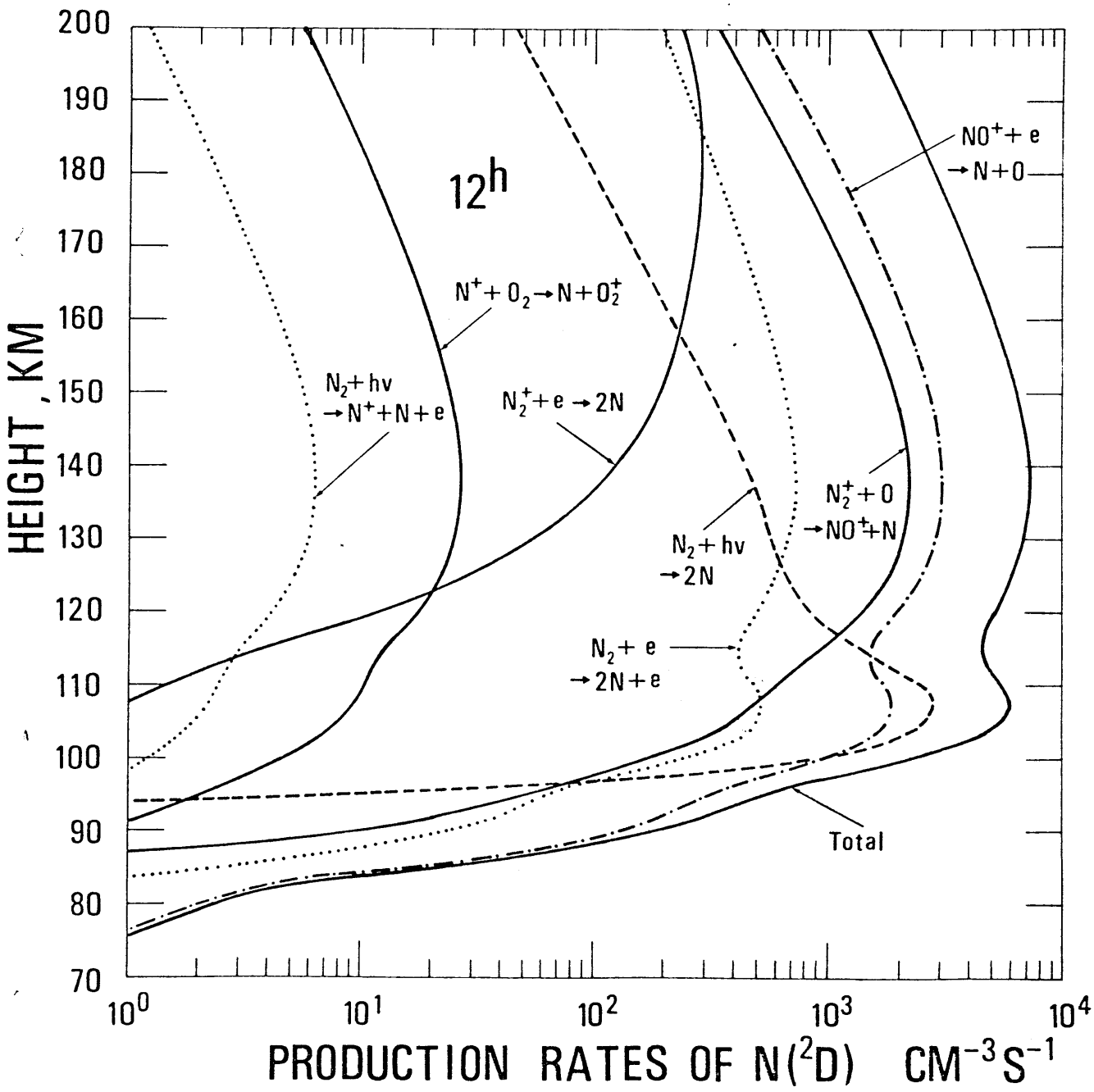

Fig. II.2a Production rates of $N(^2D)$ by varios processes at noon(SZA=45°). J2 and J3 are put together and dipicted as $N_2 + h\nu \rightarrow 2N$.

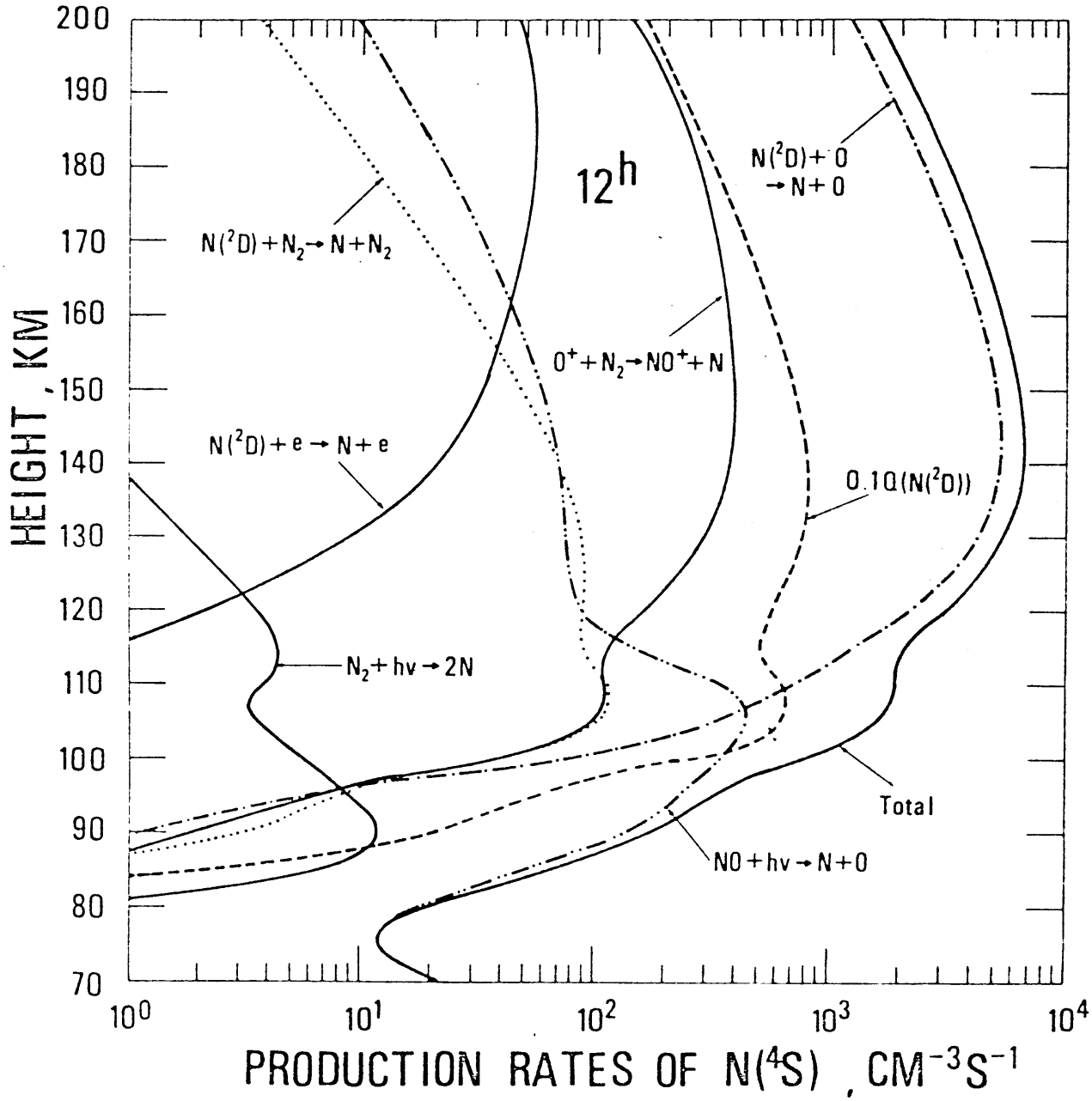

Fig. II.2b Production rates of $N(^4S)$ at noon. $Q(N(^2D))$ represents the sum of the reaction rates of J2, J3, J7, R8, RI1, RI10, RI12, and RI14.

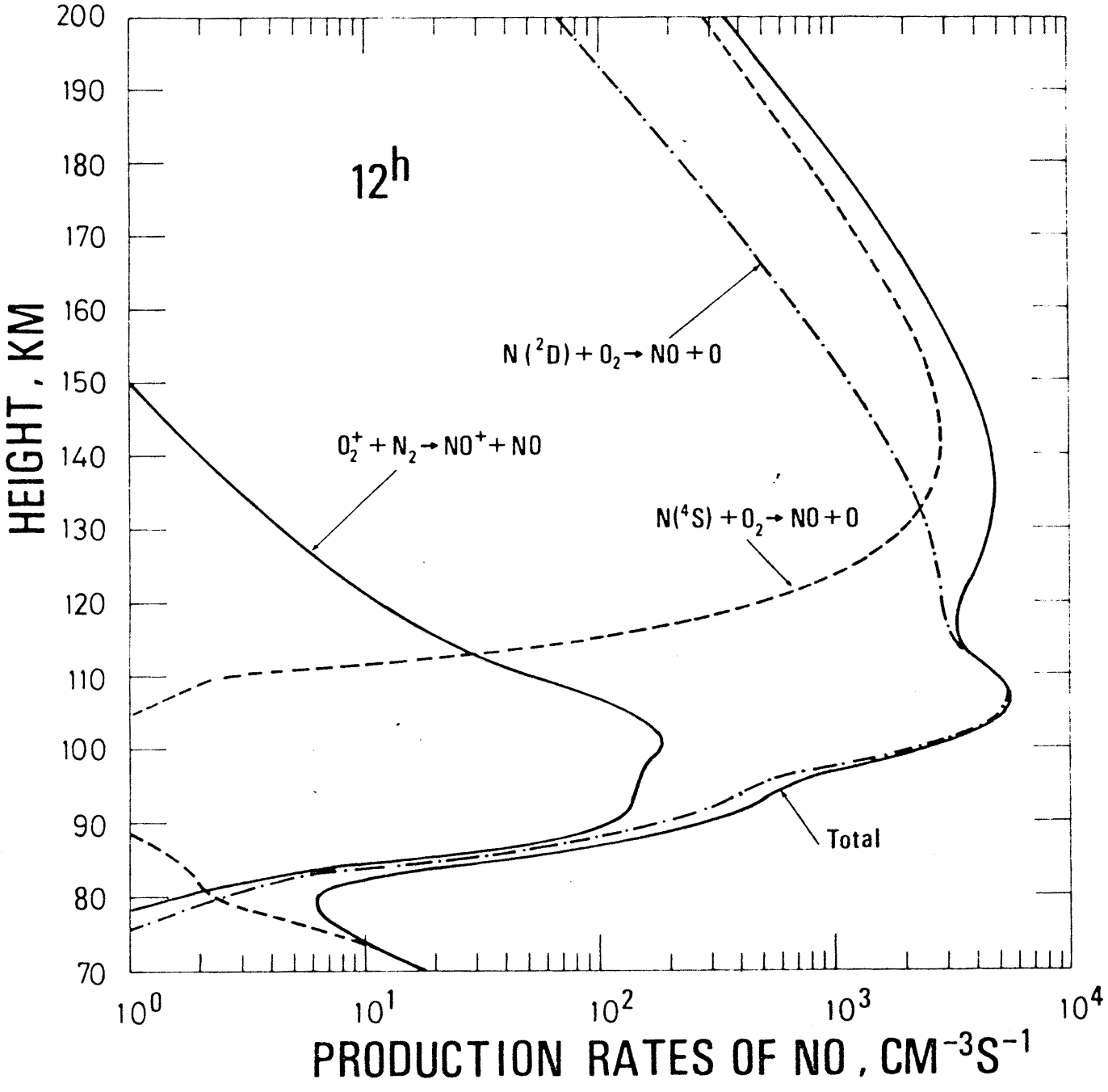

Fig. II.2c Production rates of NO at noon.

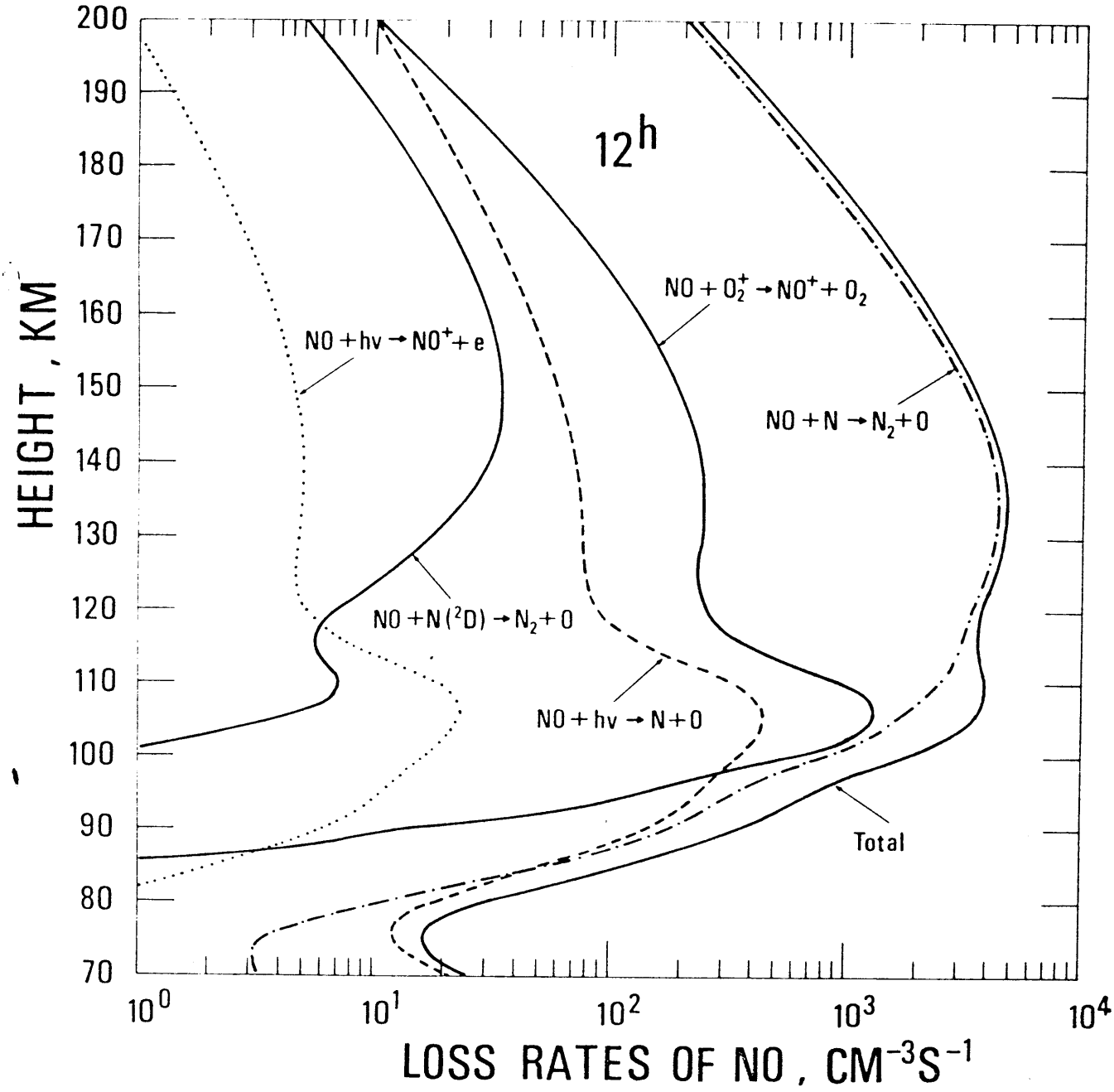

Fig. II.2d Loss rates of NO at noon.

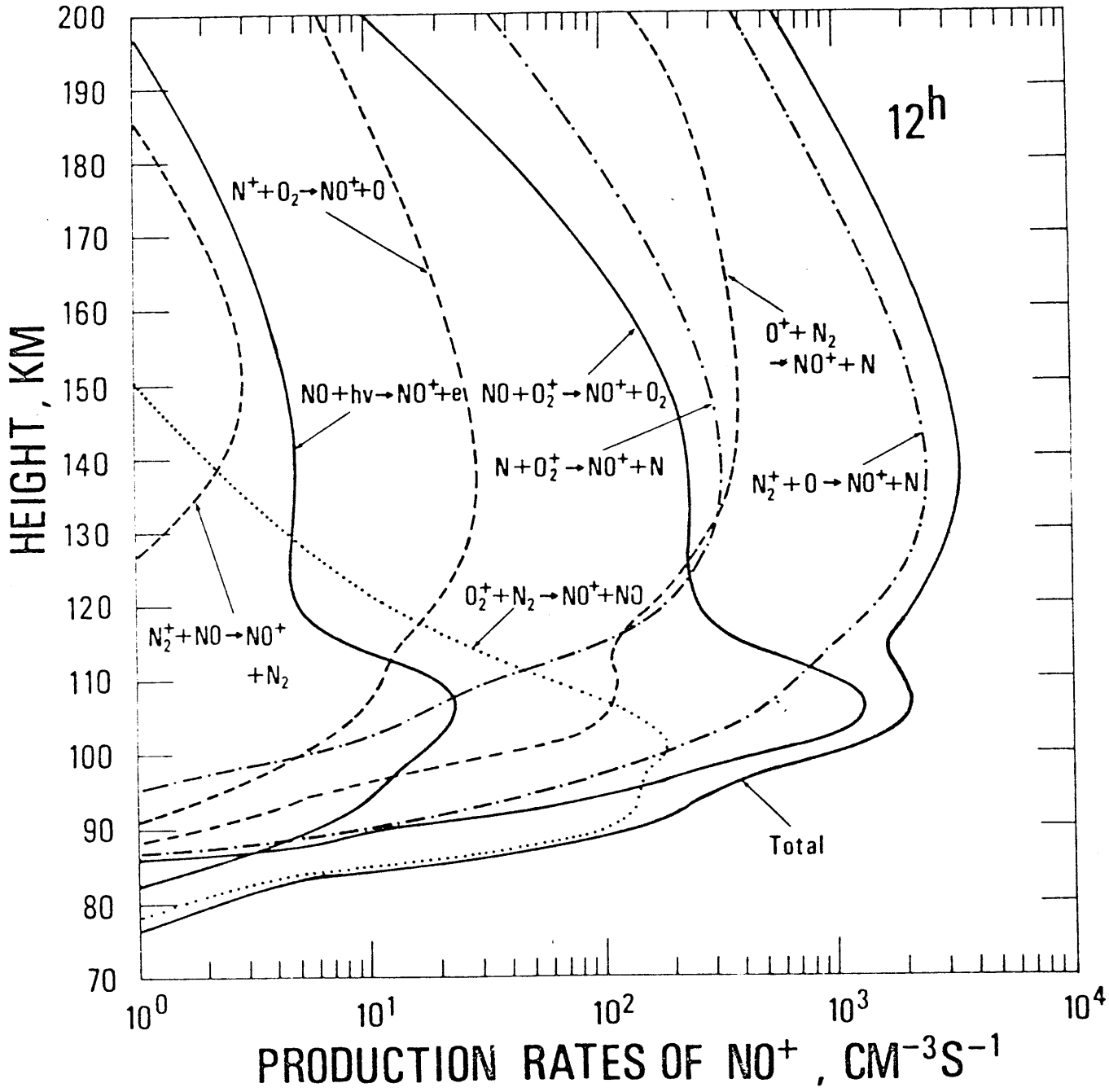

Fig. II.2e Production rates of NO^+ at noon.

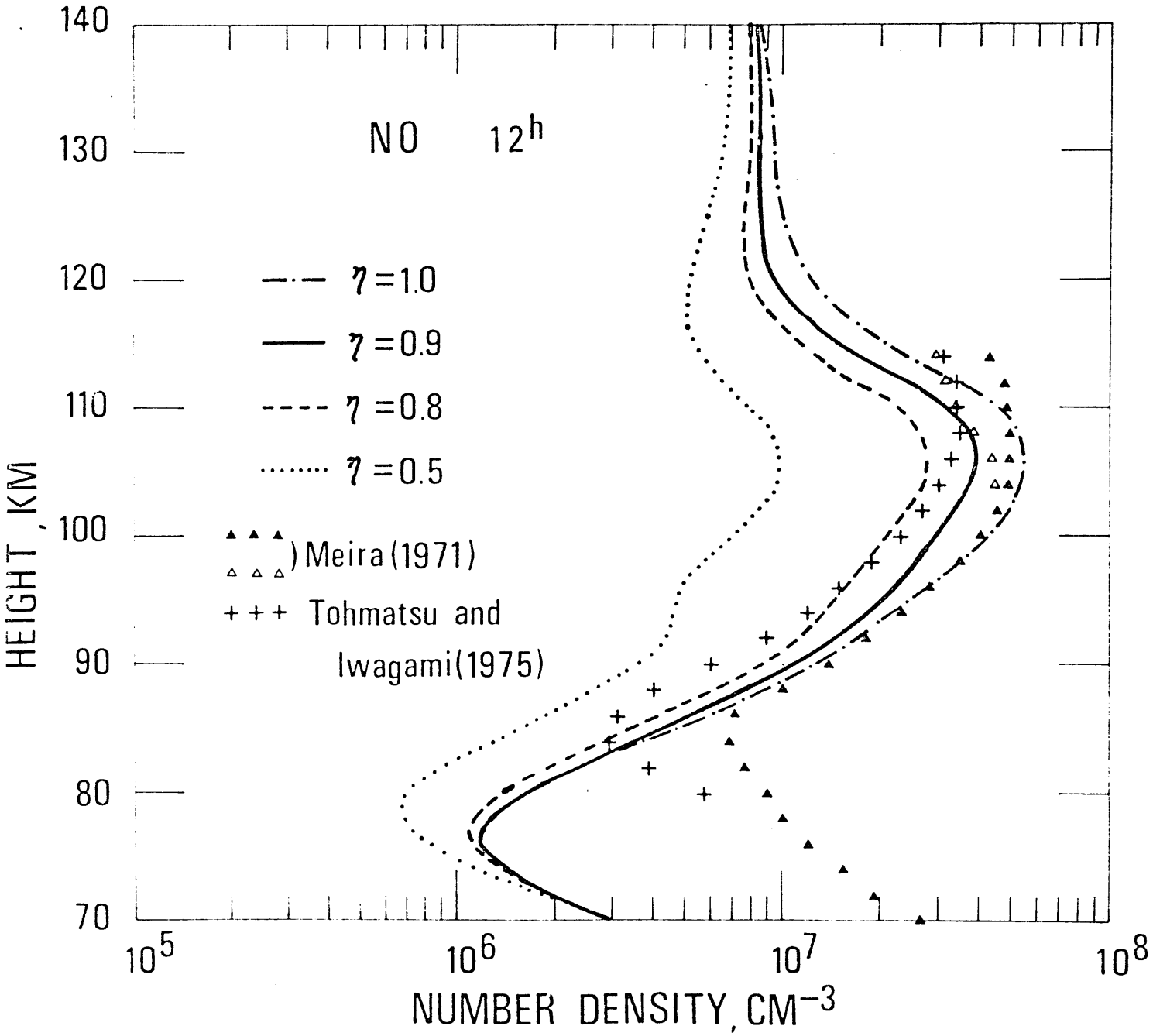

Fig. II.3 NO profiles at noon calculated for various values of η.
T_∞= 1050 K independent of local time.

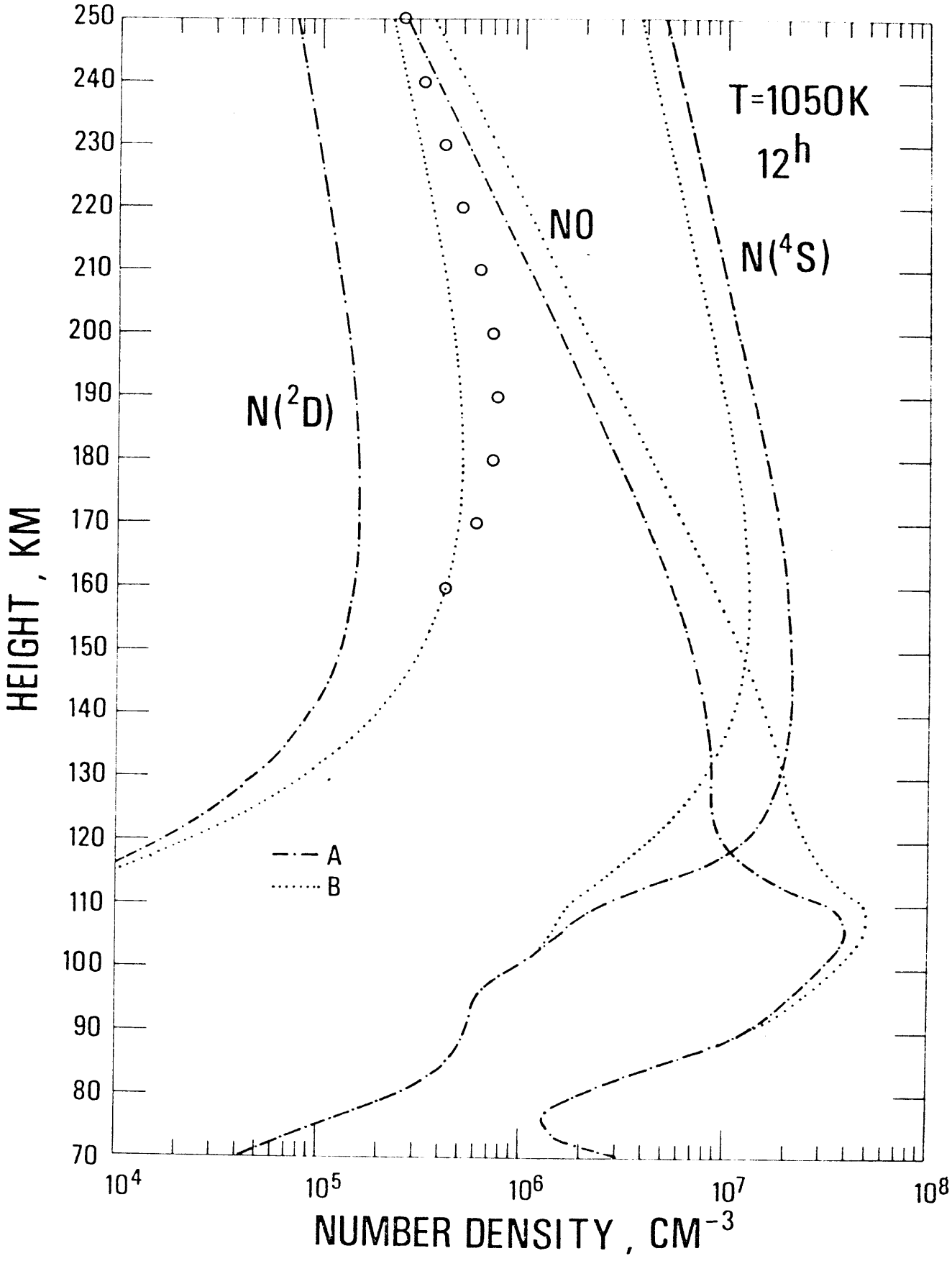

Fig. II.4 Altitude profiles of $N(^2D)$, $N(^4S)$, and NO at noon for the cases A and B. Case A: $k_3 = 8.5 \times 10^{-12} \exp(-500/T)$ $cm^3 s^{-1}$, and case B: $k_3 = 1.0 \times 10^{-12}$ $cm^3 s^{-1}$ at all altitudes. $T_\infty = 1050$ K.

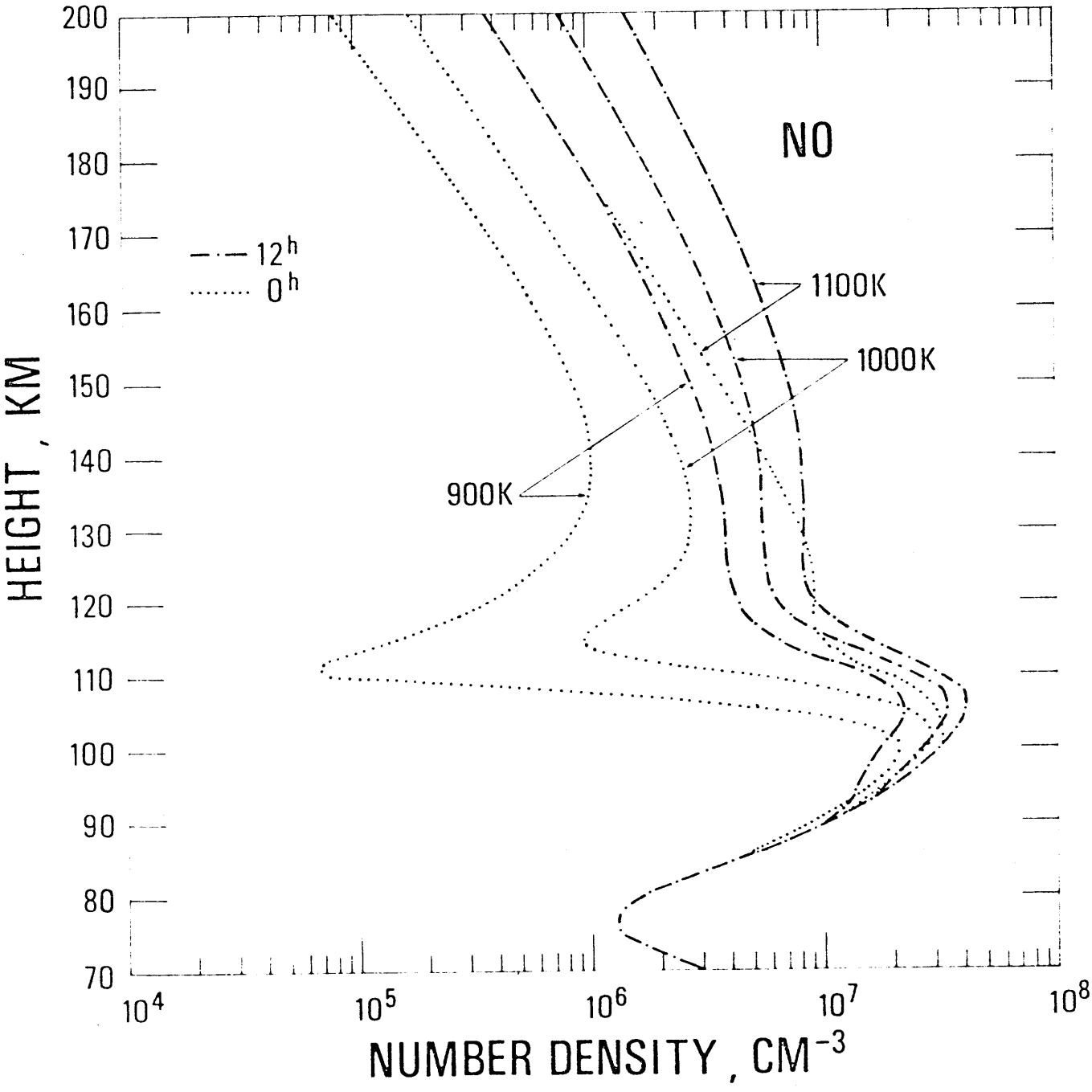

Fig. II.5 Altitude profiles of NO at noon and midnight for T_{max} = 900, 1000, and 1100 K.

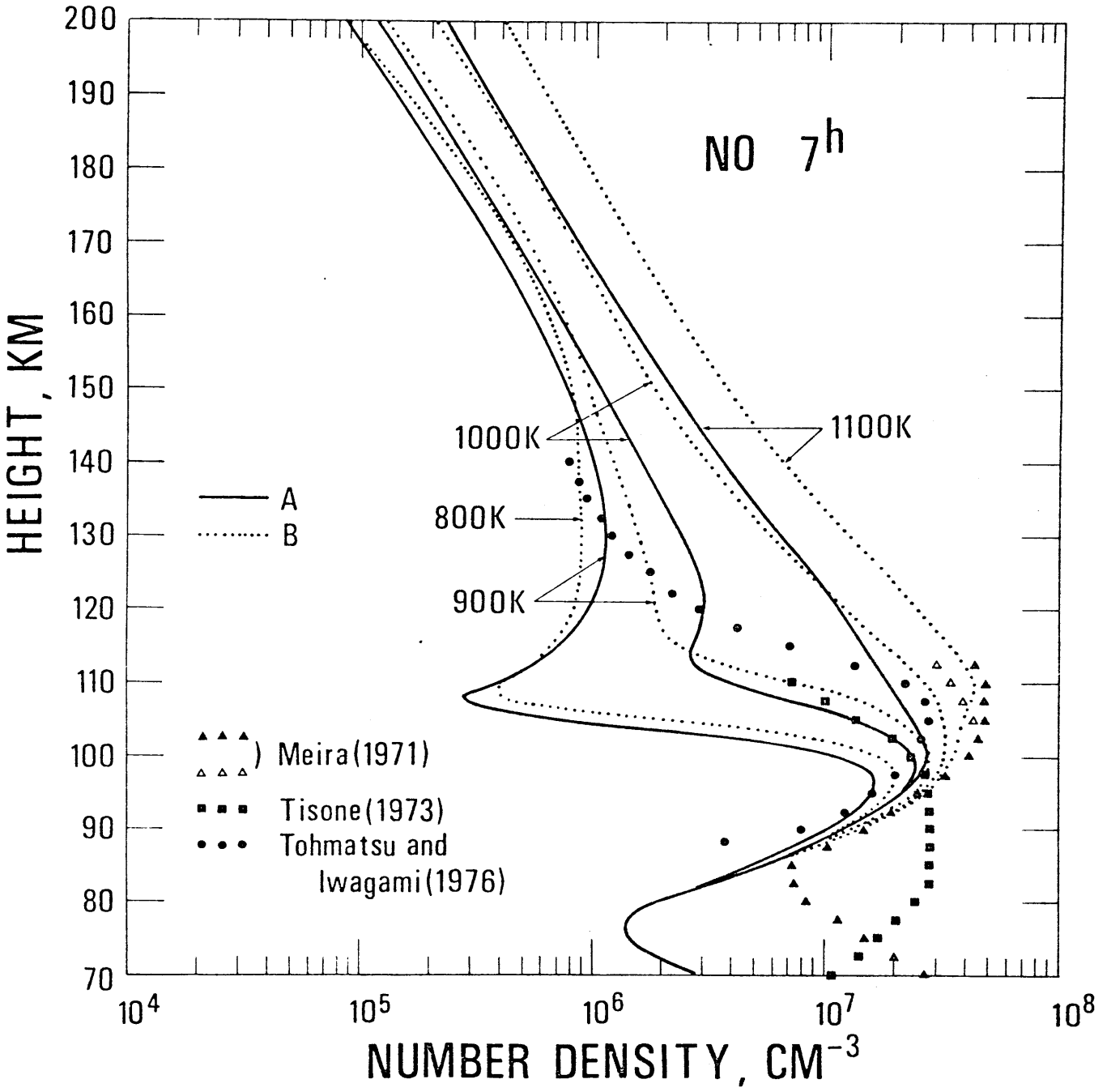

Fig. II.6 Comparison of the calculated distributions at 07 h LT for the cases A and B with the observed. The calculated profile for T_{max} = 800 K (case B) is included.

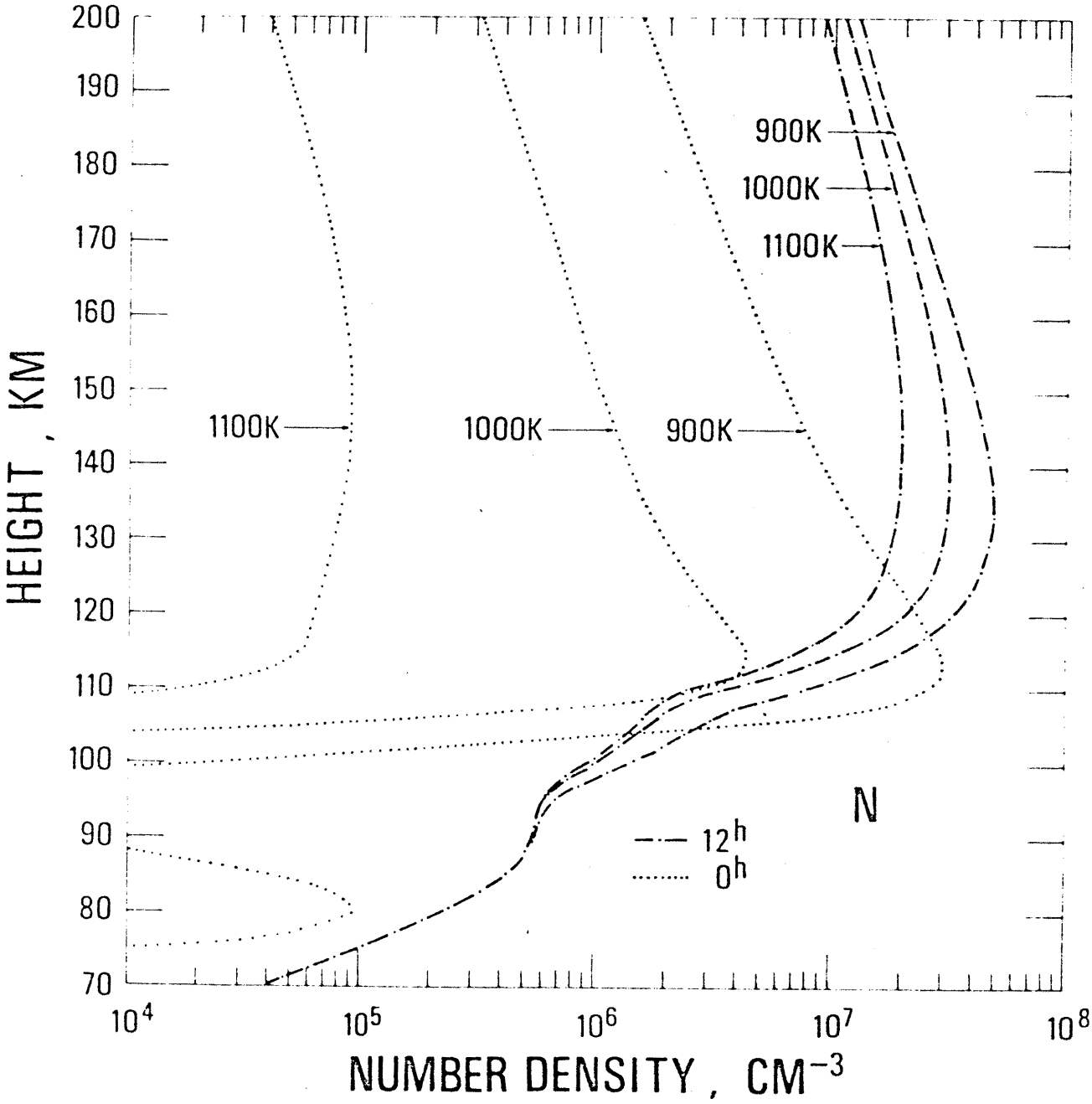

Fig. II.7 Altitude profiles of N(^{4}S) at noon and midnight for T_{max} = 900, 1000, and 1100 K.

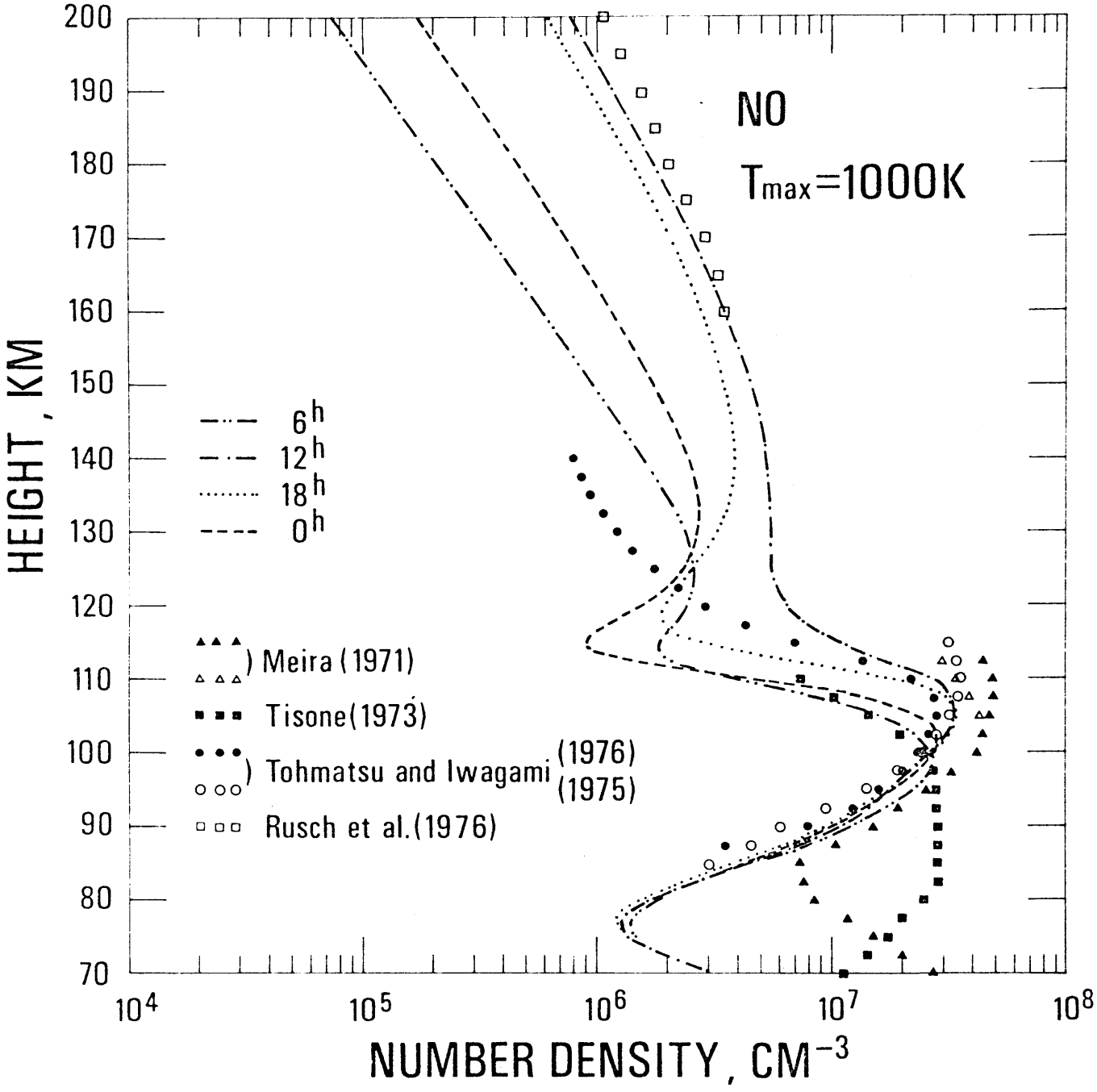

Fig. II.8 Comparison of the calculated and observed NO densities at various local times. T_{max} = 1000 K.

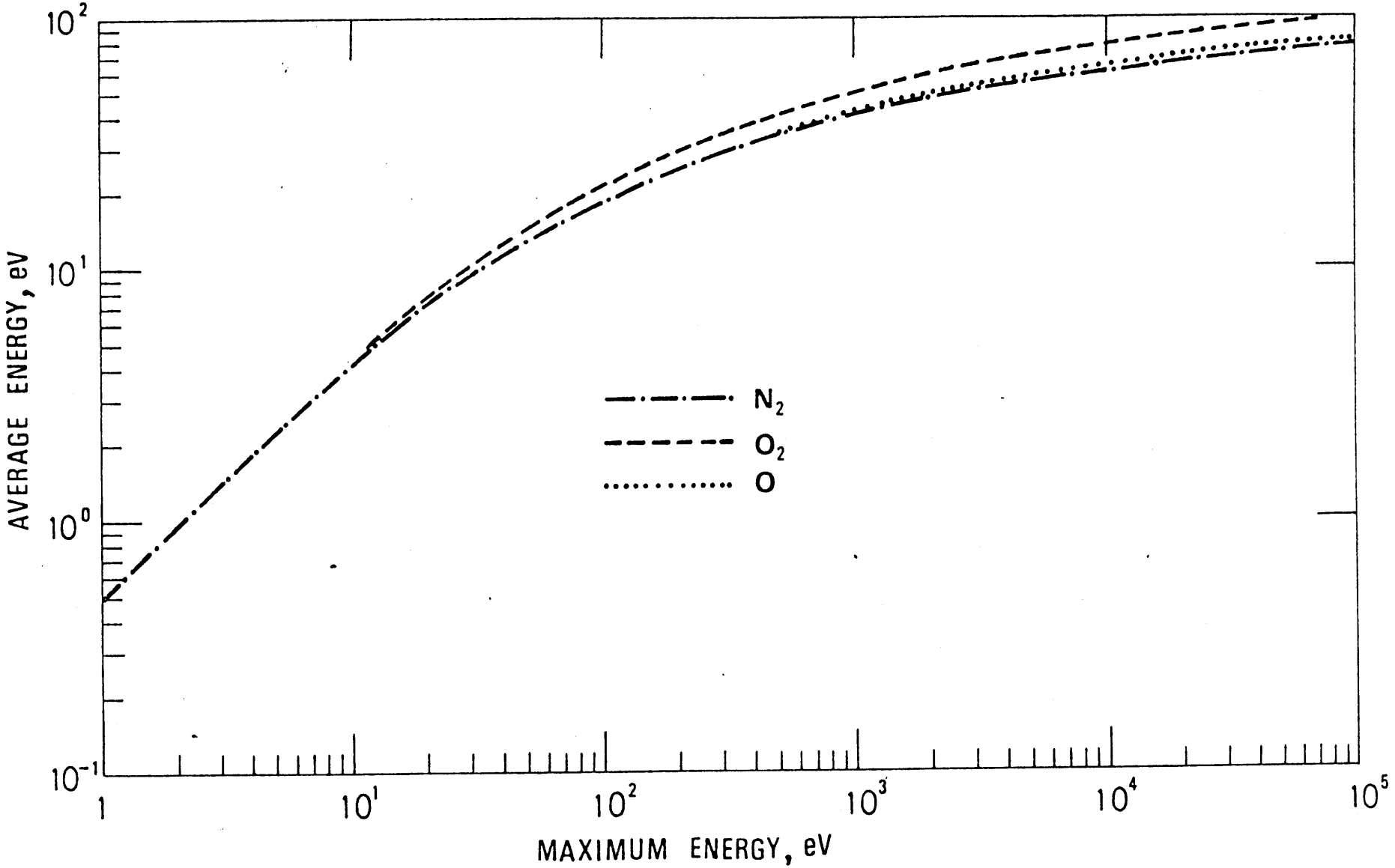

Fig. III.1 Average energy of secondary electrons as a function of the probable maximum energy of secondary electrons.

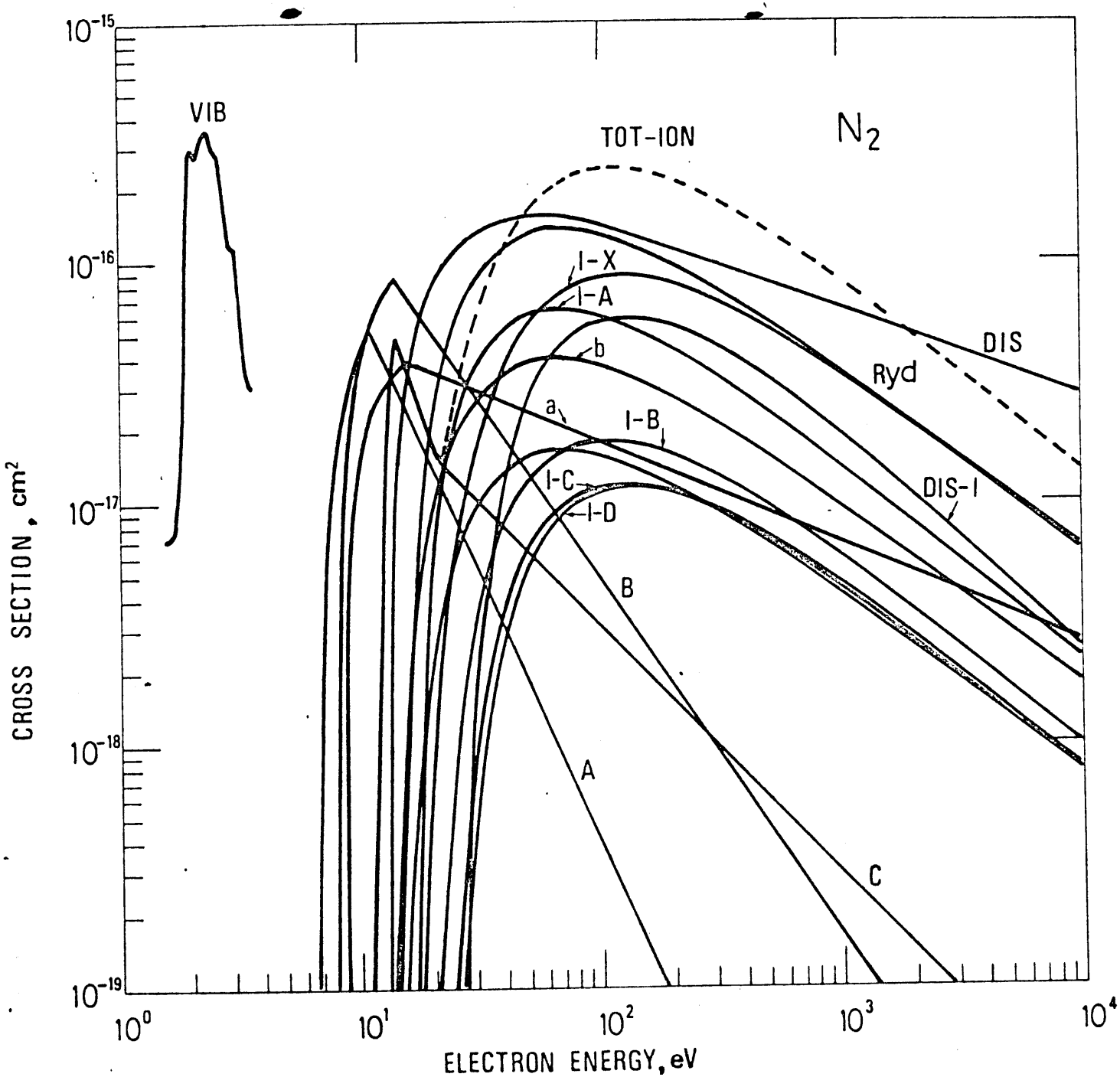

Fig. III.2a Electron collision cross section with N_2.

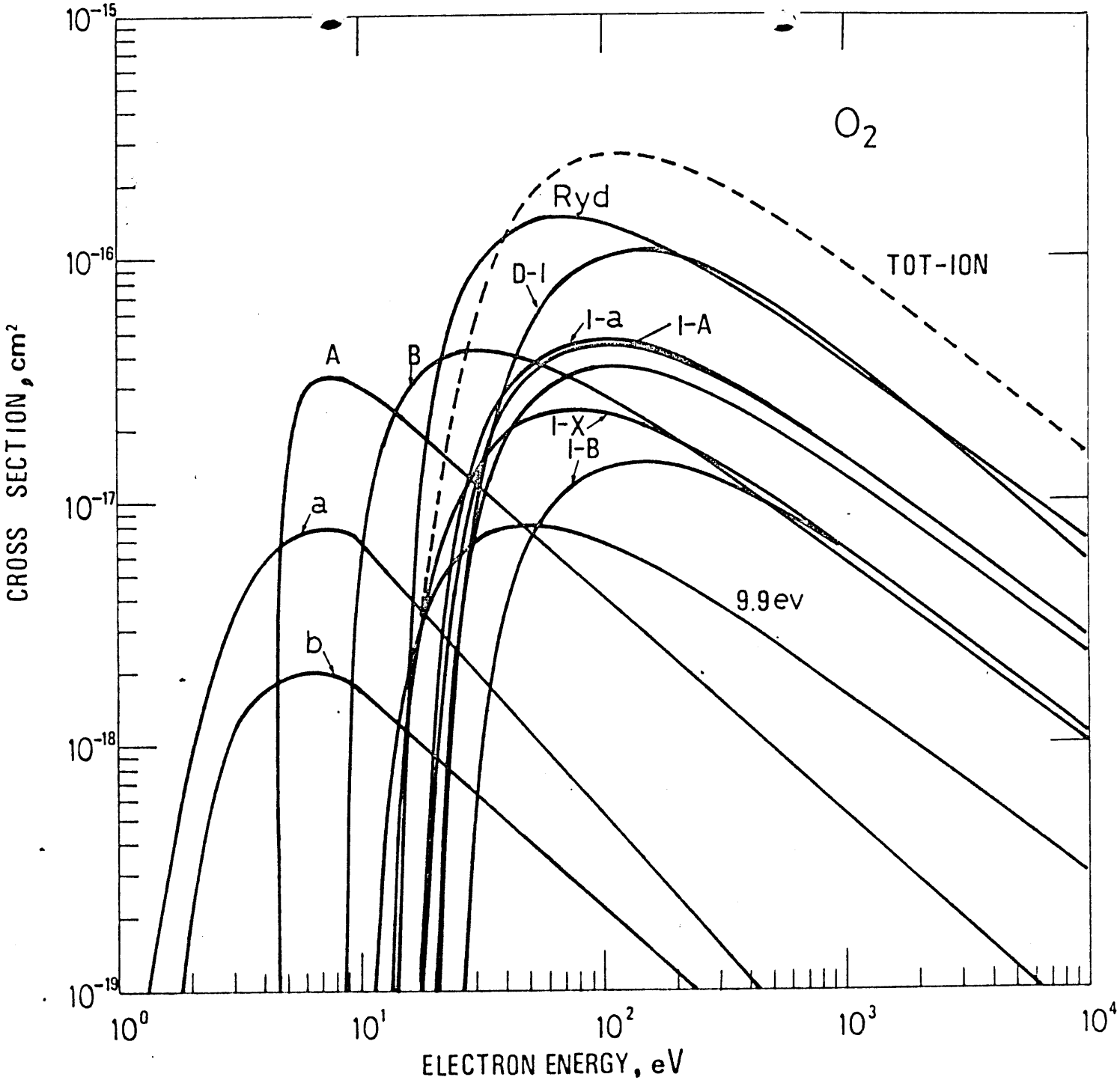

Fig. III.2b Electron collision cross section with O_2.

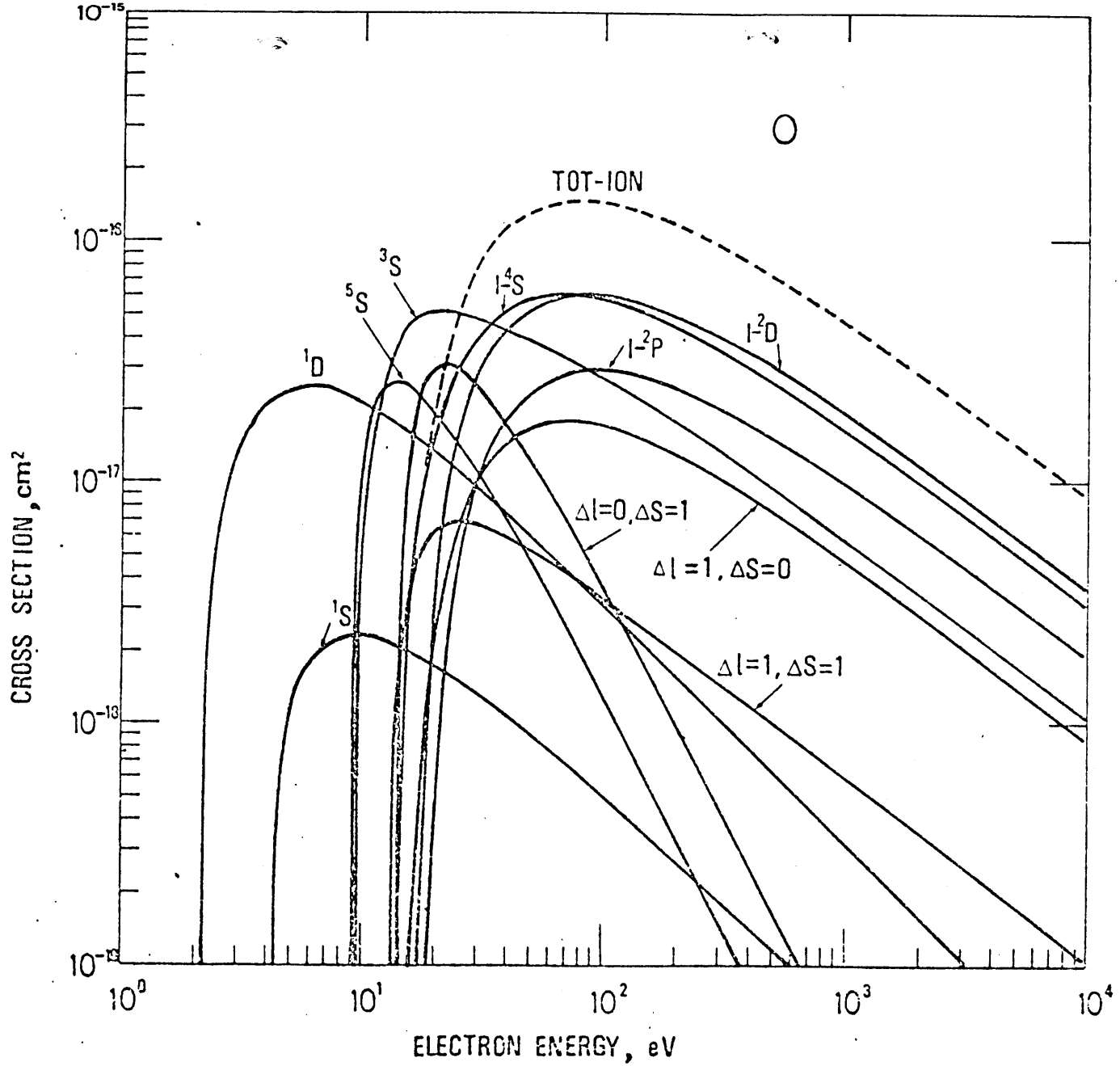

Fig. III.2c Electron collision cross section with O.

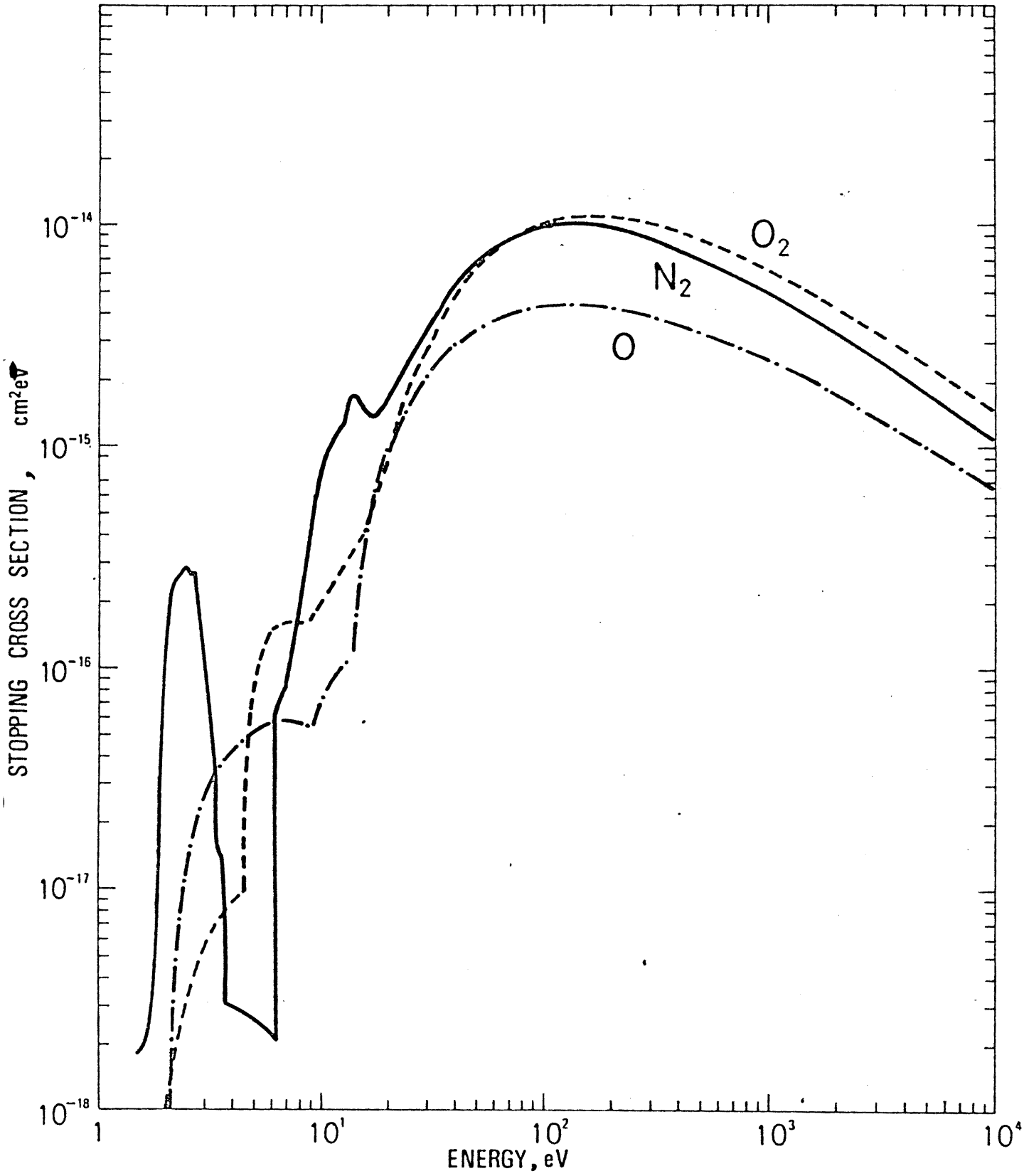

Fig. III.3 Electron stopping cross section for N_2, O_2, and O.

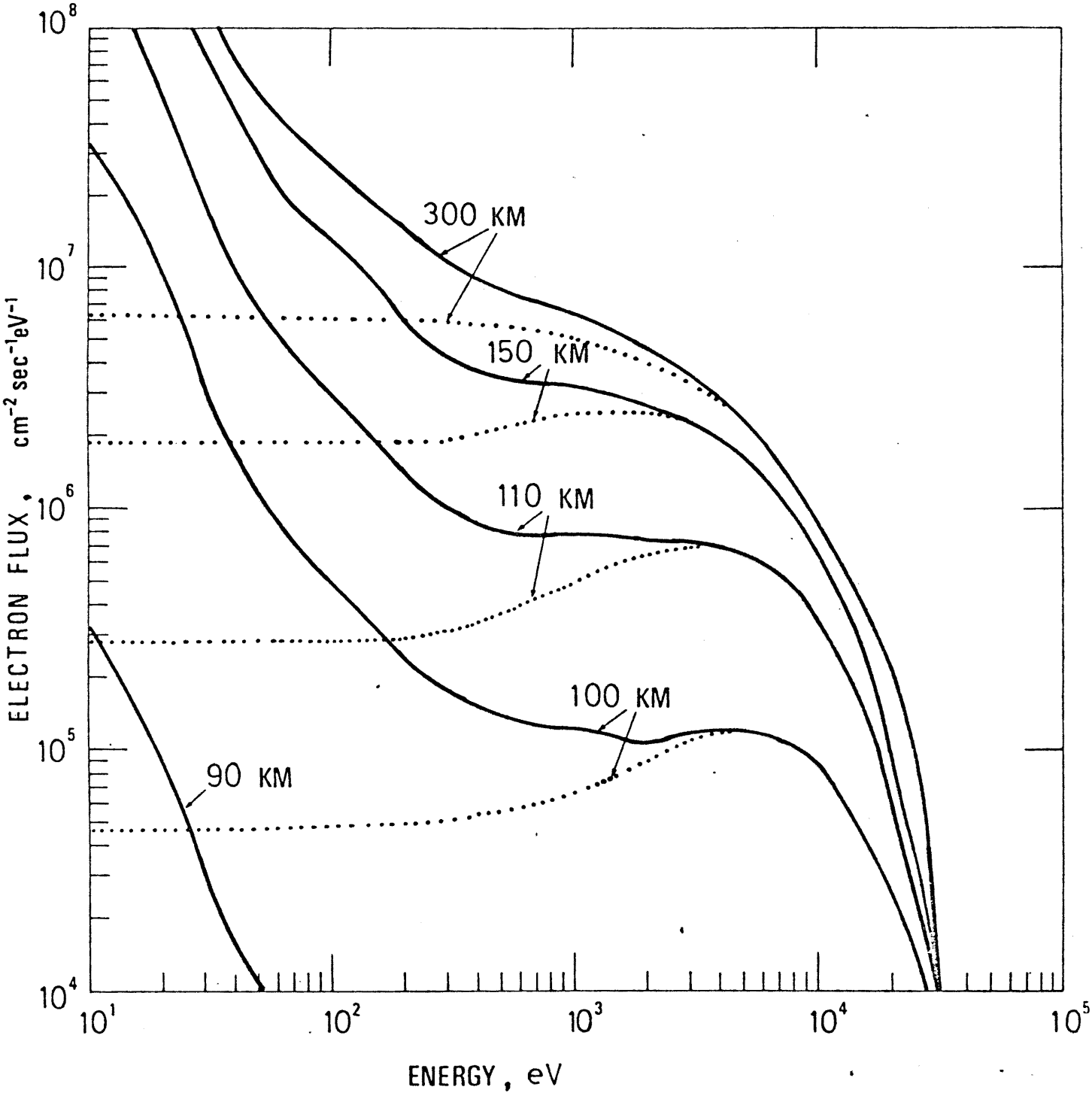

Fig. III.4 Electron fluxes at various heights calculated for the incident flux $1 \times 10^6 \exp(-E/5)$. Solid curves represent total fluxes, and dotted curves primary fluxes.

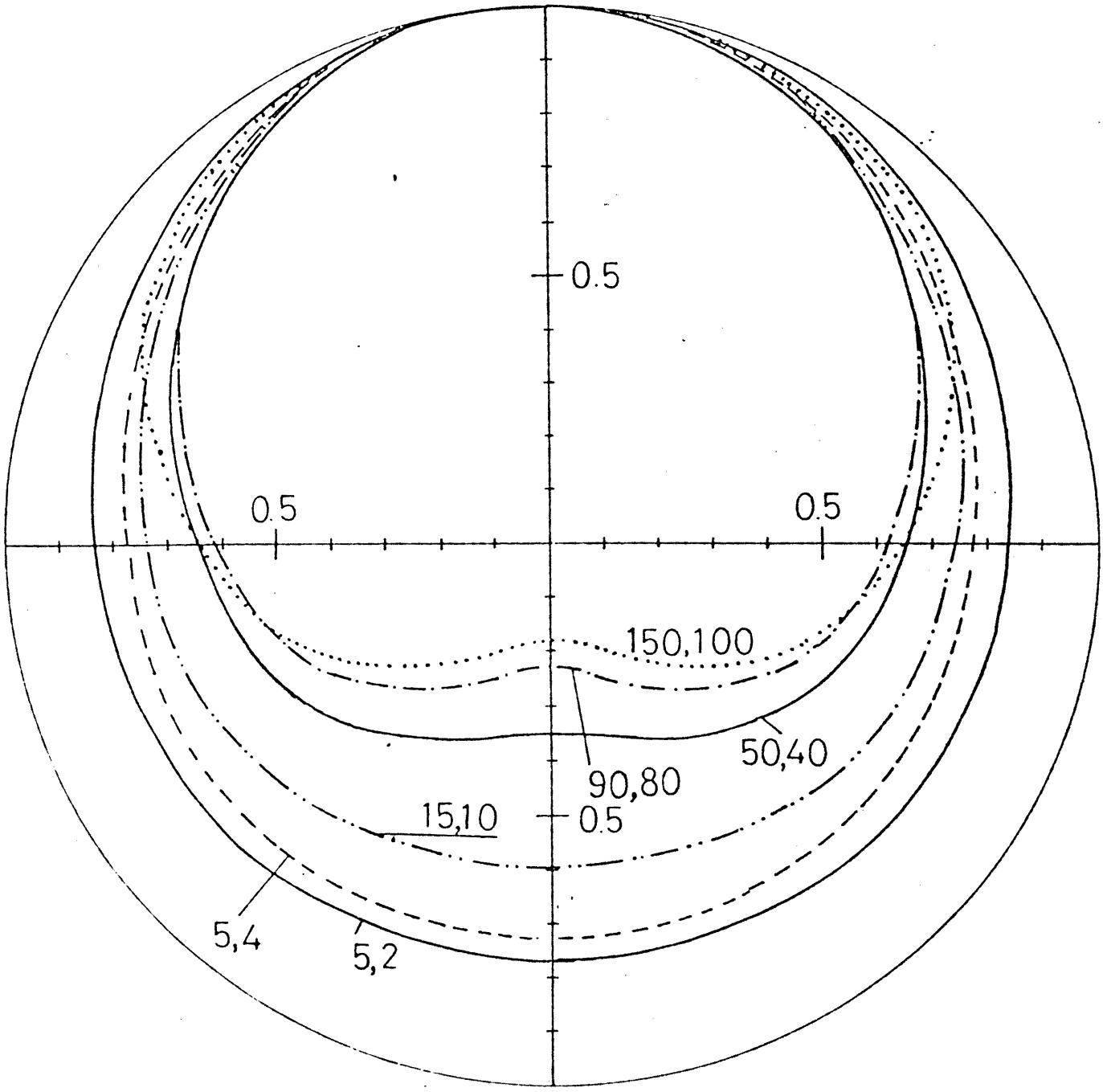

Fig. III.5 Angular dependence of the emission rate of the Bremsstrahlung X-ray for atomic nitrogen (Z =7). The direction of electron motion is assumed to be isotropic with respect to the downward hemisphere. The values given to each curve such as (15,10) represents the energies of the electron and the photon in keV.

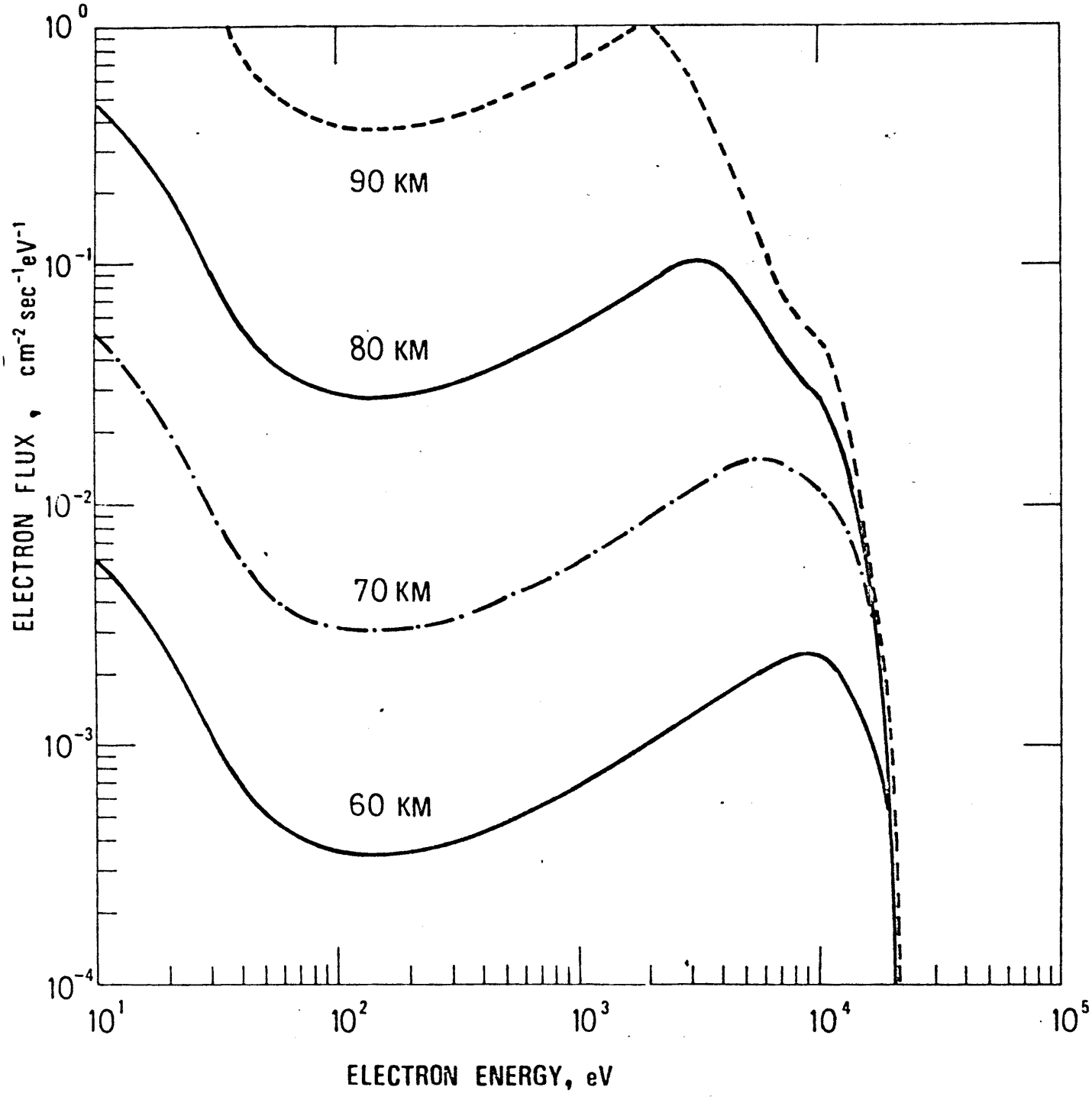

Fig. III.6 Total electron fluxes at various heights produced by the Bremsstrahlung X-ray calculated for the incident electron flux $1x10^6 exp(-E/5)$.

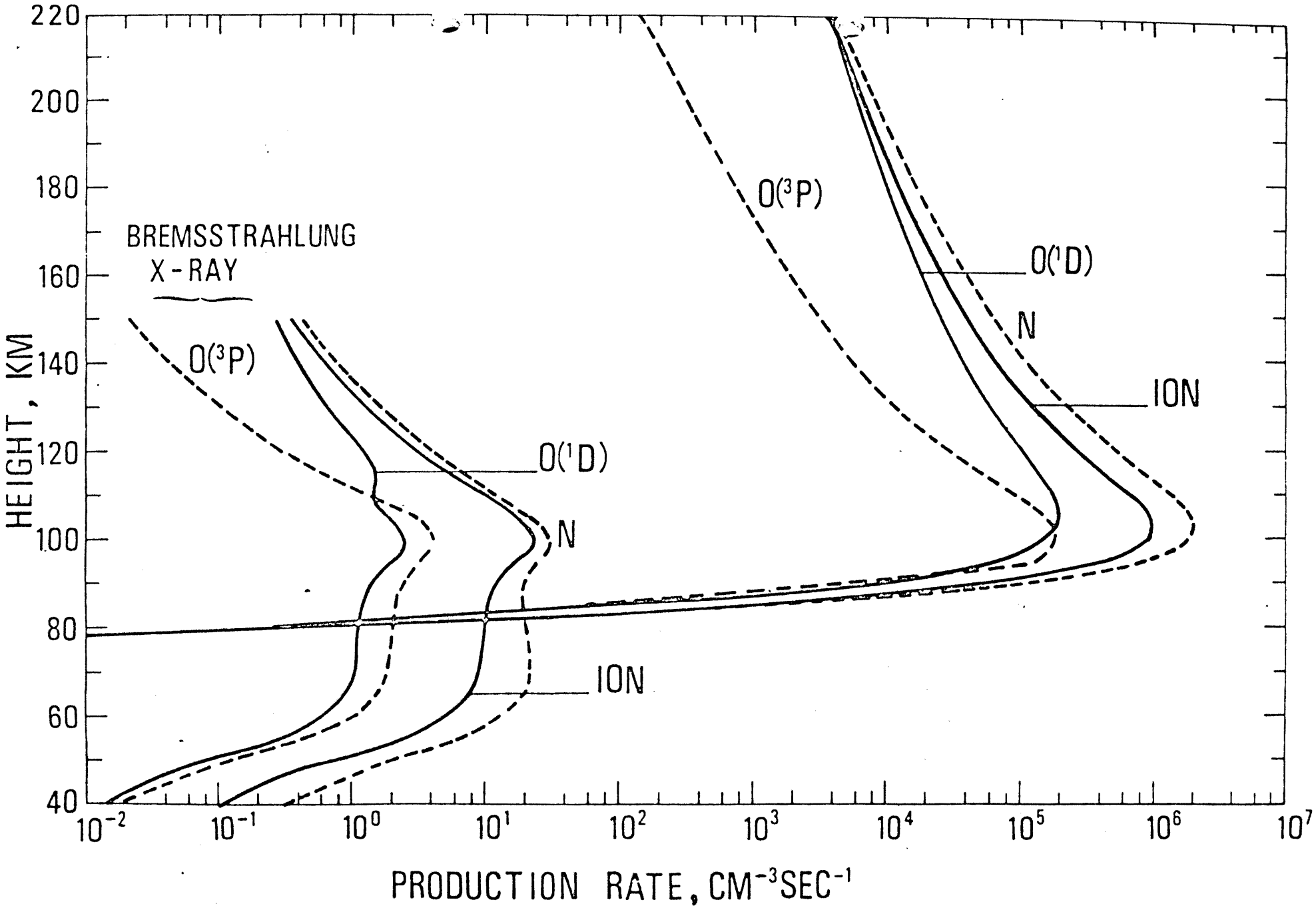

Fig. III. 7a Production rates of $O(^3P)$, $O(^1D)$, total N, and total ions for case A of the precipitating electron flux. Curves in the lower left represent those produced by the effect of Bremsstrahlung X-ray.

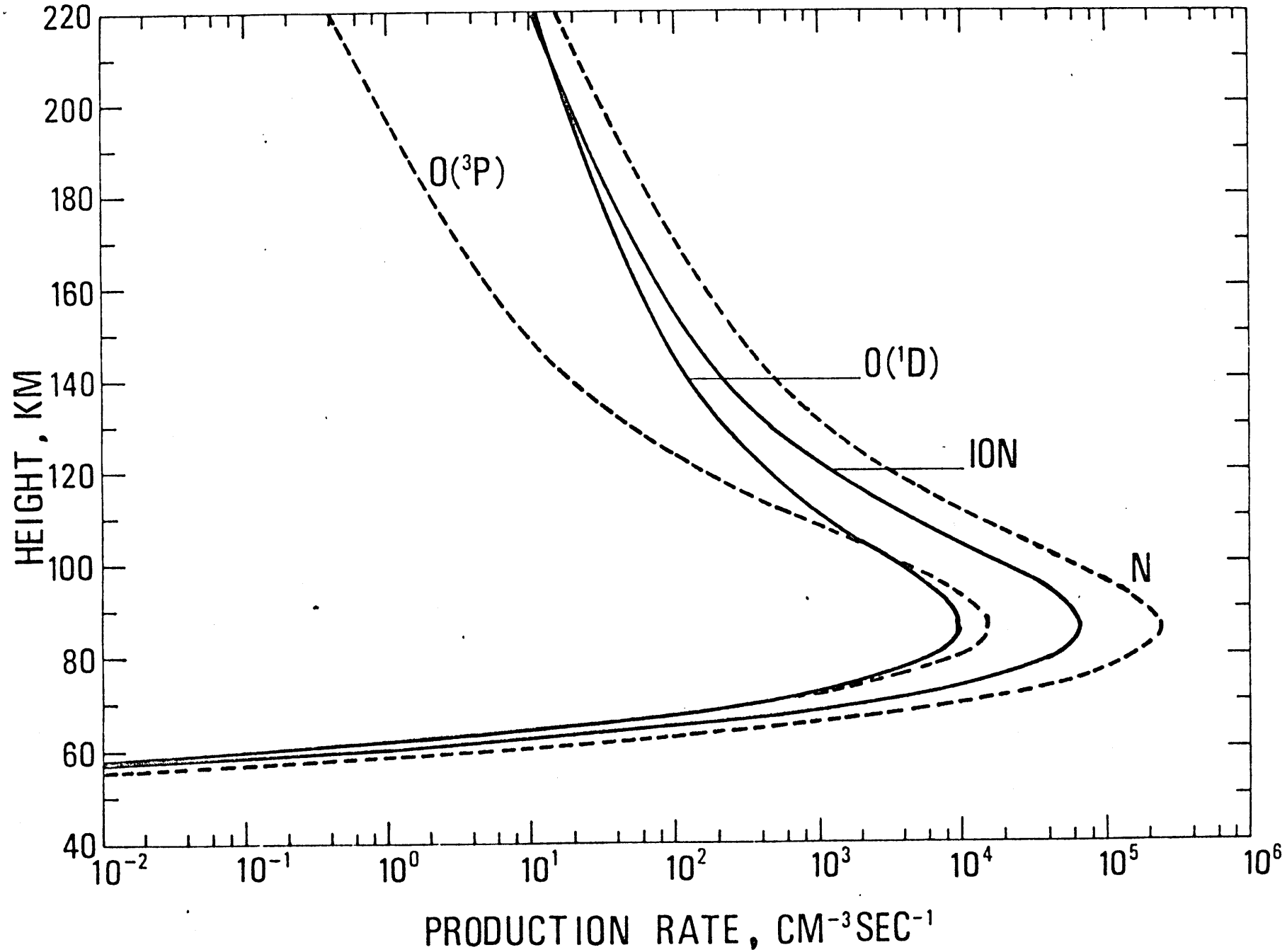

Fig. III. 7b As in Fig. III.7a but for case C of the precipitating electron flux.

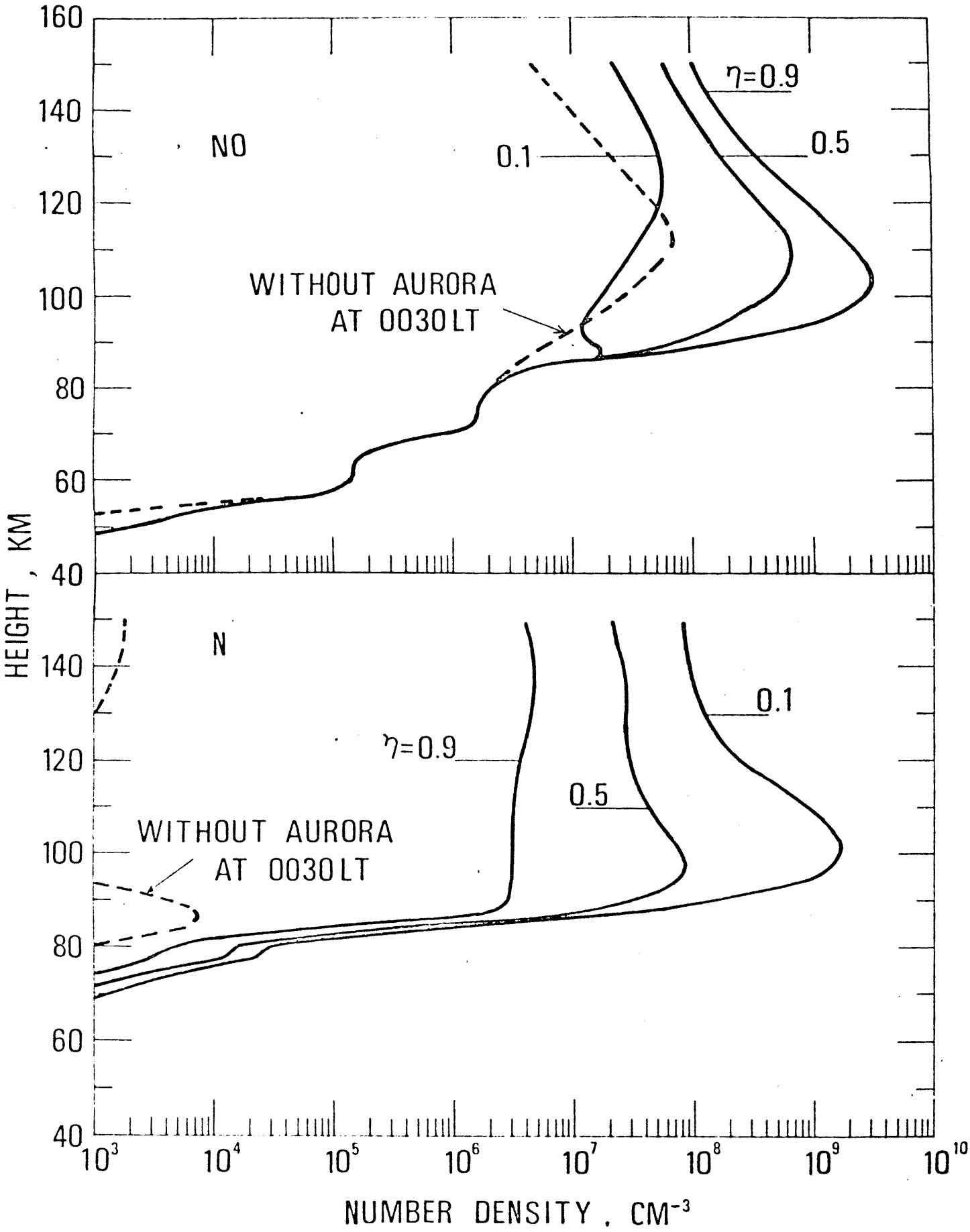

Fig. III.8 N and NO height distributions for various values of N(^{2}D) quantum yield in the electron impact dissociation of N_2, calculated for 0030 LT (i.e., after 30 minutes duration of the precipitation). and for the electron flux case A. - Height profiles of N and NO at 0030 LT under the non-auroral condition are also dipicted by dashed curves.

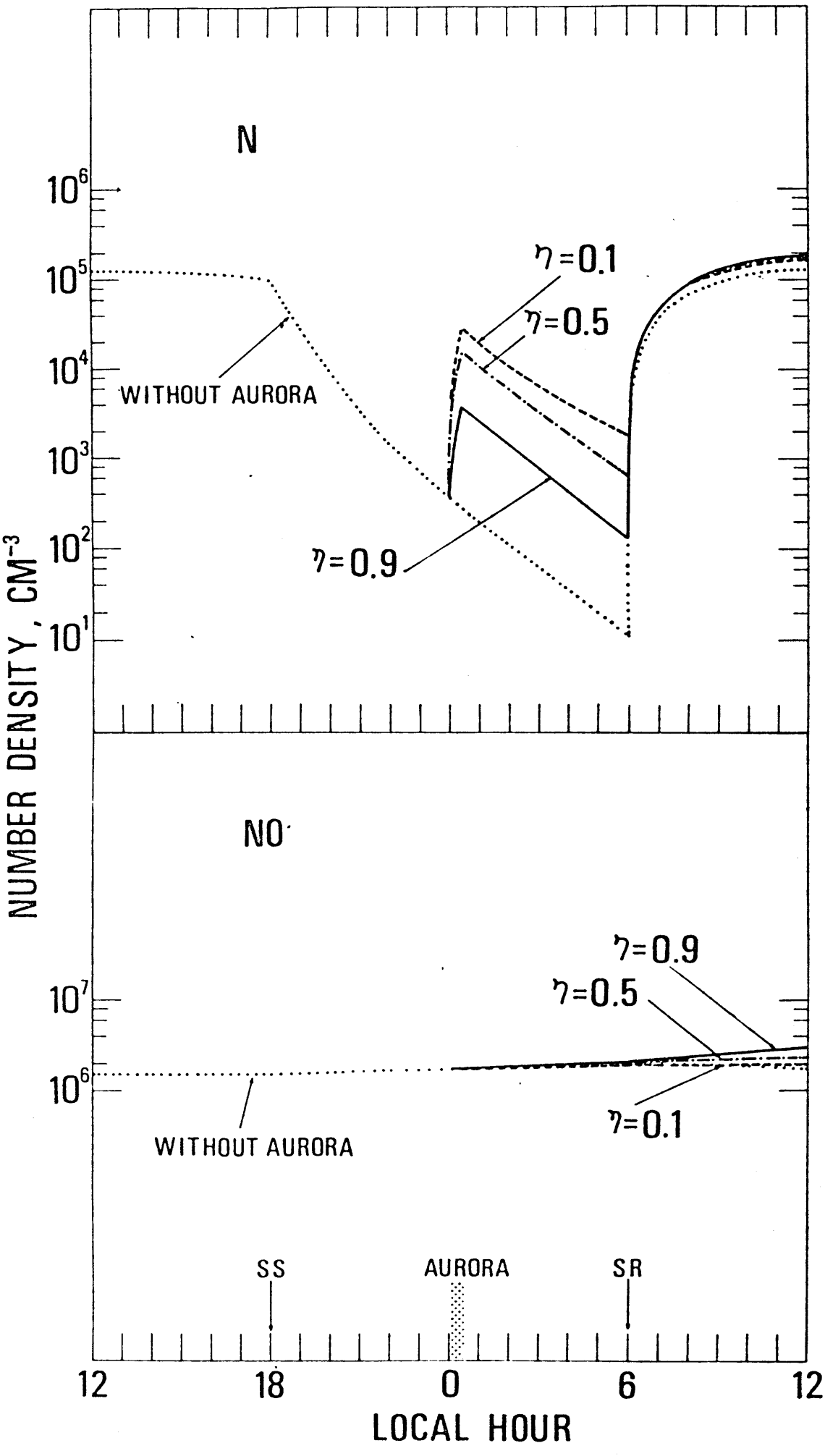

Fig. III.9a Diurnal variations of N and NO densities at 80 km, with and without auroral perturbation, and for various values of $N(^2D)$ quantum yield in the electron impact dissociation of N_2. The precipitation occurs for 0000-0030 LT, and with the flux case A.

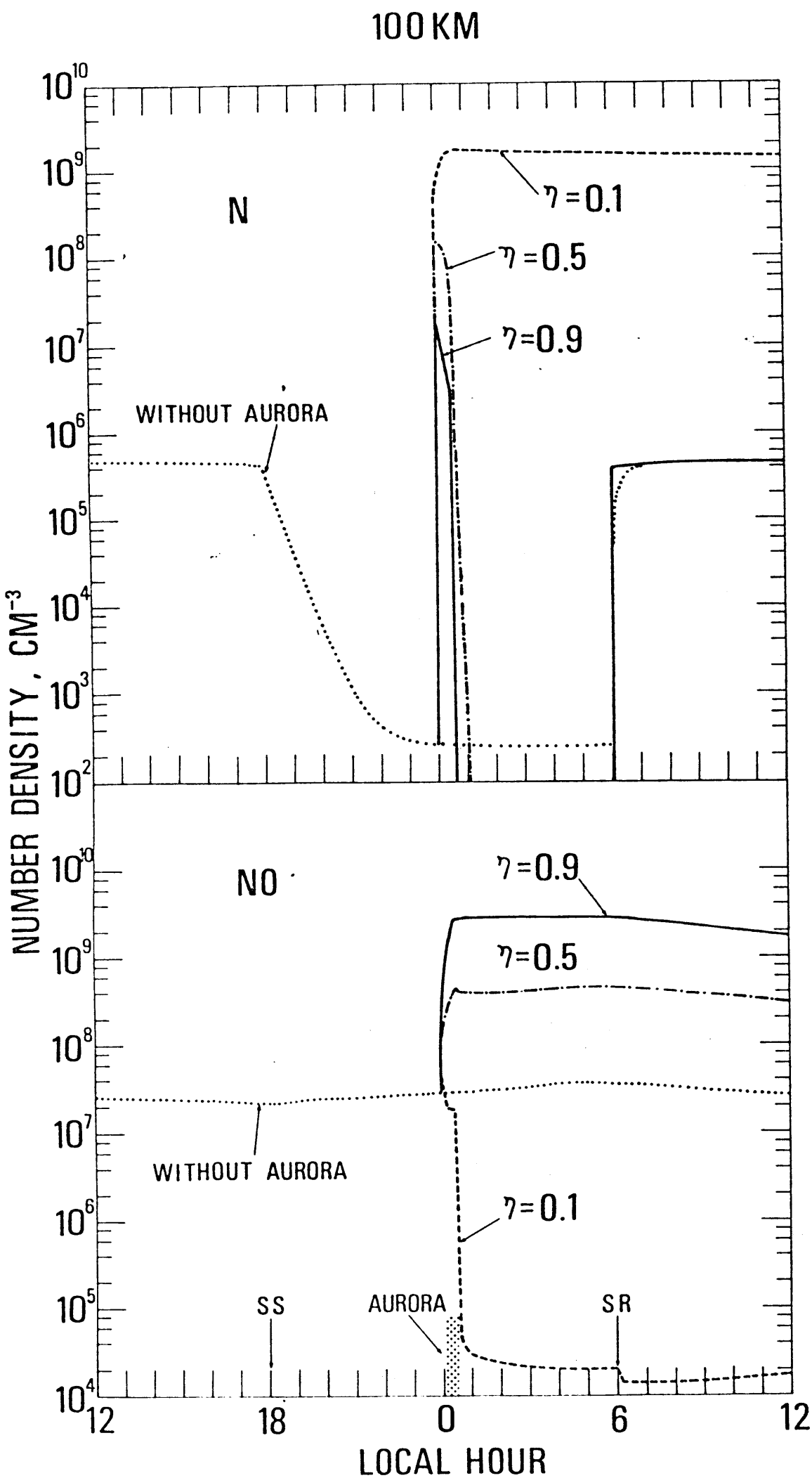

Fig. III.9b As in Fig. III.9a but at 100 km.

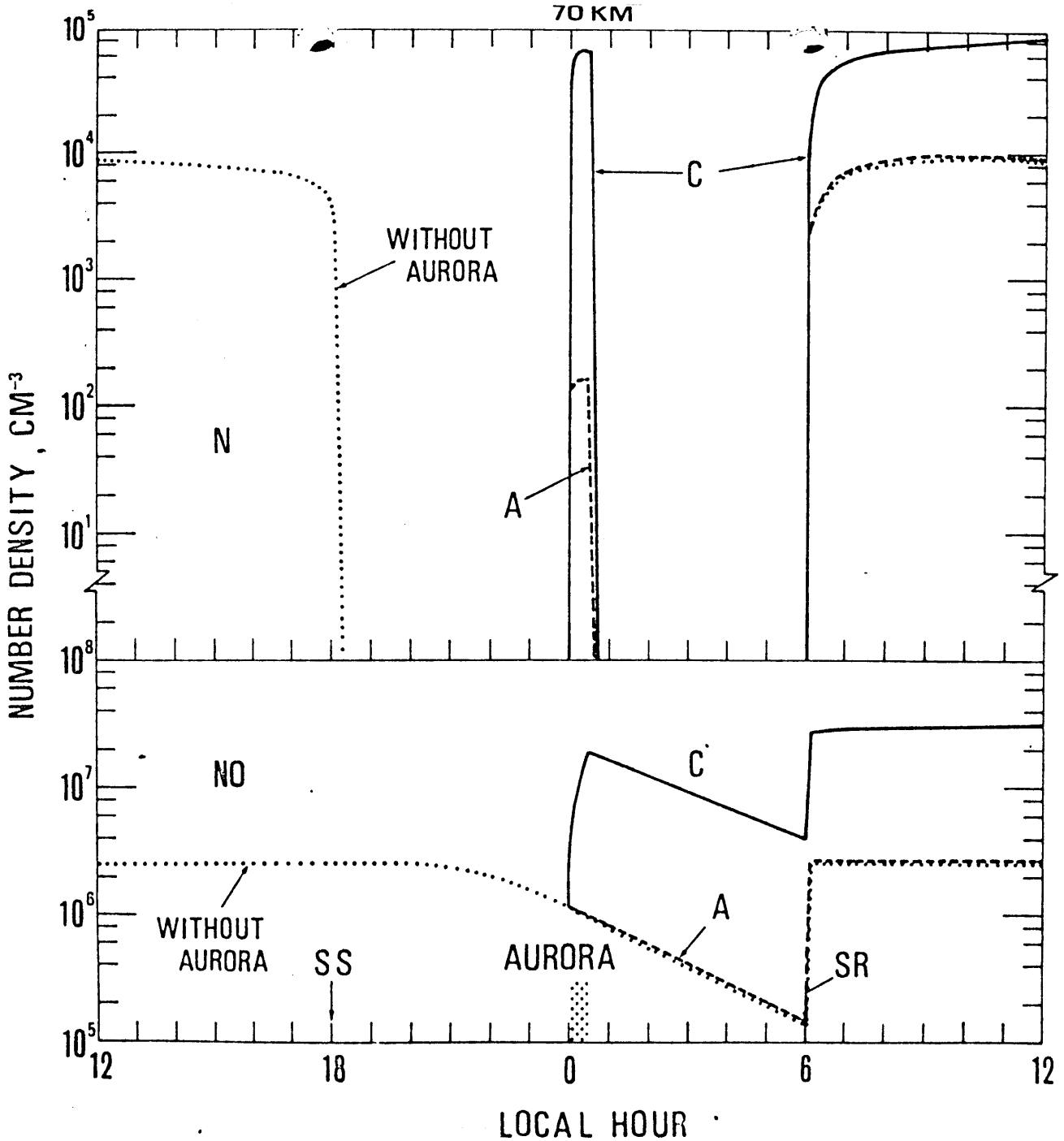

Fig. III.10a Comparison of the diurnal variations of N and NO densities at 70 km calculated for the electron fluxes case A and case C, and for a non-auroral day. η is assumed to be 0.9.

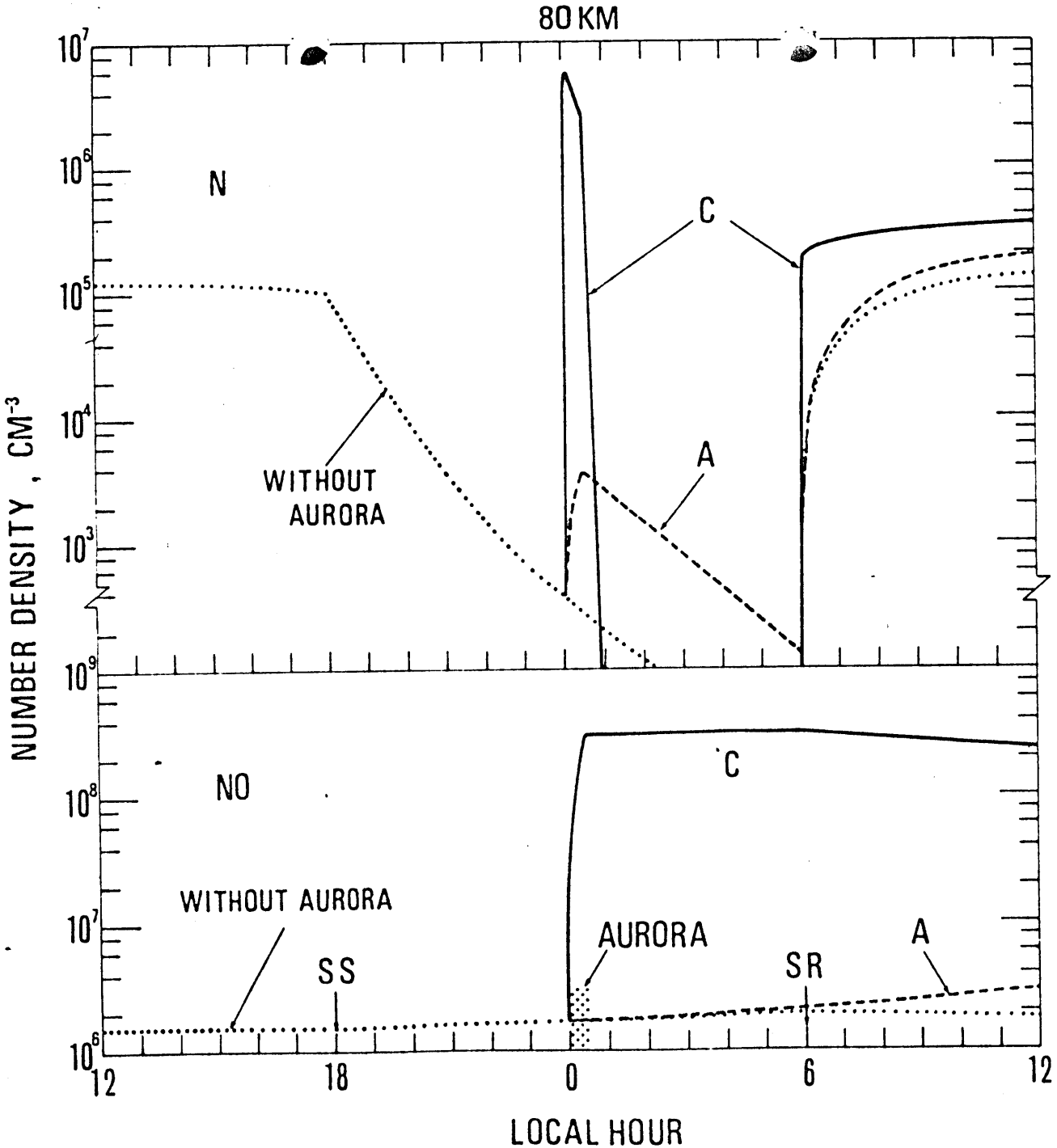

Fig. III.10b As in Fig. III.10a but at 80 km.

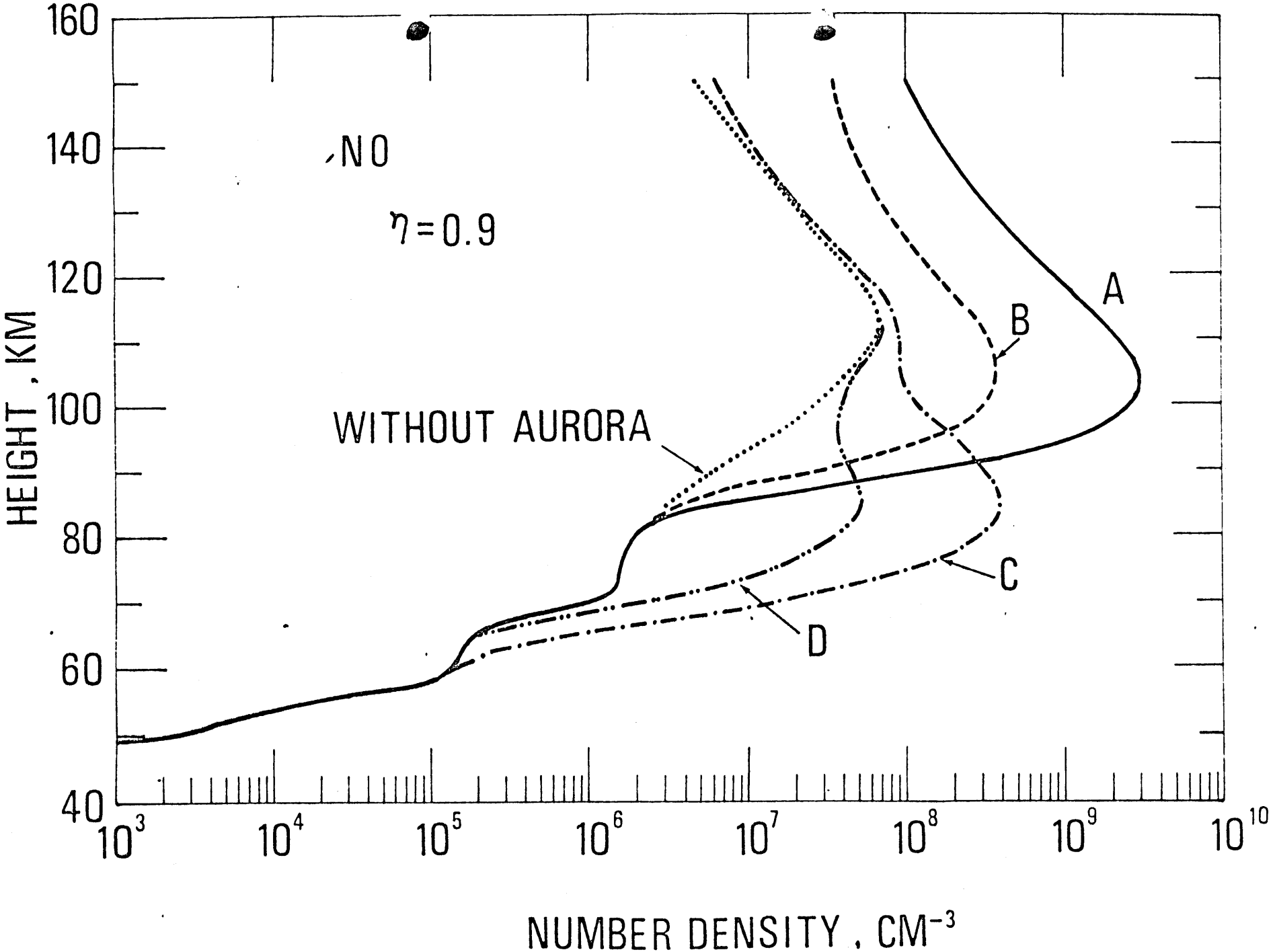

Fig. III.11 Height distribution of the NO density for various types of the electron influx and a non-influx case, after 30 minutes continuation of the electron precipitation, and in case of $\eta = 0.9$.

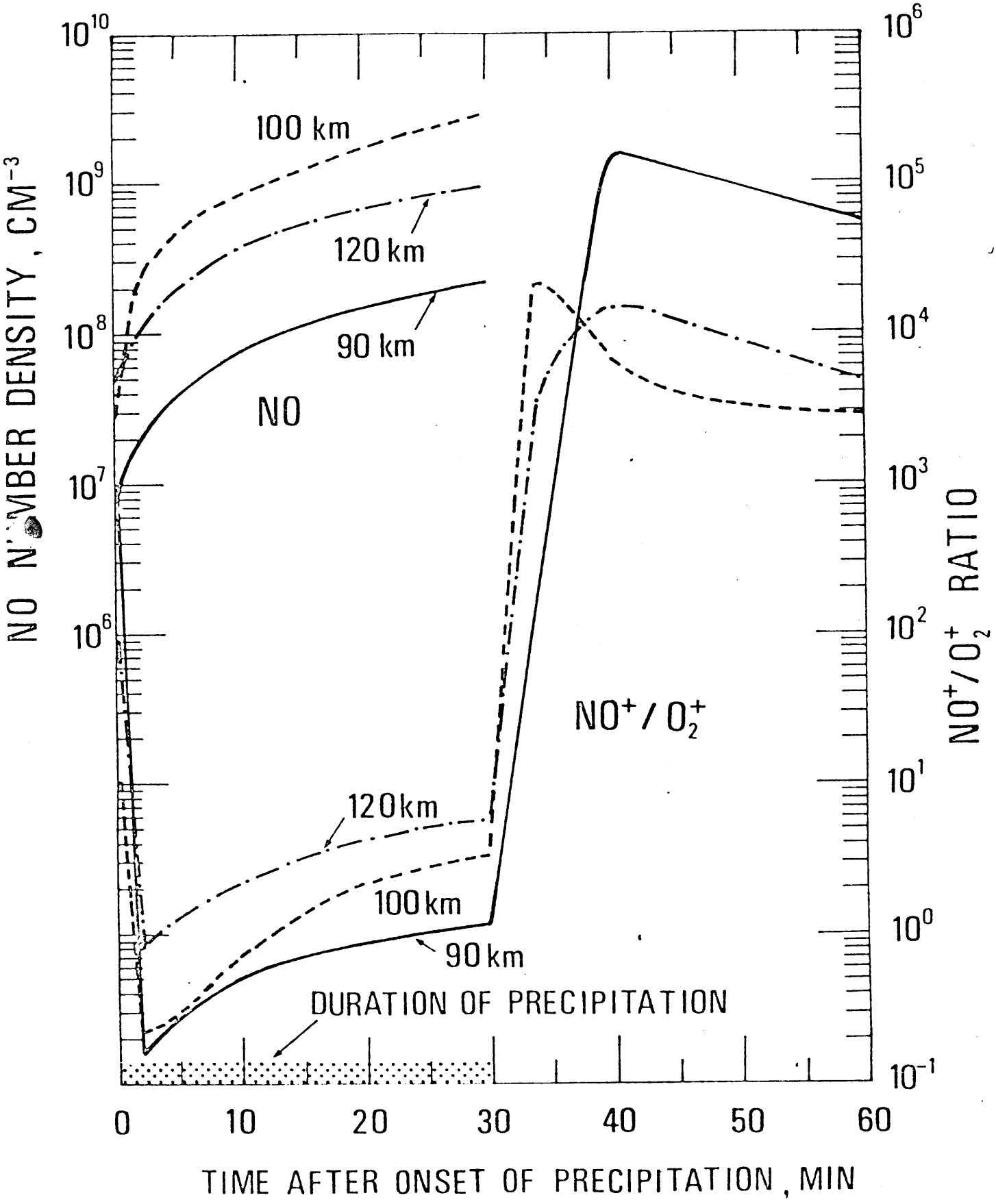

Fig. III.12 Temporal variation of $[NO^+]/[O_2^+]$ and [NO] at some chosen heights. The precipitation of the flux case A occurs during 0-30 min.

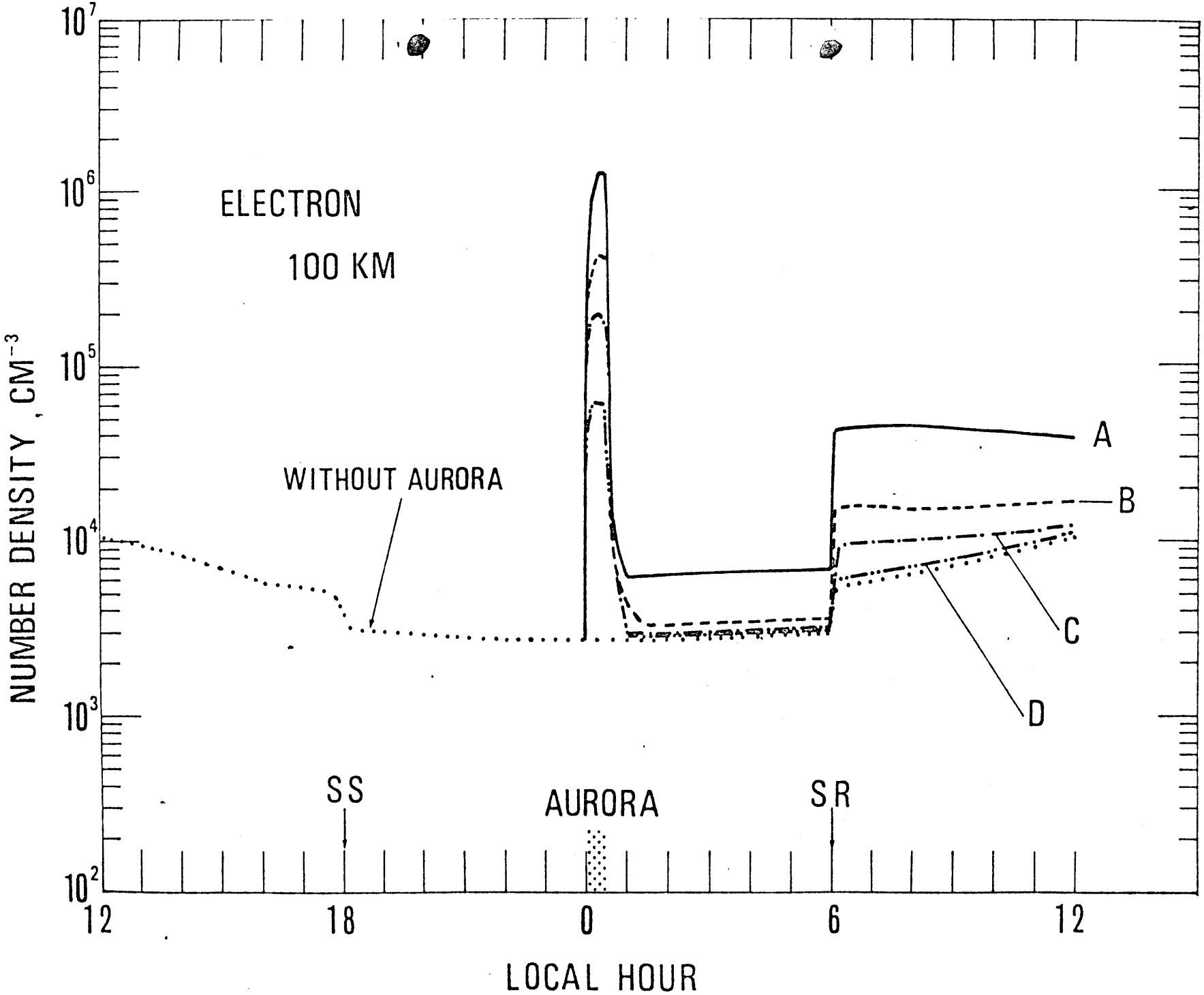

Fig. III.14b As in Fig. III.14a but at 100 km.

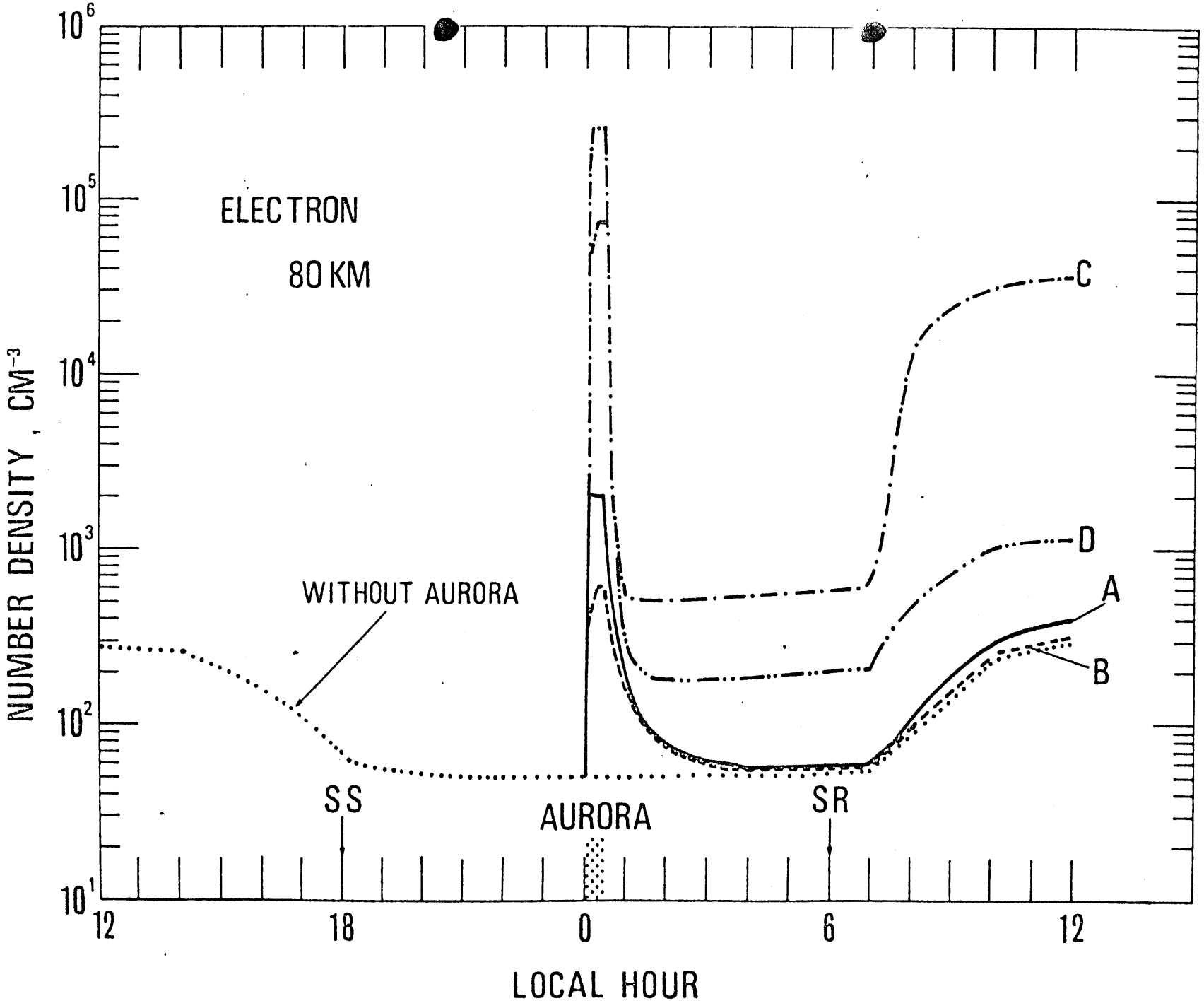

Fig. III.14a Diurnal variation of the electron density at 80 km for various spectra of precipitating electrons and for a non-auroral day.

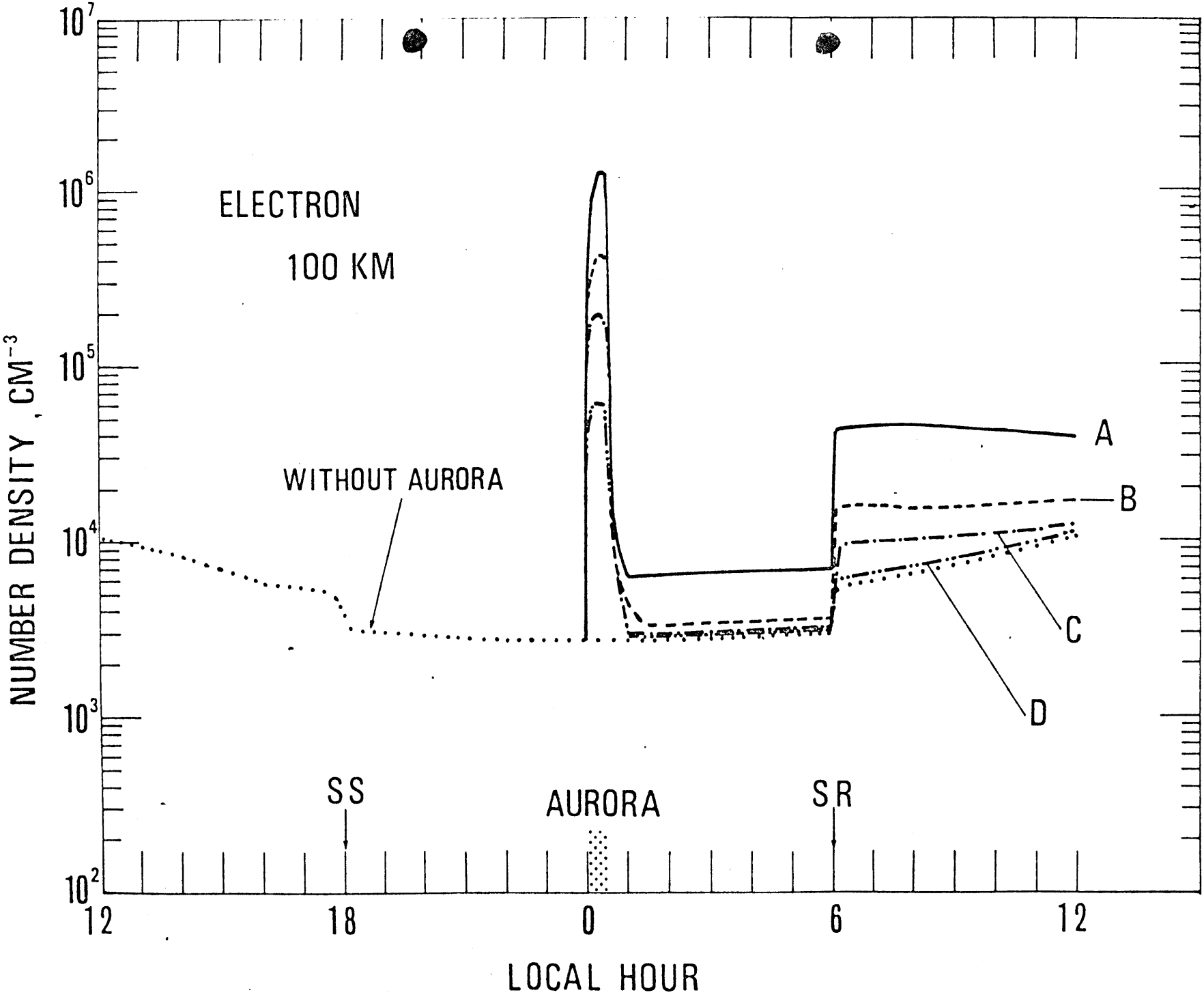

Fig. III.14b As in Fig. III.14a but at 100 km.

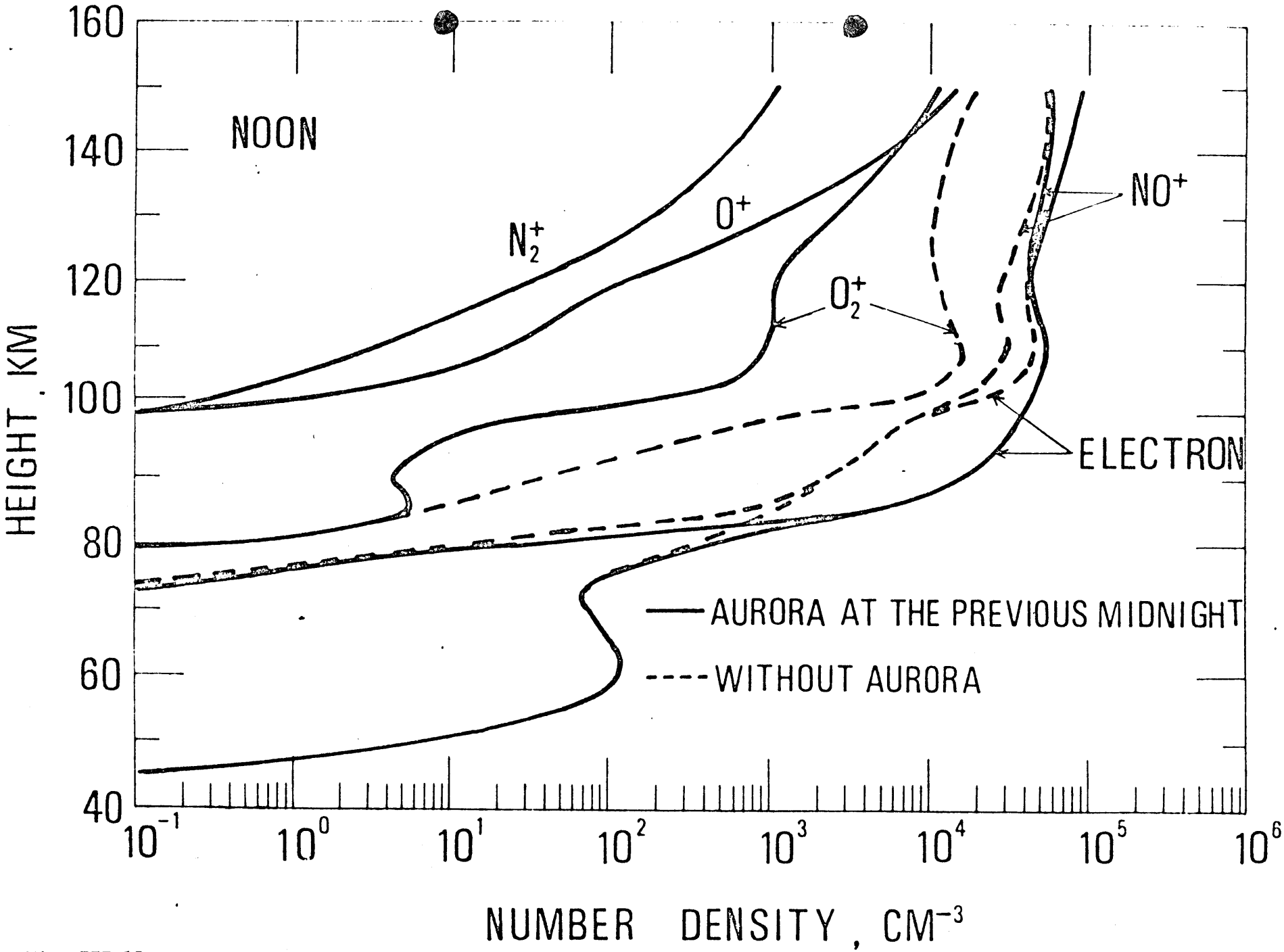

Fig. III.15 Comparison of ion compositions at noon for the case of the auroral perturbation at the previous midnight and for a non-auroral case. The precipitation occured with the flux case A during 0000-0030 LT.

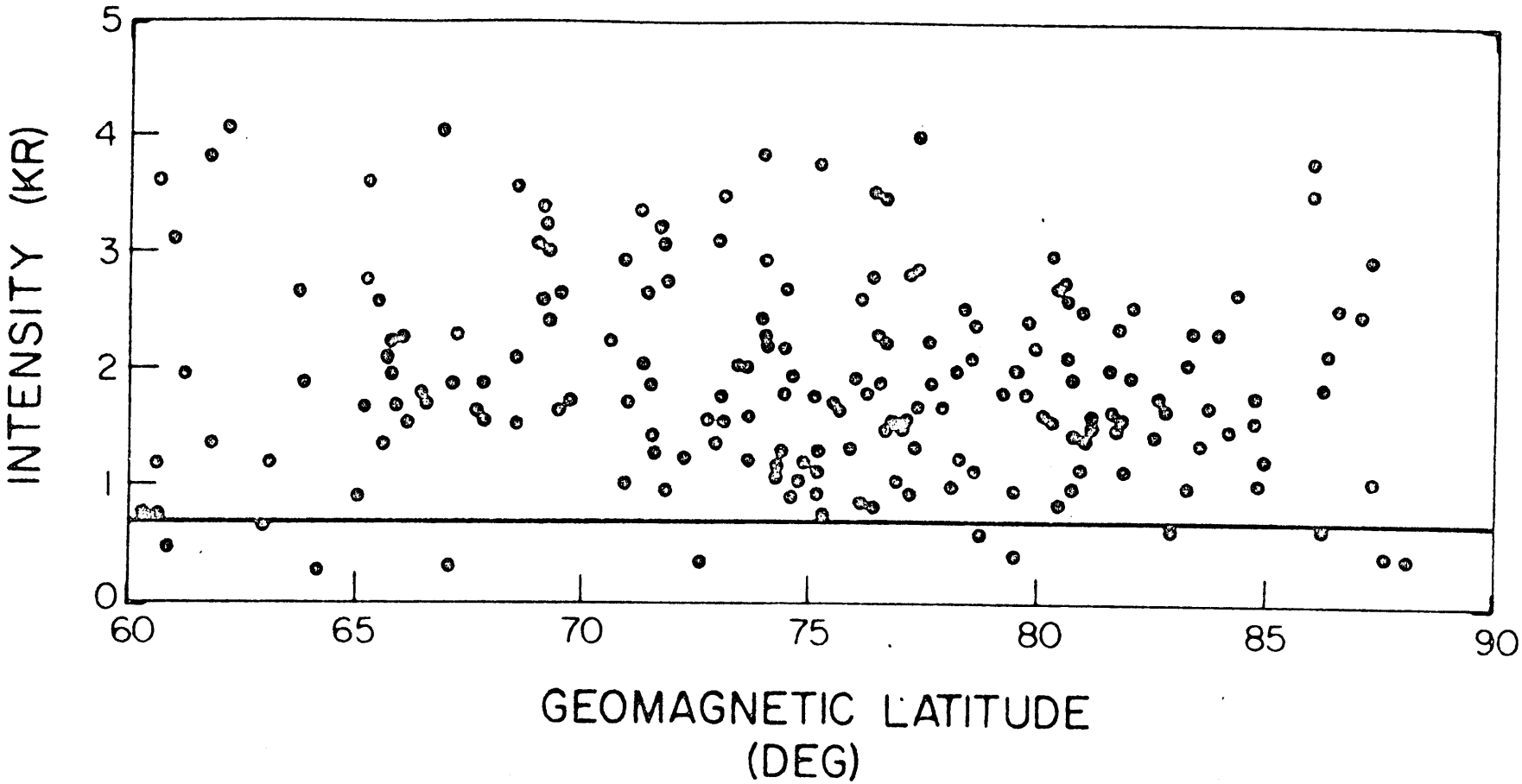

Fig. III.16 Column emission rate of the nitric oxide $\gamma(1,0)$ band as a function of geomagnetic latitude for solar zenith angles between 94° and 96°. The solid line is the average mid-latitude value of 0.75 kR.

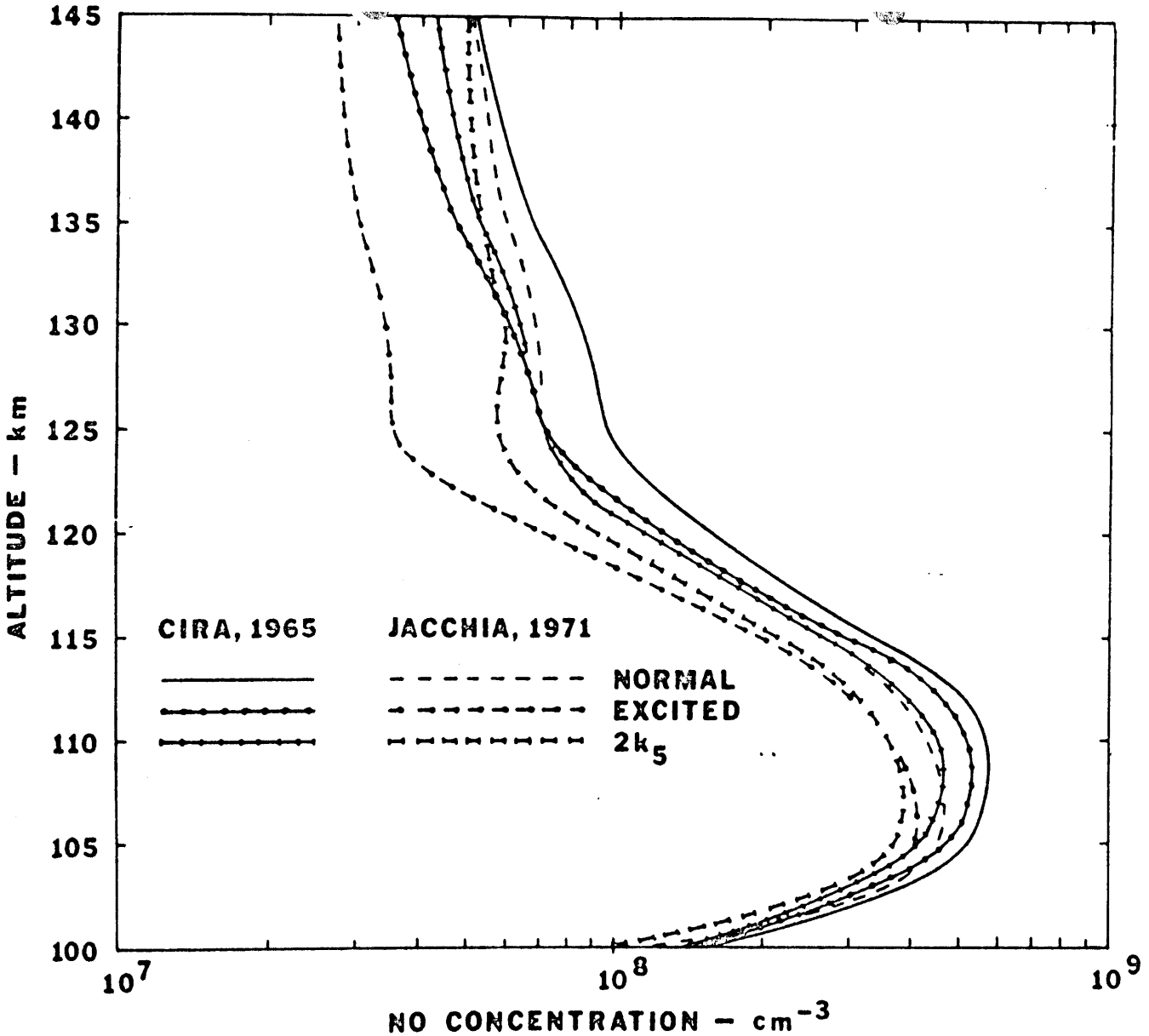

Fig. III.17 Nitric oxide concentrations deduced from the ion composition measurements using two different atmospheric models plus three variations per model.

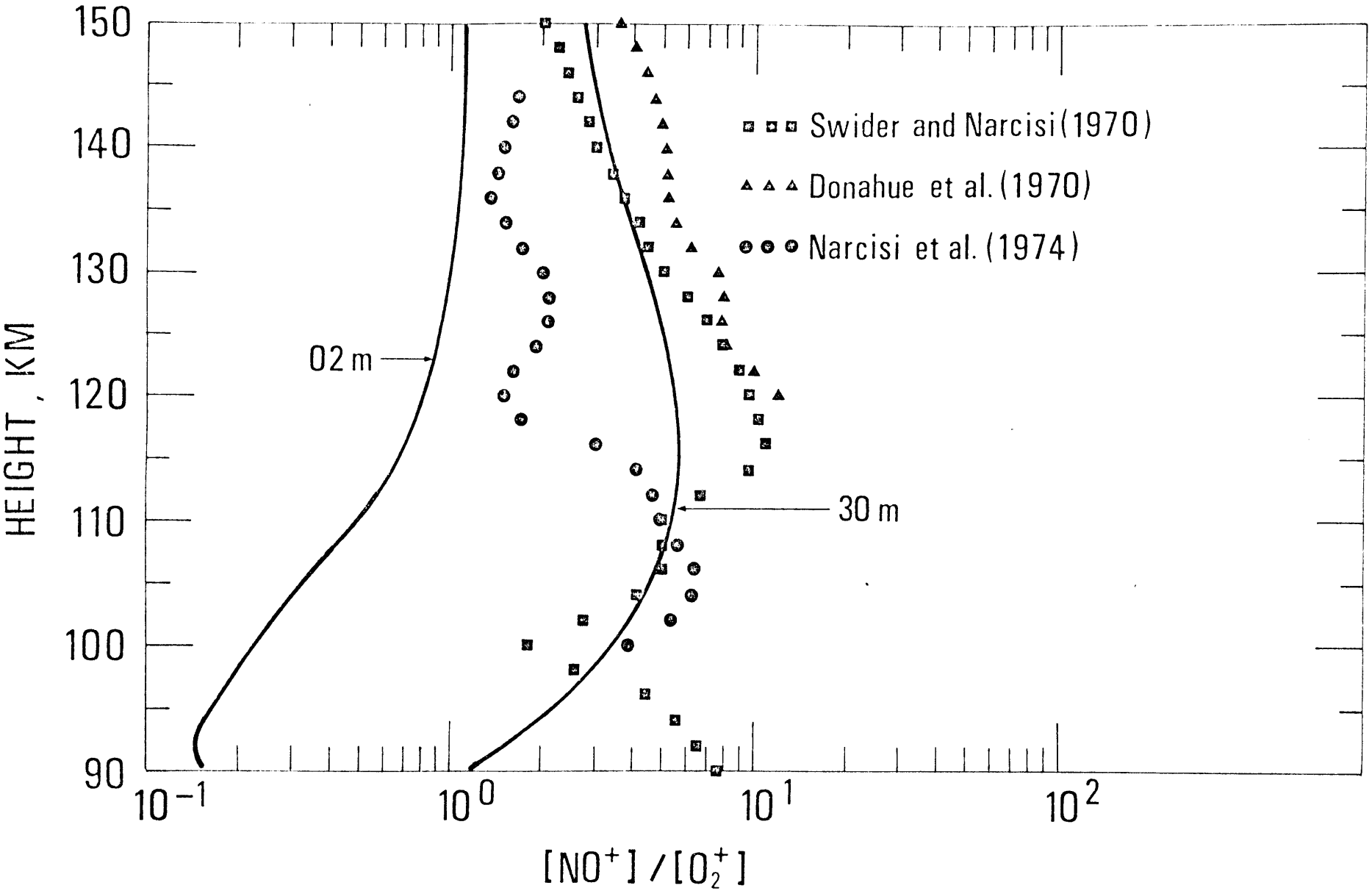

Fig. III.18 Comparison of $[NO^+]/[O_2^+]$ calculated at 00h02m and 00h30m LT for case A with those observed in the auroral ionosphere.